Aus der Medizinische Klinik mit Schwerpunkt Nephrologie und
Internistische Intensivmedizin
der Medizinischen Fakultät Charité – Universitätsmedizin Berlin

DISSERTATION

The role of Centrosomal protein 83 (CEP83) in kidney progenitor differentiation from human induced pluripotent stem cells (hiPSCs)

Die Rolle des zentrosomalen Proteins 83 (CEP83) bei der Differenzierung von Nierenvorläuferzellen aus menschlichen induzierten pluripotenten Stammzellen (hiPSCs)

zur Erlangung des akademischen Grades
Doctor rerum medicinalium
(Dr. rer. medic.)

vorgelegt der Medizinischen Fakultät Charité – Universitätsmedizin Berlin

von

Fatma Ahmed Ahmed Sayed Mansour
Kairo/Ägypten

Datum der Promotion: 30.11.2023

Table of contents

List of abbreviations

°C	Celsius degree
µg	Microgram
µl	Microliter
BB	basal body
BIH	Berlin institute of Health
BP	Biological process
bp	Base pair
BSA	Bovine serum albumin
CAKUT	Congenital anomalies of the kidney and urinary tract
Cas9	CRISPR associated protein 9
cDNA	complementary DNA
CEP164	centrosomal protein 164
CEP83	Centrosomal protein 83
CEP83$^{-/-}$	CEP83 knockout
CEP89	centrosomal protein 89
CRISPR	Clustered regularly interspaced short palindromic repeats
D	Day
DAPs	distal appendages proteins
DNA	Deoxyribonucleic acid
DPBS	Dulbecco´s Phosphate buffered saline
E	Embryonic day
E8	Essential 8
EDTA	Ethylenediaminetetraacetic acid
ESRD	End-Stage Renal Disease
FBF1	fas binding factor 1
h	Hours
hiPSCs	Human induced pluripotent stem cells
Hoxb7	Homeobox B7
HVG	Highly variable gene
IFT25	Intraflagellar Transport 25
IFT27	Intraflagellar Transport 27

IM	Intermediate mesoderm
KIF14	Kinesin Family Member 14
Kif3a	Kinesin Family Member 3A
Kif3b	Kinesin Family Member 3B
LPM	Lateral plate mesoderm
LRRC45	leucine-rich repeat-containing 45
min	Minutes
ml	Milliliter
mRNA	Messenger RNA
NPHP	Nephronophthisis
PCR	Polymerase chain reaction
qPCR	Real-time quantitative PCR
RNA-seq	mRNA sequencing
rpm	Rotation per minute
RT	Room temperature
SCLT1	sodium channel and clathrin linker 1
scRNA seq	Single cell RNA sequencing
SD	Standard deviation
SDS	Sodium dodecyl sulfate
sec	Seconds
TFs	transition fibers
TPM	Transcripts per million
TPMmax	Maximum TPM across samples
TZ	transition zone
UMAP	Uniform Manifold Approximation and Projection for Dimension Reduction
UMI	Unique molecular identifier

List of figures

List of tables

Abstract (English)

Background: Centrosomal protein 83 (CEP83) is a component of the distal appendages proteins (DAPs) of centrioles, which is necessary for the assembly of primary cilia. Primary cilia play an essential role in early embryonic development, organ development, and tissue homeostasis. Loss of many ciliary proteins in mice models results in kidney agenesis, or embryonic lethality before kidney development. The kidney develops from human induced pluripotent stem cells (hiPSCs) in a stepwise process involving the induction of specialized nephron progenitors (NPs) in the intermediate mesoderm, then differentiation into kidney epithelia.

Methods: Here, we used a hiPSCs derived system that models the induction of NPs followed by kidney epithelial differentiation to analyze the role of CEP83 in human kidney epithelial differentiation. We used CRISPR-cas9 technology to induce inactivating deletions of CEP83 in hiPSCs. Then, we differentiated the hiPSCs into NPs and kidney organoids. We used morphological analyses, gene expression studies, and immunostaining to analyze NPs and kidney epithelial differentiation.

Results: CEP83$^{-/-}$ hiPSCs failed to differentiate into nephron epithelia compared with the WT hiPSCs, which successfully differentiated into kidney organoids containing differentiated nephron epithelia. In contrast, CEP83$^{-/-}$ differentiated cells and organoids upregulate regulatory genes of lateral plate mesoderm (LPM), including OSR1, FOXF1, FOXF2, and FENDRR. In addition, CEP83$^{-/-}$ organoids upregulate marker genes of cardiovascular progenitors including TBX1, and ISL1. The shifted differentiation of CEP83$^{-/-}$ hiPSCs was associated with defective ciliogenesis.

Conclusion: In a human system modeling kidney epithelial differentiation from hiPSCs, our data provide new insight into the essential role of CEP83 in early NPs differentiation. That may help to better understand the pathogenesis of CEP83-associated renal developmental defects.

Abstract (German)

Hintergrund: Das zentrosomale Protein 83 (CEP83) ist eine Komponente der distalen Anhängselproteine (DAPs) der Zentriolen, die für den Aufbau der primären Zilien notwendig sind. Primäre Zilien spielen eine wesentliche Rolle in der frühen Embryonalentwicklung, der Organentwicklung und der Gewebehomöostase. Der Verlust von Zilienproteinen in Mausmodellen führt zu Nierenagenesie oder embryonaler Letalität vor der Nierenentwicklung. Die Niere entwickelt sich aus humanen induzierten pluripotenten Stammzellen (hiPSCs) in einem schrittweisen Prozess, der die Induktion spezialisierter Nephronvorläuferzellen (NPs) im intermediären Mesoderm und die anschließende Differenzierung in Nierenepithelien umfasst.

Methoden: Wir haben ein von hiPSCs abgeleitetes System verwendet, das die Induktion von NPs und die anschließende Differenzierung zu Nierenepithelien modelliert, um die Rolle von CEP83 bei der epithelialen Differenzierung der menschlichen Niere zu analysieren. Mit der CRISPR-Cas9-Technologie wurden inaktivierende Deletionen von CEP83 in hiPSCs induziert (CEP83$^{-/-}$). Anschließend wurden die CEP83$^{-/-}$ und Wildtyp (WT) hiPSCs in NPs und Nierenorganoide differenziert. Mit Hilfe von morphologischen Analysen, Genexpressionsstudien und Immunfärbung wurde die Differenzierung von NPs und Nierenepithelien analysiert.

Ergebnisse: CEP83$^{-/-}$ hiPSCs, anders als WT hiPSCs, konnten sich nicht erfolgreich in Nierenorganoide mit differenzierten Nephronepithelien differenzieren. CEP83$^{-/-}$ Zellen und Organoide zeigten eine erhöhte Expression von regulatorischen Genen des lateralen Plattenmesoderms, einschließlich OSR1, FOXF1, FOXF2 und FENDRR. Darüber hinaus wurden CEP83$^{-/-}$ Organoiden Markergene für kardiovaskuläre Vorläufer hochreguliert (TBX1 und ISL1). Die veränderte Differenzierung von CEP83$^{-/-}$ hiPSCs war mit einer gestörten Ziliengenese verbunden.

Schlussfolgerung: Unsere Daten liefern neue Erkenntnisse über die wesentliche Rolle von CEP83 bei der frühen Differenzierung von NPs. Dies könnte dazu beitragen, die Pathogenese von CEP83-assoziierten Nierenentwicklungsstörungen besser zu verstehen.

1.   Introduction

Primary cilia are microscopic sensory antennae projecting from most mammalian cells that play an essential role in organ development and tissue homeostasis by regulating several signaling pathways[1-12]. Disruption in primary cilium assembly or function results in a group of disorders known as ciliopathies, defined as genetically heterogeneous disorders associated with a wide range of phenotypes affecting most of the body organs. Renal ciliopathies include nephronophthisis (NPHP)[13-16], renal cysts[17,18], and impaired renal development[19-26]. Therefore, studying the functional role of newly identified ciliary proteins and their mechanistic role in renal ciliopathies may help to better understand renal pathophysiology and the onset of kidney disease.

1.1.   Structure and composition of the primary cilium

There are two types of cilium: motile and immotile (primary cilium), the motile cilium is distributed in limited tissues such as the lungs, respiratory tract, middle ear, and embryonic node, while the primary cilium is an immotile sensory finger-like organelle that projects from the surface of most mammalian cells. The primary cilium is composed of a cytoskeletal core termed axoneme that comprises nine outer pairs of microtubules and a central pair that controls motility (9 + 2 axoneme) in the motile cilium, and only 9 outer pairs of microtubules (9 + 0 axoneme) in the immotile cilium[27-29]. The base of the primary cilium is composed of the basal body (BB), the transition zone (TZ), and the Inversin compartment[30-33], as shown in **Fig. 1A**.

1.2.   Assembly of the distal appendages proteins (DAPs) at the ciliary base
The BB comprises important structures named the transition fibers (TFs) or distal appendages (DAPs) that link the mother centriole to the plasma membrane, and are composed of a group of proteins called distal appendages proteins. To date, six DAPs proteins have been identified namely: centrosomal protein 83 (CEP83), sodium channel and clathrin linker 1 (SCLT1), centrosomal protein 164 (CEP164), centrosomal protein 89 (CEP89), fas binding factor 1 (FBF1), and leucine-rich repeat-containing 45 (LRRC45)[27,34-36]. DAPs proteins play an essential role in the initiation of ciliogenesis by docking the primary ciliary vesicle to the plasma membrane[34,37].
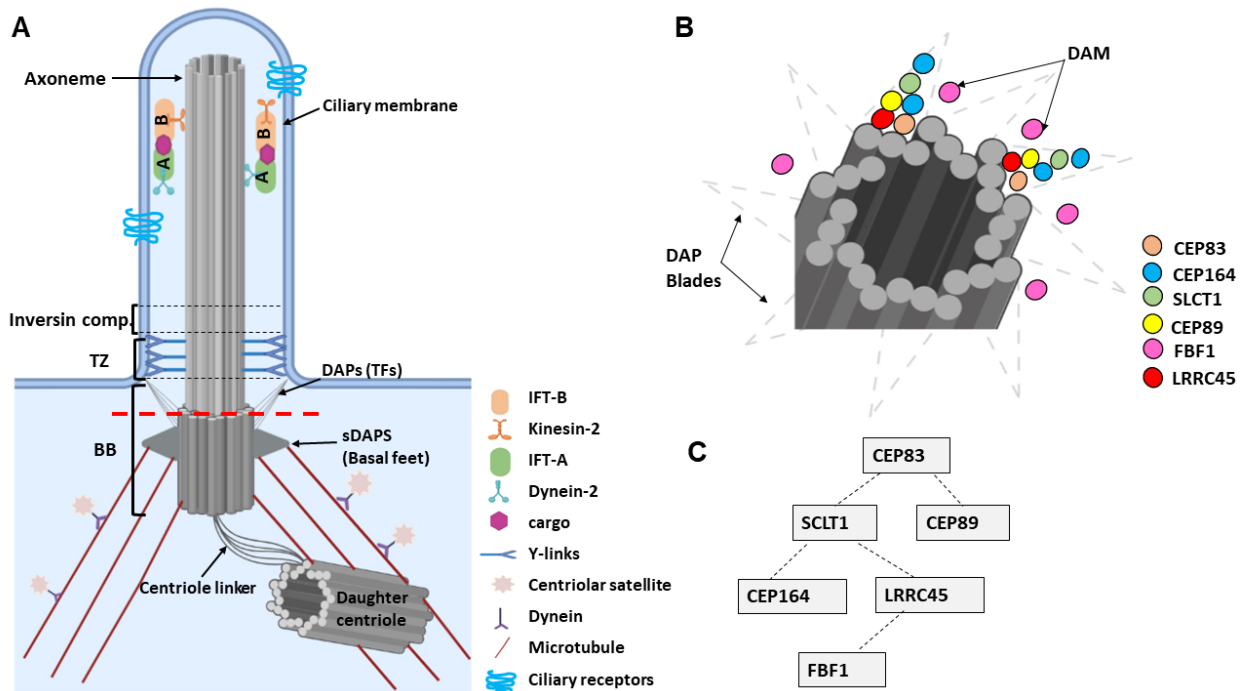
Figure 1: Primary cilium structure. (**A**) A simplified diagram of the primary cilium demonstrates its basic structures. The ciliary base comprises three essential compartments namely: a basal body (BB) that is composed of a mother centriole that is connected to the daughter centriole via the centriole linker, a transition zone (TZ), and the inversin compartment. The BB harbors two structures, the subdistal appendages (sDAPs), and the distal appendages (DAPs) that were previously known as transition fibers (TFs). (**B**) High magnification of the DAPs at the ciliary base is shown in Figure 1B, as referred to by the non-continuous red line in Figure 1A. The diagram shows that the DAPs are arranged as DAP blades, and DAP matrix (DAM) [16]. (**C**) The illustration shows that the DAPs are arranged in a hierarchical assembly at the base of the mother centriole (adapted from own publication: Mansour *et al*, 2021[37]).

Previous studies that used super-resolution microscope techniques showed that the DAPs proteins are organized in pinwheel-like structures[28,35] **(Fig. 1B)**, and the recruitment of the DAPs at the base of the cilium occurs in a hierarchical sequence as shown in **Fig. 1C**. Mutations in genes encoding CEP83[38], CEP164[26,39,40], and SCLT1[18,41] proteins have been associated with NPHP and cystic kidney disease[18,38,41-43]. NPHP is an autosomal recessive kidney disease that commonly leads to End-Stage Renal Disease (ESRD) in children and young adults. NPHP comprises three forms: infantile, juvenile, and adolescent with the onset of ESRD at 3, 13, and 19 years old, respectively[15,17,44-53].

1.3.   Functional role of ciliary proteins in embryo and kidney development

Mutations of *Kif3a* and *Kif3b*, major components of the kinesin-II ciliary anterograde motor, in mice[23,25] resulted in early embryonic lethality with holoprosencephaly, an

edematous pericardial sac, cardiac looping defects, and a truncated posterior trunk at E9.5 and E10.5. Interestingly, the same phenotype has been recorded in global *Cep164* knockout mice[26]. Additionally, *Kif3a* mutant mesoderm has been associated with reduced nephron numbers[23,24]. Moreover, biallelic loss of function mutation of Kinesin-like protein 14 (*KIF14*), a key regulator protein of cilia formation, resulted in bilateral renal agenesis in human and zebrafish[19,20]. Similarly, mutations in genes that encode the ciliary intraflagellar transport proteins including intraflagellar transport protein 25 (IFT25) and intraflagellar transport protein 27 (IFT27) in mice have been previously associated with renal agenesis or renal hypoplasia[21,22].

1.4. Differentiation of Human induced pluripotent stem cells into kidney organoids

In the last few years, several studies were interested in differentiating induced pluripotent stem cells (iPSCs) into kidney organoids in vivo[54-59]. The engineering of such a cellular model of kidney cells could be applied to studies of kidney development and disease modeling studies of many genetic disorders. Interestingly, **Takasato *et al*., 2015** established a protocol that could successfully differentiate human induced pluripotent stem cells (hiPSCs) into most nephron epithelial cells[57].

1.5 Aim of the study

Genome editing studies have used the advantage of in vivo induction of kidney organoids from stem cells to study congenital renal disease[58,60-64]. In our research, we were interested in generating genetically modified hiPSCs that lack the CEP83 protein using CRISPR-cas9 technology. Then we differentiated the *CEP83*^{-/-} hiPSCs into nephron progenitors followed by kidney organoids to understand the functional role of CEP83 in the differentiation of the early nephron progenitors and kidney development. Phenotypical characterization of the structural, molecular, and functional defects in the designed CEP83 deficient cellular model provides novel findings on the functional role of CEP83 protein in nephron progenitor's differentiation from hiPSCs and in kidney development.

2. Methods

2.1. Human induced pluripotent cells (hiPSCs) Cell line

The BIHi005-A hiPSCs line was used to generate CEP83 mutated hiPSCs, the cell line was provided by the stem cell facility at Max Delbruck center for molecular biology (MDC) and produced by the Berlin Institute of Health (BIH). Further information about the cell line is available at https://hpscreg.eu/cell-line/BIHi005-A.

2.2. Generation of CEP83 knockout clones using CRISPR- CAS9 Technology:

We used the advance of the Clustered Regularly Interspaced Short Palindromic Repeats (CRISPR) technology to generate CEP83 knockout hiPSCs clones. The CRISPOR web tool (http://crispor.tefor.net/, V 4.97)[65] was used to design two highly specific (specificity score more than 80) crispr RNA (crRNA), that are targeting exon 7 (**Table 1**). Homo sapiens was used as the reference genome and 5'-NGG-3' as the protospacer adjacent motif (PAM).

Table 1: List of designed crRNAs:

CEP83 (EXON 7)	Sequence-PAM sequence	Specificity Score
crRNA1/ 155 FW	GGCTGAAGTAGCGGAATTAA-AGG	88
crRNA2/218 FW	AAGAATACAGGTGCGGCAGT-TGG	88

2 nmol crRNA were dissolved in 20 µl of 1X IDTE buffer (11-04-02-01, IDT) to obtain a stock concentration of 100 µM (150 pmol/µl). Equimolar volumes of crRNA and tracrRNA (1072532, IDT) were annealed to form two guide RNAs (gRNAs) with cycling conditions: (95°C- 5 min, 70°C- 10 min, 45°C- 5 min, and 4°C- ∞). The gRNAs were diluted with IDTE buffer to 20 µM and kept on ice. Cas9 protein (Alt-R® S.p. Cas9 Nuclease V3, 1081058, IDT) was diluted to a working concentration of 1 µg/µl. 1 µl of each gRNA was mixed with 0.5µl Cas9 protein and incubated at RT for 1 h to generate RNP complexes (**Fig. 2**). Cultured hiPSCs on matrigel (354277, Corning®) in Essential 8 medium (E8, A1517001, Thermo Fisher Scientific) supplemented with ROCK inhibitor (Rocki, Y-27632), were split one day before by accumax (07921, Stem Cell Technologies), and cultured in an equal proportion of E8 medium and StemFlex medium (A3349401, Thermo Fisher Scientific).

Before the transfection, the cells with a density of 40–50% were dissociated again by accumax. Then cells were collected, and resuspended in buffer R, a resuspension buffer from the Neon™ transfection 100 µl kit (MPK10096, Invitrogen)[66]. After that, cells were transfected in 3 ml of buffer E, Electrolytic buffer using a Neon transfection system (Invitrogen), the Neon transfection 10µl tip, voltage (1200 V), width (30 ms), and pulse (1). The transfection step was performed by Narasimha Swamy Telugu. Finally, the transfected cells were seeded for 48 hours in StemFlex medium with Rocki, with daily medium change.
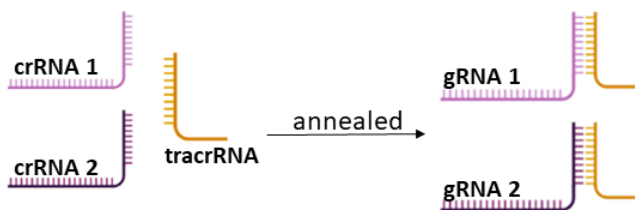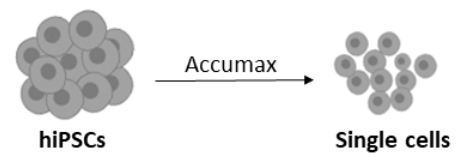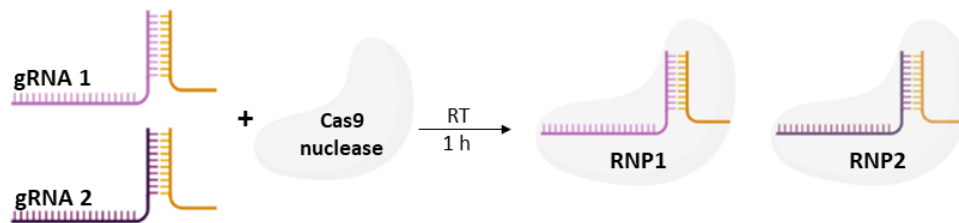
Figure 2: Experimental design of hiPSCs transfection with gRNAs.

(A) Annealing of two crRNAs and tracrRNA to form gRNAs. tracrRNA carries a complementary sequence to the crRNA. **(B)** hiPSCs were dissociated with accumax, and 2x tubes of hiPSCs were prepared for transfection. **(C)** Cas9 protein and gRNAs were incubated at room temperature for 1 h to form RNP complexes. **(D)** The prepared suspension of cells was transfected with RNP complexes using a nucleotransfection system. Then, cells were seeded in a 6-well plate for 48 h.

2.3. Testing edited genomic DNA for transfection efficiency

Quick DNA extraction and PCR were done using the Phire™ Tissue Direct PCR Master Mix (F-140WH, Thermo Scientific, Waltham, MA, USA) according to the manufacturer's instructions to test transfection efficiency. Primers were designed using the Primer3 webtool (V. 0.4.0, SourceForge, USA, Table 3), ordered from BioTeZ (Berlin, Germany) as 100 µM stock solutions, and diluted to 10 µM in nuclease-free H2O (AM9937, Thermo Fisher Scientific) and stored at -20°C. The used PCR mix included 10 µl Buffer, 7.8 µl H_2O, 0.4 µl Primer forward, 0.4 µl Primer reverse, 0.4 µl Polymerase, and 1 µl genomic DNA, and was subjected to the following PCR cycling conditions: 98°C- 5 min, for 35 cycles (98°C- 5 sec, 63.5°C- 30 sec, 72°C- 1 min), 72°C- 10 min, and 4°C- ∞. The size of the produced PCR product was checked on a 1.5% agarose gel (9012-36-6, Carl Roth GmbH, Karlsruhe, Germany). After confirming the success of the transfection, the cells were dissociated and seeded at three different low densities of 10, 25, and 50 x 10^3 cells per well for 24 h.

2.4. Single cell picking, cloning, and selection of biallelic mutated clones.

Under a picking hood S1, we picked twenty-four single cells, that were cultured in StemFlex medium for two weeks. Then, DNA extract from the cultured clones was tested for CEP83 mutation using Phire™ Tissue Direct PCR Master Mix[67]. Clones that showed biallelic mutation for CEP83, were expanded in culture and frozen in a bambanker medium (BB01, Nippon Genetics) for further characterization.

2.5. Differentiation of hiPSCs into kidney organoids
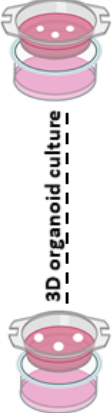
Following the Takasato protocol, cultured hiPSCs with 70-80% density were trypsinized using 1X Trypl E Select (12563011, Thermo Fisher Scientific). The collected cells were seeded on a matrigel-coated 6-well plate with a density of 15 × 10^3 cells per cm^2. Then, cells were cultured in E8 medium supplemented with 10µM ROCKi, and incubated at 37 °C CO_2 incubator for 48 h. The cells were supplied daily with a fresh medium, till reached 40–50% confluence after two days. Then, cells were differentiated using the differentiation medium, APEL2 medium (05270, Stem Cell Technologies). The differentiation medium

was previously prepared by adding 5% Protein Free Hybridoma Medium II (12040077, Thermo Fisher Scientific), and antibiotic–antimycotic (15240-062, Thermo Fisher Scientific). The cells were cultured for 7 days to induce inter-mediate mesoderm (IM) differentiation[67], as summarized in **Table (2).**

The cells were washed at the end of day 7, with 1X DPBS, trypsinized with trypsin EDTA 0.05% (25300-062, Thermo Fisher Scientific), and incubated at 37°C for 3 min. To neutralize the trypsin, 9 ml of MEF culture medium (AR005, R& D) was added to the dissociated cells. The cells were seeded by centrifugation and, finally resuspended in 1 ml APEL2 medium. Then, to prepare the organoids, the total number of the cells was counted and divided to reach 1×10^6 cells per organoid. Finally, we picked up each cell pellet by a wide-bore tip (P1,000 or P200). We carefully seeded the cell pellet onto the polyester membrane of the transwell cell culture 6- well plate (CLS3450-24EA, Sigma Aldrich) with minimal medium carryover[67]. The supplied medium is described in **table 2**.

Table 2: Steps of the differentiation protocol

Duration	Cell stage	Medium supplement	Experimental design
Day -2 to 0	Pluripotent	2 ml E8 medium supplemented with Rocki. Medium changed daily.	Monolayer culture
Day 0 to 5	Posterior primitive steak induction	2 ml APEL2 medium supplemented with 8 µMCHIR99021 (4423/10, R& D). Medium changed every 2 days.	
Day 5 to 7	Intermediate Mesoderm induction	4 ml APEL2 medium supplemented with 200 ng FGF9 (273-F9-025, R& D) and 1 µg/ml heparin (H4784-250MG, Sigma Aldrich). Medium changed every 2 days.	
Day 7	Organoids seeding	1.2 ml APEL2 medium supplemented with 5 µMCHIR99021 for 1 hour.	3D organoid culture
Day 7 to 12	Organoid stage	1.2 ml APEL2 medium supplemented with 200 ng FGF9 and heparin. Medium changed every 2 days.	
Day 12 to 25	Organoid stage	1.2 ml APEL2 medium supplemented with heparin only. Medium changed every 2 days.	

2.6. Molecular Biology Methods

2.6.1. DNA isolation and Polymerase Chain Reaction (PCR)

The cultured *WT* and KO hiPSCs clones were washed and collected with a maximum of $5x10^6$ cells/ml. The DNA was extracted using DNeasy Blood & Tissue Kits (Qiagen, 69504) following the manufacturer's instructions. The concentrations and quality of the extracted DNA were measured using Nanodrop (Thermo Scientific, Waltham, MA, USA). We used the Phusion high-fidelity DNA polymerase (M0530, Biolabs, New England) to amplify 200 µg DNA by PCR[67].

The used master mix is 4 µl Phusion 5x buffer, 0.4 µl Dntps10Mm, 12.4 µl H_2O, 1 µl Primer forward, 1 µl Primer reverse, 0.2 µl Polymerase, and 1 µl genomic DNA. The PCR cycling conditions: (98°C- 30 sec, for 35 cycles (98°C- 10 sec, 63.5°C- 30 sec, 72°C- 1 min), 70°C- 10 min, and hold at 4°C- ∞).

The PCR results were checked on a 1.5% agarose gel and analyzed using a Bio-Doc Analyze dark hood and software system (Biometra, Göttingen, Germany).

2.6.2. RNA extraction and mRNA sequencing

At three time points of differentiation (D0, D7, and D25), the total RNA was isolated from a maximum of $1x10^7$ cells from both *WT* and *KO* clones, following the manufacturer's instructions of RNAasy Mini Kit (74104, Qiagen, Hilden, Germany) following the manufacturer's instructions. During the extraction, the RNA was treated with RNase-free DNase I (79254, Qiagen, Hilden, Germany) at RT for 15 min. Then, we measured the concentration, integrity, and quality of the extracted RNA using a Nanodrop, an Agilent 2100 Bioanalyzer, and the Agilent RNA 6000 Nano kit (5067-1511, Agilent Technologies, Santa Clara, CA, USA). For RNA sequencing, the extracted RNA with high purity (OD260/280 = 1.8-2.2 and OD260/230 ≥ 1.8) and high integrity (more than 6.8) was prepared for submission to sequencing by Novogene (Cambridge, United Kingdom)[68].

Raw data were transformed into sequenced reads and recorded in FASTQ files by Christian Hinze[68]. He aligned the FASTQ files to build 19 of the human genome provided by the Genome Reference Consortium (GRCh19) using the TOPHAT2 aligner tool[67,68]. The featureCounts were used to obtain the raw counts[69]. The Integrative Genomic Viewer (IGV, V 2.3.68, Broad Institute, USA) tool was used to visualize the mutation of CEP83 in the KO sequencing data[70]. Then, we performed normalization of the sequence reads to

the sequence length, to calculate the transcripts per million (TPM) values that were used for gene expression analysis[67,68,71].

2.6.3. Quantitative polymerase chain reaction (qPCR)

Using the RevertAid First Strand cDNA synthesis kit (K1622, Thermo Scientific, Waltham, MA, USA), 500 ng of the extracted RNA was reverse transcribed to cDNA. 1 µL of synthesized cDNA was used for qPCR using FastStart Universal SYBR Green Master (ROX,4913914001, Roche Diagnostics, Mannheim, Germany) according to the manufacturer's instructions. Relative mRNA expression measures of the target genes at each time point of the differentiation (D0, D7, and D25) were normalized to the mRNA expression level of Glyceraldehyde-3-Phosphate Dehydrogenase (GAPDH) gene. Then we used the ΔΔCt method for expression analysis. Primer 3 was used to design all primer pairs (**Table 3**).

Table 3: List of primers.

Gene	Forward primer sequence (5' →3')	Reverse primer sequence (5' →3')
CEP83	AGACAGCAAACGAGTGGAAC	GGATCTGACTGTAGCCTGCA
OSR1	CCTTCCTTCAGGCAGTGAAC	CGGCACTTTGGAGAAAGAAG
GAPDH	AGCCACATCGCTCAGACAC	GCCCAATACGACCAAATCC
POU5F1	AGCAAAACCCGGAGGAGT	CCACATCGGCCTGTGTATATC
NANOG	AAGGCCTCAGCACCTACCTA	ATTGGAAGGTTCCCAGTCGG
SOX2	CAAAAATGGCCATGCAGGTT	AGTTGGGATCGAACAAAAGCTATT
HOXD11	CAGCAGCGCAGTTGCC	CGGTCAGTGAGGTTGAGCAT
EYA1	AACAGCTCACCGTATCCAGC	TGTGCTGTACTCTGCTGTGG
GATA3	GCCCCTCATTAAGCCCAAG	TTGTGGTGGTCTGACAGTTCG
HOXB7	AAGCTCAGGAACTGACCGC	CCCTGTCTTGGCCGGTG

2.6.4. Single cell RNA (scRNA) experiment.

On day 7 of the differentiation of hiPSCs to intermediate mesodermal, the cells were collected from two experiments: The first experiment (*WT1* and *KO1*), and the second experiment (*WT2* and *KO2*) cells as illustrated in (**Fig. 3**). The collected cells were washed with 1x DPBS, then were dissociated with Accumax. After that, cells were filtered through a 40 µm filter, and counted to reach 10,000 cells per sample. Finally, cells were stained by Trypan blue (T10282, Thermo Fisher Scientific) to check for viability.

Bead-in-Emulsion (GEM) generation, cDNA synthesis, and library preparation were performed according to the 10x Genomics single cell protocol using 10X Genomics toolkit version v3.1 (1000121, Pleasanton, CA)[72], Chromium Next GEM Chip G (1000120), and 10X Genomics Chromium Controller. The quality of the generated cDNA and library was tested using the Agilent 4200 TapeStation system. Generated libraries were sequenced on Illumina HiSeq 4000 sequencers (paired-end, ~10,000 reads/nucleus). Sequencing was performed by the Genomics Facility (Berlin Institute for Medical Systems Biology (BIMSB), Berlin, Germany).
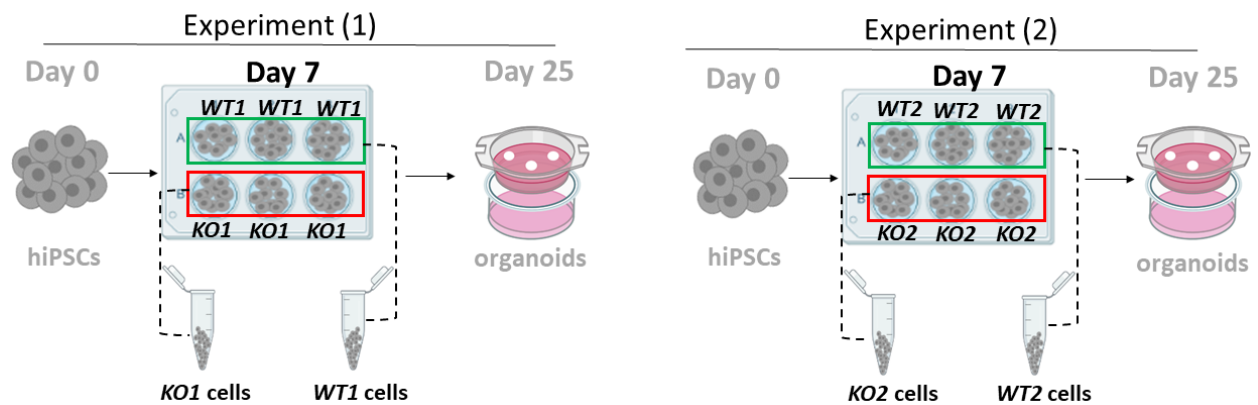
Figure 3: The figure illustrates the experimental design of the two scRNA experiments on day 7.

A gene expression matrix from a pair of FASTQ files was produced for each sample by Christian Hinze and analyzed using Cellranger version 3.0.2. Reads were aligned to the GRCh38 reference genome[67,68]. Gene expression matrices were subjected to further analysis to perform quality control analysis, cell clustering, cell type sorting, and differential gene expression using the Seurat R package (version 3)[73]. Cells derived from each sample were filtered separately using a lower cutoff of gene number (nGene) equal to 500 and an upper cutoff nGene is 6000.

Then, log normalization and scaling of the filtered data were performed in R (R Foundation for Statistical Computing Platform, 4.0.4), followed by the merging of the data from the four samples into one merged Seurat object. Clustering was performed based on highly variable genes (HVGs). Unique molecular identifiers (UMIs) plots were generated. Then, the first 20 principle components were used to perform a principal component analysis (PCA), using the factoextra, FactoMineR, and ggplot2 libraries. Marker gene lists that differentiate between clusters were extracted using the Seurat FindAllMarkers function with a log fold change threshold ±0.25. Only positive marker genes that expressed in at least 25 % of cells were used to identify different cell types.

2.7. Protein Isolation from hiPSCs and immunoblotting

The protein was extracted from both *WT* and *KO* hiPSCs to test the expression of the CEP83 protein. Up to $1*10^6$ cells per sample were firstly washed with cold 1x DPBS, then the washed cells were centrifuged for 5 min at 300 g. The cell pellets were suspended in ice-cold 100 µl of radioimmunoprecipitation assay (RIPA) buffer (R0278, Sigma-Aldrich) buffer, that was premixed with Proteinase Inhibitor (11697498001, Hoffmann-La Roche, Basel, Switzerland). The cell suspensions were kept with constant agitation at 4°C for 30 min, and were centrifuged for 20 min at 12,000 rpm at 4°C. After centrifugation, the supernatant was transferred to a new tube. Then, we used the Bicinchoninic acid protein assay (BCA, 23225, Thermo Scientific, Waltham, MA, USA) for protein quantification.

30 µg of the protein were used for immunoblotting, and were mixed with the same amount of the reducing 10% β-mercaptoethanol (24896800, Sigma-Aldrich, Saint Louis, MO, USA). Then, the protein mixture was denatured at 70°C for 10 min. after denaturation, the protein was loaded on a precast polyacrylamide NuPage 4-12% Bis-Tris protein gel (Invitrogen, Carlsbad, CA, USA). The protein electrophoresis was done in 1x MOPS using the XCell SureLock® Mini-Cell using 100V, 200mA for 2 h[67,74].

Proteins were blotted on Immobilon-P Polyvinylidene difluoride (PVDF) membrane with 0.45 µm pore size. The PVDF was pre-activated in methanol for 20 sec, and was equilibrated in 1X NuPage Transfer buffer (1.25 mM bicine, 1.25 mM BisTris, 0.05 mM EDTA, and 10% ethanol) for 30 min at RT. The blotting was performed in 1X NuPage Transfer buffer using the XCell II™ Blot Module. The membrane was blocked in 5% BSA (T844.2, Carl Roth GmbH, Karlsruhe, Germany) in 1X TBS-T pH 7.6 (50 mM TrisBase, 150 Mm NaCl, 0.05% Tween-20 (1662404, Bio-Rad)) for 1 h at RT. After the blocking, the membrane was incubated with the primary antibodies (Table 4) at 4°C overnight:

Table 4: List of primary antibodies used in immunoblotting.

Antibody	Dilution	Company
Anti- CEP83 produced in Rabbit	1:500	Sigma-Aldrich, Saint Louis, MO, USA
Anti-α-Tubulin produced in Mouse	1:500	T9026, Sigma-Aldrich

Then, the membrane was incubated with horseradish peroxidase (HRP)-conjugated secondary antibodies (1:2000 dilution) for 1 h at RT. After that, the protein was

detected using Chemiluminescent reagent (34076, Thermo Scientific, Waltham, MA, USA). Finally, the spectra^{TM} Multicolor Broad Range Protein Ladder (26623, Thermo Scientific, Waltham, MA, USA) was used to evaluate the corresponding protein bands' molecular weight.

2.8. Histology

2.8.1. Fixation and Paraffin embedding of kidney organoids

The organoids were washed in cold1X DPBS, and fixed in BD cytofix (554655, BD Biosciences, Franklin Lakes, USA) on ice for 1 hour. After fixation, organoids were dehydrated in a gradually increased concentration of ethanol (E7023, Millipore Sigma) as follows: 70%, 90%, 100%, and 100 %, each 15 min. Then, toluol was used for clearing the organoids for three turns, each 20 min. Cleared organoids were infiltrated with melted paraffin (CN48.2, Carl Roth GmbH, Karlsruhe, Germany) at 65°C, three changes, each 30 min. Then, organoids were embedded in paraffin blocks, which were processed into a HM 355S microtome to obtain 3.5 µm-thick sections.

2.8.2. Hematoxylin and Eosin staining (H&E)

Sections were incubated at 62 °C for 15 min, then were dried for 30 min at RT. After drying, the sections were cleared with xylol (9713.3, Carl Roth, Karlsruhe, Germany) twice each 2 min then the sections were dehydrated in decreasing concentrations of ethanol as follows: 100 %, 96 %, 80 %, and 70 %, each twice for 2 min. Then sections were washed twice with distilled water, and were stained as follows: 1x 3 min Hematoxylin, 1x 3 min H2O tap water, 1x 2 min Eosin (1 % in ddH2O, 3137.2, Sigma-Aldrich, Saint Louis, MO, USA), and 1x 5 min ddH2O. Then, the sections were dehydrated using increasing EtOH concentrations (96 % and 2x 100 %, 2 min each) and xylol, were mounted with Kaiser´s glycerol gelatin-based mounting medium (03989, Sigma-Aldrich, USA), and analyzed using a bright field microscope.

2.8.3. Immunofluorescence staining

The cultured cells on the glass slides (day 7 differentiated cells) and the growing organoids on the polyester membrane of the transwell cell culture 6- well plate (day 25) were fixed for 10 minutes on ice in BD Cytofix buffer. Then, the cells and the organoids

were washed using BD Perm/Wash (554723, BD Biosciences, USA) twice, 15 min each. Then, cells and organoids were blocked for 2 h at RT in a preprepared blocking solution (1% BSA + 0.3% triton-X-100 (3051.3, Carl Roth, Karlsruhe, Germany) in 1X DPBS). After blocking, cells and organoids were incubated with primary antibodies (**Table 5**) overnight at 4°C.

Table 5: List of primary antibodies used in immunofluorescence staining.

Antibody	Dilution	Company
Monoclonal Anti-Tubulin, acetylated antibody (T6793)	IF: 1:2000	Sigma-Aldrich, Saint Louis, MO, USA
anti-Cdh1	IF: 1:200	BD Bioscience, San Jose, CA, USA
Lotus tetragonolobus lectin (LTL)	IF: 1:200	Vector lab, Burlingame, USA
Anti-NPHS1	IF: 1:300	R&D System, Minneapolis, MN, USA
Anti- CEP83	IF: 1:200	Sigma-Aldrich, Saint Louis, MO, USA

After that, cells were washed in 1X DPBS twice (10 min each). The washed cells were incubated with fluorescence-labeled secondary antibodies overnight at 4°C. The secondary antibodies include Cy3, Cy5, Alexa488, and Alexa647 (dilution of 1:500, Jackson ImmunoResearch, Newmarket, UK), and Cy3 Streptavidin (dilution of 1:500, Vector lab, Burlingame, USA). Then, nuclear staining was performed using DAPI (D1306, Invitrogen, Carlsbad, CA, USA), diluted 1:300000, for 1 h at RT. Finally, Dako fluorescent mounting medium (K3461, Dako, Carpinteria, CA, USA) was used to mount the slides. Then, the slides were examined and imaged using a SP8 confocal microscope (Carl Zeiss GmbH, Germany). Then, the taken images were processed in ImageJ software (V-1.48; National Institutes of Health, Bethesda, MD) for quantitative analysis.

2.9. Statistics

All differentiation experiments were performed using three clones per group. Molecular and histological characterization experiments were performed using three biological replicates per group. Bulk RNA sequencing experiments were done using three biological replicates per group at each time point of the differentiation, while the scRNA-seq was only performed on two biological replicates per group. The experiment analysis was done using the unpaired 2-tailed t-test to compare between *WT* and *KO* groups. We used GraphPad Prism 7.04 (GraphPad Software, San Diego, CA) for the generation of graphs comparing the two groups, and data are presented as mean ± SD.

3. Results

3.1. Generation of CEP83⁻/⁻ hiPSCs clones

We used CRISPR Cas9 technology to induce deletion of the *CEP83* gene in hiP-SCs. Three *KO* clones carried different deletions in exon 7. These deletions resulted in an induction of a premature stop codon in both alleles (*KO1*) or one allele (*KO2, and KO3*), or frameshift mutation in one allele (*KO2, and KO3)*, associated with complete loss of CEP83 protein **(Fig. Fig.4 A- F)**.

Clones	Reads count (deleted bps)/ induced mutation	Mutated mRNA (EXON 7)	Predicted amino acid sequence
WT1	24	GAG-GCT-GAA-GTA-GCG-GAA-TTA-AAG-GCT-GAA-AAG-GAG-AAT-TCT-GAG-GCT-CAG-GTG-GAA-AAT-GCC-CAA-AGA-ATA-CAG-GTG-CGG-CAG-TTG-GCT	EAEVAELKAEKEN SEAQVENAQRIQV RQLA
WT2	23		
WT3	31		
KO1	8 (-63)/ Stop codon induction (TAG)	GAG-GCT-GAA-GTA-GCG-GAA-**TAG**-TTG-GCT	EAEVAE*
KO2	**First allel** 9 (-63)/ Stop codon induction (TAG)	**First allel** GAG-GCT-GAA-GTA-GCG-GAA-**TAG**-TTG-GCT	**First allel** EAEVAE*
	Second allel 2 (-62)/ Frame shift mutation induction	**Second allel** GAG-GCT-GAA-GTA-GCG-GAA-TCA-GTT-GGC-T	**Second alleL** EAEVAE**SVG**
KO3	**First allel** 12 (-63)/ Stop codon induction (TAG)	**First allel** GAG-GCT-GAA-GTA-GCG-GAA-**TAG**-TTG-GCT	**First allel** EAEVAE*
	Second allel 7 (-74)/ Frame shift mutation induction	**Second allel** GAG-GCT-GAA-GTA-GCG-GAA-TTT-GGC-T	**Second allel** EAEVAE**FG**

Figure 4: Generation of CEP83 mutated hiPSCs clones. (A) PCR on the WT and transfected (with gRNAs) hiPSCs showed two different-sized PCR products on agar gel. The first product is 180 bp as expected by the designed primer pair for CEP83 detection. While, the other product is around 120 bp pair as expected by the designed CRISPR- cas9 approach, indicating the success of mutation induction. Then, twenty-four *KO* clones were picked and grown for two weeks, after that the clones were tested for mutation

induction by PCR. (B) PCR showed that three clones (KO1, KO2, and KO3) showed one DNA product, which was sized around 120 bp (the mutated DNA product). (C) q RT-PCR showed significantly downregulated expression of CEP83 in the mutated hiPSCs. (D) Immunoblotting shows a complete loss of CEP83 protein which is 83 KD in the KO clones compared with the WT clones. (F) Bulk RNA sequencing was done on three WT clones and three KO clones, the mutation was visualized using IGV, and reads of each clone were used to characterize the type of mutation, the newly edited mRNA sequence, and the expected amino acid sequence of CEP83 protein. Data are mean ± SD.*$P < 0.05$.

Pluripotency marker genes and gene expression analyses between the WT and KO hiPSCs clones indicated similar gene expression profiles **(Fig. 5)**.
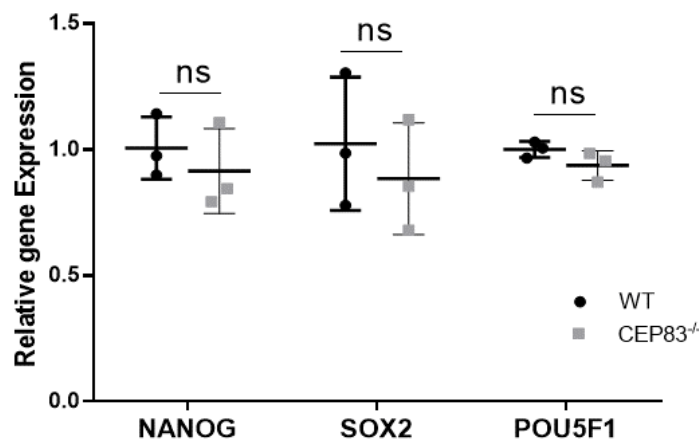
Figure 5: complete loss of CEP83 didn't alter either the gene expression or expression of the pluripotency markers of hiPSCs. The KO hiPSCs showed non-altered expression of the pluripotency markers compared with the WT hiPSCs using qRT- PCR. Data are mean ± SD. ns, not significant. Figures 5 A-D are adapted from Mansour et al., 2022[67].

3.2. CEP83−/− hiPSCs failed to differentiate into kidney organoids

To assess the functional role of CEP83 on the differentiation of the kidney progenitors and renal epithelial cells, a two-step manner protocol was used to differentiate both *WT* and *CEP83−/−* hiPSCs **(Table 2)** towards kidney organoids[57]. The first step is to differentiate hiPSCs (**Fig. 6A**) into intermediate mesoderm (IM) cells for seven days in a monolayer culture. IM cells give rise to two main kidney progenitors: metanephric mesenchyme (MM) and ureteric bud (UB)[57,75-80]. The MM differentiates into glomeruli, proximal and distal tubules epithelial cells, while UB gives rise to collecting duct (CD) epithelial cells[81]. The second step is to differentiate the IM cells into kidney organoids in 3D culture for 18 days. On day 7, the differentiated *CEP83−/−* and *WT* cells showed the same morphology in culture (**Fig. 6B**). However, on day 25, the *WT* organoids exhibited a well-

organized convoluted structure under a bright field microscope, while *CEP83$^{-/-}$* organoids showed no unique structures **(Fig. 6C)**.
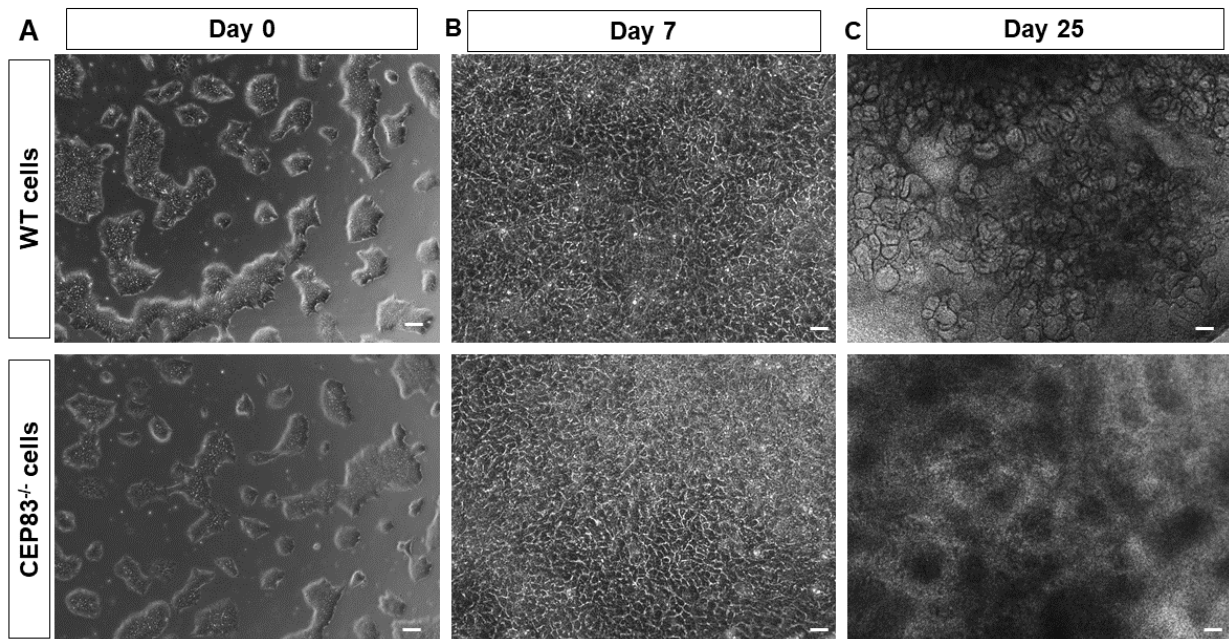
Figure 6: CEP83$^{-/-}$ hiPSCs differentiate into intermediate mesoderm (IM) cells, and failed to differentiate into kidney organoids. (A) However, hiPSCs didn't show morphological alteration on both day 0 (hiPSCs stage), and (B) day 7 (intermediate mesodermal cells) of the differentiation. (C) On day 25, the WT organoids showed convoluted structures in almost organoids while the KO organoids showed non-specific structures and instead appeared as homogenous growing cells (C). Bar = 50 µm.

Hematoxylin and eosin (HE) staining of the *WT* organoid sections displayed well-organized structures, while the *CEP83$^{-/-}$* organoids didn't show any defined structures **(Fig. 7A and 7B)**. Immunostaining for some renal epithelial markers, including NPHS1, LTL, and CDH1 showed positive staining in the *WT* organoids and negative staining in the *KO* organoids **(Fig. 7C and 7D)**. Bulk RNA sequencing of the CEP83$^{-/-}$ and *WT* organoids confirmed that the CEP83 deficient cells are unable to differentiate into renal epithelial cells **(Fig. 7 E-I)**.

3.3. CEP83$^{-/-}$ differentiated cells show defective ciliogenesis.

Previous studies have shown that CEP83 loss resulted in a complete loss of cilium in Retinal pigmented (RPE) cells[34,82], and the renal tubule epithelial cells[38]. In our study, we stained the differentiated cells at day 7 (IM cells) and day 25 (organoids) for acetylated tubulin to investigate the functional role of CEP83 protein loss on primary cilium assembly **(Fig. 8A,** and **B)**. The *CEP83$^{-/-}$* cells and organoids showed downregulation in the number

of ciliated cells compared to the *WT* cells and organoids **(Fig. 8C,** and **E)**. Additionally, measuring the ciliary length showed that *KO* cells and organoids showed longer cilium than the *WT* cells and organoids (**Fig. 8D,** and **F)**.
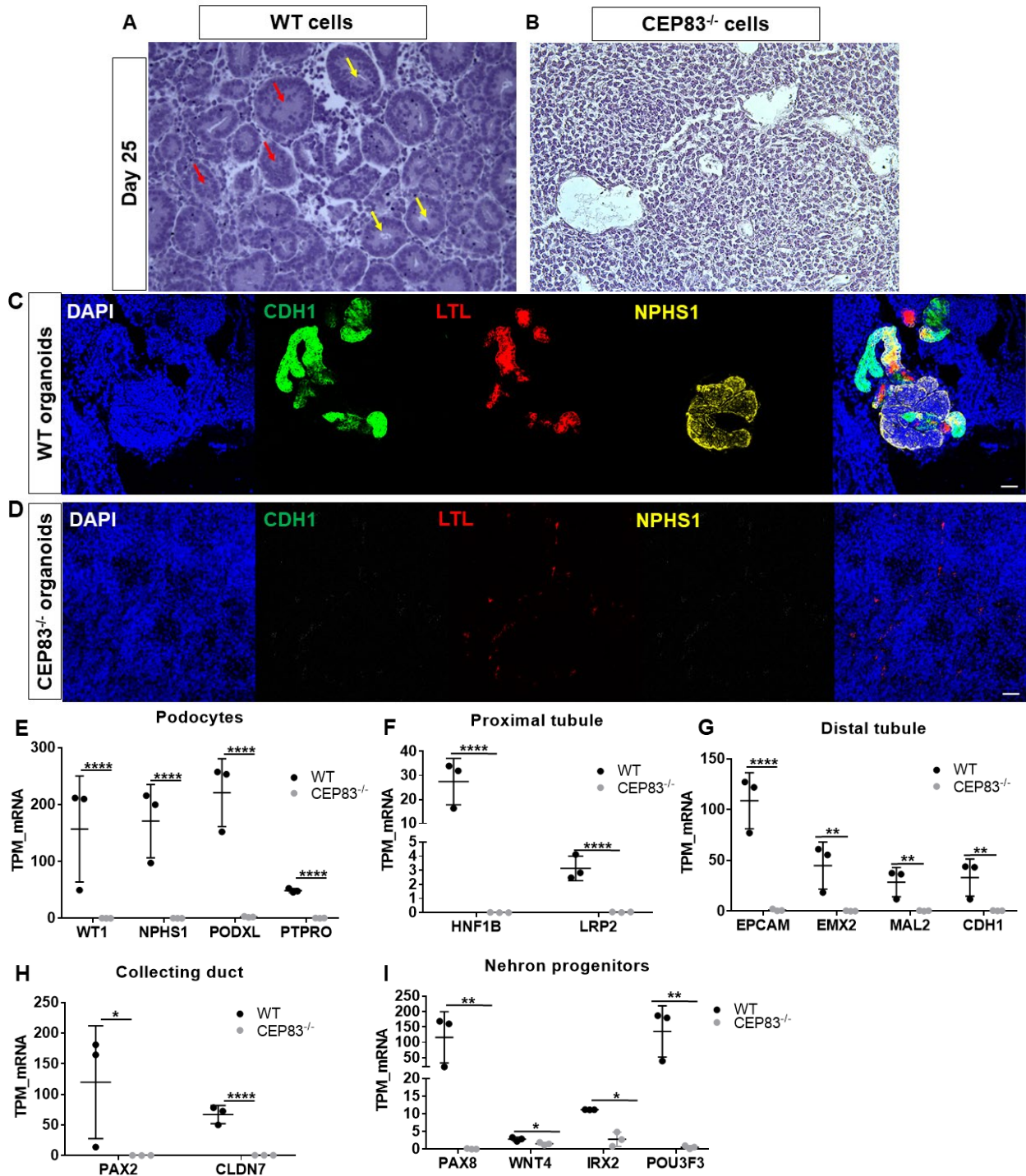
Figure 7: CEP83⁻ᐟ⁻ organoids show a failure of renal epithelial cells on day 25. (A) Histological staining of the cross sections of the WT organoids at day 25 using hematoxylin and eosin stain showed two different structures. The first structure is a round-to-oval structure with a nuclear arrangement on the periphery and a central lumen-like structure (referred to by the yellow arrows) while the other structure is a compact round-to-oval structure with a multinuclear structure in the center (referred by red arrows). Immunofluorescence

staining of both WT and KO organoids for the podocyte marker; NPHS1, proximal tubule stain; LTL, and the distal tubule marker; CDH1 was performed. (C) The WT organoids showed positive staining for the three markers, indicating the successful differentiation of the WT hiPSCs toward renal epithelial cells. (D) While the KO organoids showed negative staining for the three markers, indicating the failure of the mutated cells to differentiate into renal epithelial cells. Bulk RNA sequencing analysis show downregulated expression of renal epithelial markers in CEP83$^{-/-}$ organoids, (E) including WT1, NPHS1, PODXL, and PTPRO for podocytes, (F) HNF1B and LRP2 for proximal tubule epithelial and precursor cells, (G) EPCAM, EMX2, MAL2, and CDH1 for distal tubule epithelial cells, (H) PAX2 and CLDN7 for collecting duct cells, and (I) PAX8, WNT4, IRX2, and POU3F3 for nephron progenitor cells (E). Bar = 50 μm. n = 3 clones per group. Data are mean ± SD. *P < 0.05, **P < 0.01, and ****P < 0.0001.
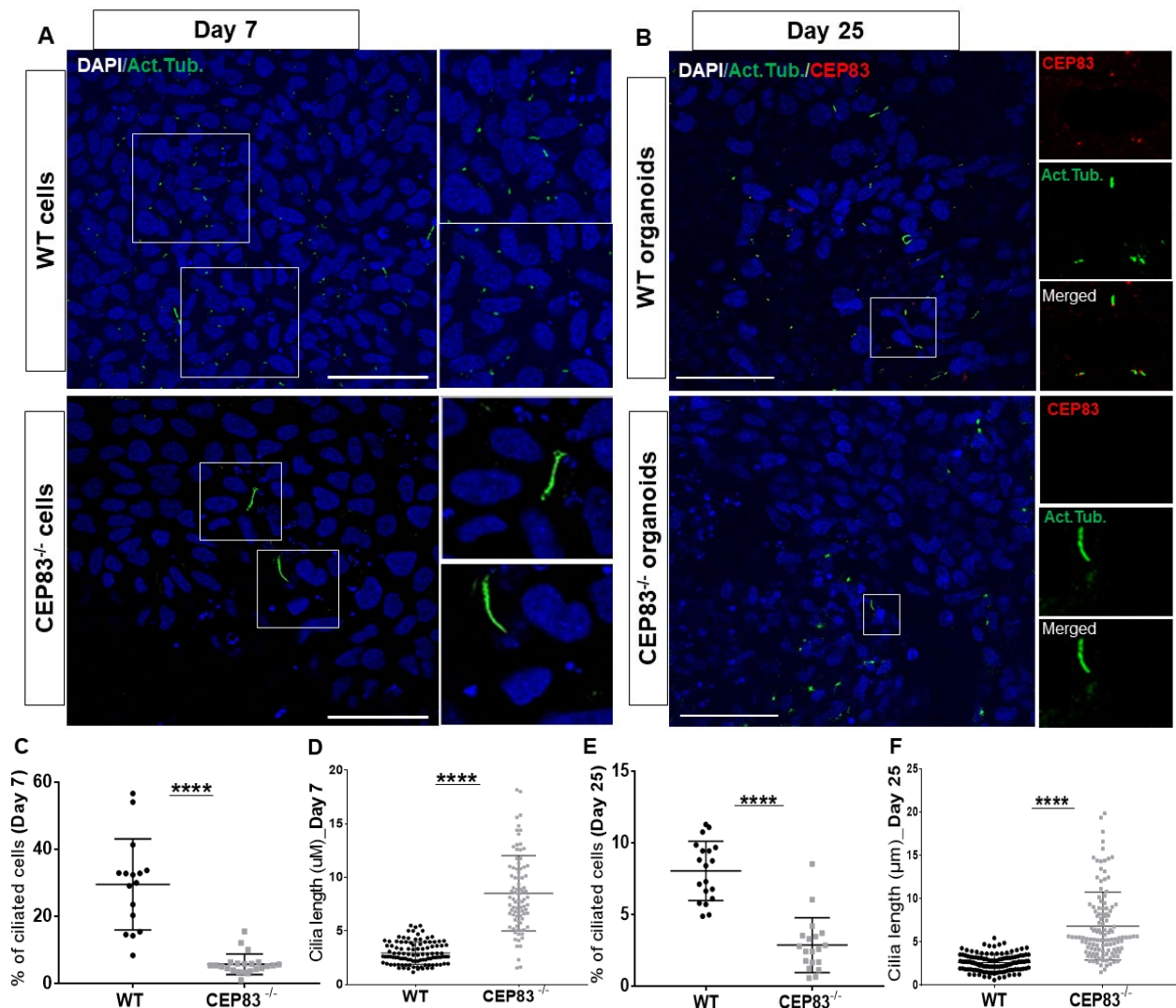
Figure 8: CEP83 knockout in hiPSCs resulted in defective ciliogenesis at both days 7 and 25 of differentiation. WT and CEP83$^{-/-}$ differentiated cells at (A) day 7 and (B) day 25 were stained for acetylated tubulin (shown in green) to evaluate the functional role of CEP83 loss on primary cilium formation. As shown in A, and B, the mutated cells showed defective ciliogenesis in the number of the ciliated cells, in addition to longer cilium formation. (B)The defective ciliogenesis at day 25 in the KO organoids was associated with missing CEP83 protein (shown in red), which appeared to be localized at the base of the cilium in WT

organoids. The ciliated cells were quantitatively analyzed using image J for the number of the ciliated cells and ciliary length. The analysis showed a significant downregulated number of the ciliated cells in CEP83$^{-/-}$ cells at day 7 (C) and day 25 (E). additionally, the analysis revealed that the ciliated CEP83$^{-/-}$ cells form longer cilium (D) at day 7 and (F) at day 25. n = 3 clones per group. Data are mean ± SD. ****$P < 0.0001$. Panel A: Bar = 50 µm.

3.4. CEP83$^{-/-}$ hiPSCs differentiated into Intermediate mesoderm in a monolayer cell culture.

To understand the differentiation efficiency of hiPSCs into nephron progenitors, we measured the relative gene expression of UB marker genes including *GATA3*[83,84] and *HOXB7*[85,86], and the expression of MM marker genes, including *HOXD11*[87,88] and *EYA1*[89,90] using qRT- PCR **(Fig. 9A-D)**, and bulk RNA sequencing data **(Fig. 9E-H)**.
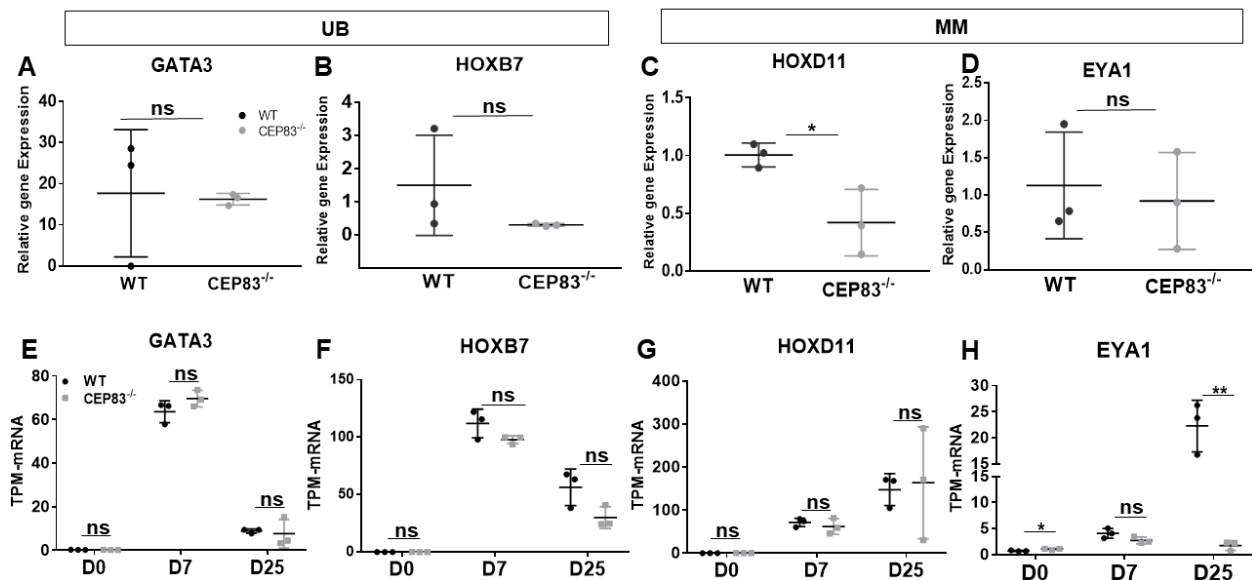
Figure 9: CEP83 mutated cells show similar expression profiles to WT cells for UB and MM marker genes. (A) Relative gene expression analysis shows that CEP83 mutated cells express intermediate mesoderm marker genes similarly to WT cells at day 7. This includes ureteric bud (UB) marker genes including GATA3 (A) and HOXB7 (B), and metanephric mesenchyme (MM) including HOXD11 (C) and EYA1 (D). Using the bulk RNA sequencing data, (E-H) the UB and MM marker genes were plotted across the different differentiation points (D0, D7, and D25), and showed no significant difference compared with the WT cells at day 7. n= 3 clones per group. Data are mean ± SD. *P < 0.05, and **P < 0.01. ns= not significant.

3.5. Single cell RNA (scRNA) sequencing analysis reveals the clustering of *KO* cells and *WT* cells.

Single-cell RNA (scRNA) sequencing analysis was performed on the differentiated cells on day 7 to exclude the nonspecific differentiation of hiPSCs. We clustered 27,328

cells derived from four samples *WT1* (3,768 cells), *WT2* (5,793 cells), *KO1* (8,503 cells), and *KO2* (9,264 cells), derived from two experiments as shown in **Fig. 3**. PCA of the WT samples and *KO* samples using the average expression of the top highly variable genes revealed that Dim 1 and Dim 2 contribute to the high percentage of variation 54% and 31.3%, respectively. **(Fig. 10A)**. Our clustering revealed ten different cell clusters (0- 9), some clusters are consistent with previous studies[91,92] **(Fig. 10B, and C)**. Interestingly, three clusters are identified as nascent nephron cells. To understand the defective differentiation of the mutated cells into kidney organoids, we focused on the molecular changes of the nascent nephron clusters between the *WT* and the *KO* cells.
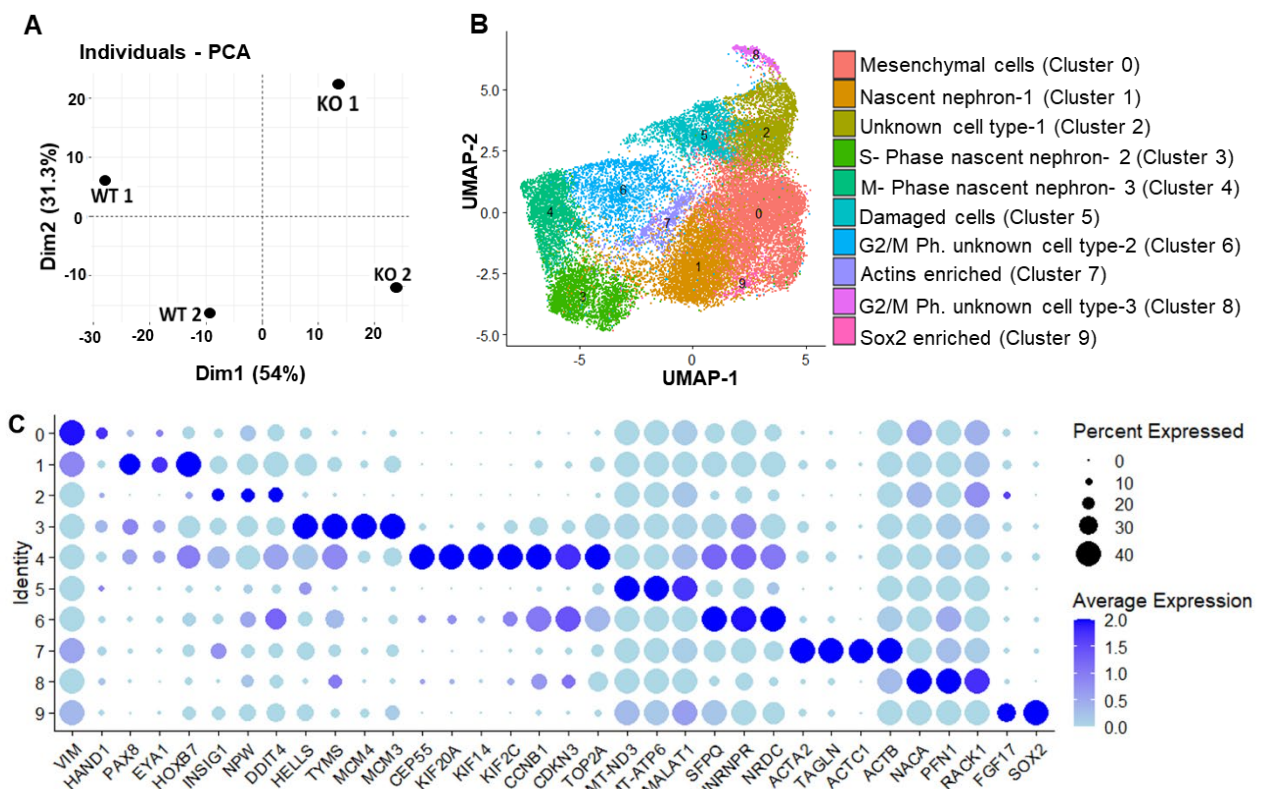
Figure 10: Single cell RNA (scRNA) sequencing analysis reveals ten different clusters at day 7. The experimental design of the scRNA sequencing was performed on four clones (WT1, WT2, KO1, and KO2) derived from two different experiments on day 7, as shown in **Figure 3** (Methods section). (A) Principal component analysis (PCA) of WT and CEP83^{-/-} cells was performed using the first 20 principle components (see methods section). Dimension 1 (Dim1) resembles 54 % of the expression differences and splits the KO samples from the WT samples. While Dimension 2 (Dim2) resembles 31.3 % of the expression differences and splits the two different experimental conditions (experiment 1 and experiment 2). (B) UMAP derived from clustering of the four samples (WT1, WT2, KO1, and KO2) after integration in a Seurat object (as described in the methods section) reveals 10 clusters as annotated. (C) The dot plot shows the average expression of top-expressed genes that characterize the individual clusters. The figure is adapted from Mansour et al.,2022[67].

3.6. *CEP83⁻ᐟ⁻* differentiated cells downregulate marker genes of the nascent nephron in three clusters.

The three nascent nephron clusters 1, 3, and 4 express nephron progenitors' marker genes including PAX8, EYA1, and HOXB7. Interestingly, the cellular contribution to cluster 1 (Nascent nephron-1) is highly shared by the *WT* cells compared with the *KO* cells (**Fig. 11A**). However, the cell proportion of the *WT* cells is mildly increased compared to the *KO* cells in both clusters 3 and 4. Additionally, the *KO* cells of those clusters downregulated the expression of PAX8, EYA1, and HOXB7 genes compared to the *WT* cells **(Fig. 11B)**.
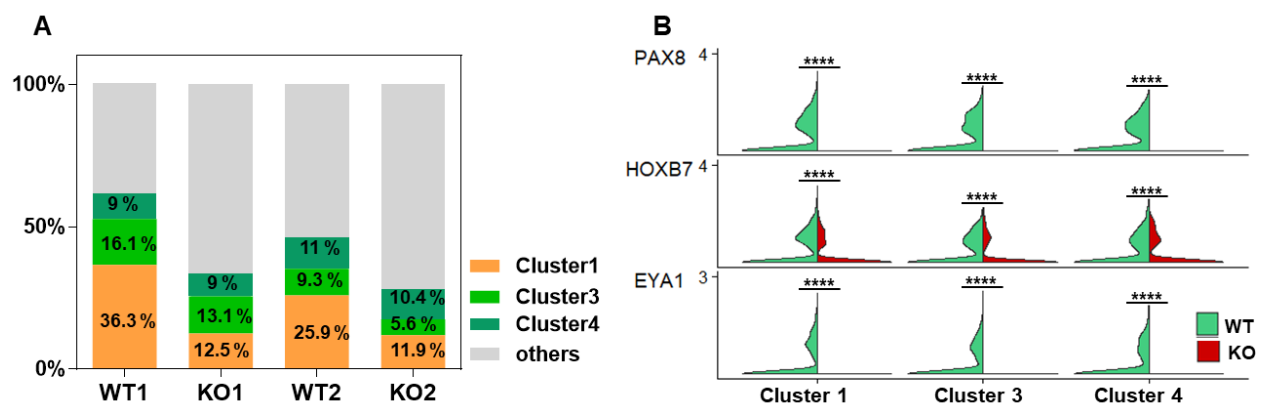
Figure 11: *CEP83⁻ᐟ⁻* **cells showed a defect in the differentiation of kidney progenitor at the early monolayer induction stage.** (A) The figure shows the different cell proportions between *WT* (*WT1, WT2*) and *KO* (*KO1, KO2*) groups in the three clusters that contain the nascent nephron cells (clusters 1, 3, and 4). (B) Focusing on these three clusters, the average expression of the kidney progenitor gene *PAX8*, the UB marker gene *HOXB7*, and the MM marker gene *EYA1* was plotted between the *WT* and *KO* cells, as shown in the violin plots. The plot shows that the KO cells significantly downregulate the expression of the three genes. N= 2 per group. *$P < 0.05$ and ****$P < 0.0001$.

3.7. CEP83⁻ᐟ⁻ cells upregulated marker genes of early lateral plate mesoderm.

Differential expression analysis between *WT* and *KO* cells was performed using bulk RNA sequencing data on day 7, the analysis was done by selecting genes with TPM >2, fold change between *WT* and KO groups > 1.5 (up or down-regulated genes), and *P*-value calculated on log10 TPM < 0.05. The analysis showed upregulation of many genes including OSR1, FOXF1, FOXF2, FENDRR, HAND1, HAND2, CXCL12, GATA5, and GATA6, these genes were expressed in early lateral plate mesoderm (LPM)[93-117]. Differential expression was confirmed by pseudobulk scRNA sequencing **(Fig.12A-I).**

3.8. CEP83^{-/-} organoids upregulated cardiovascular progenitor marker genes at day 25 of differentiation.

To assess the differentiation pattern of the CEP83^{-/-} organoids at day 25, we investigated the upregulated genes in *KO* cells at day 25 for other LPM genes. We found that *KO* organoids upregulate markers genes of cardiac mesoderm, which is a derivative of the LPM, including *ISL1*, and *TBX1*[118-125] **(Fig. 13A and 13B)**.
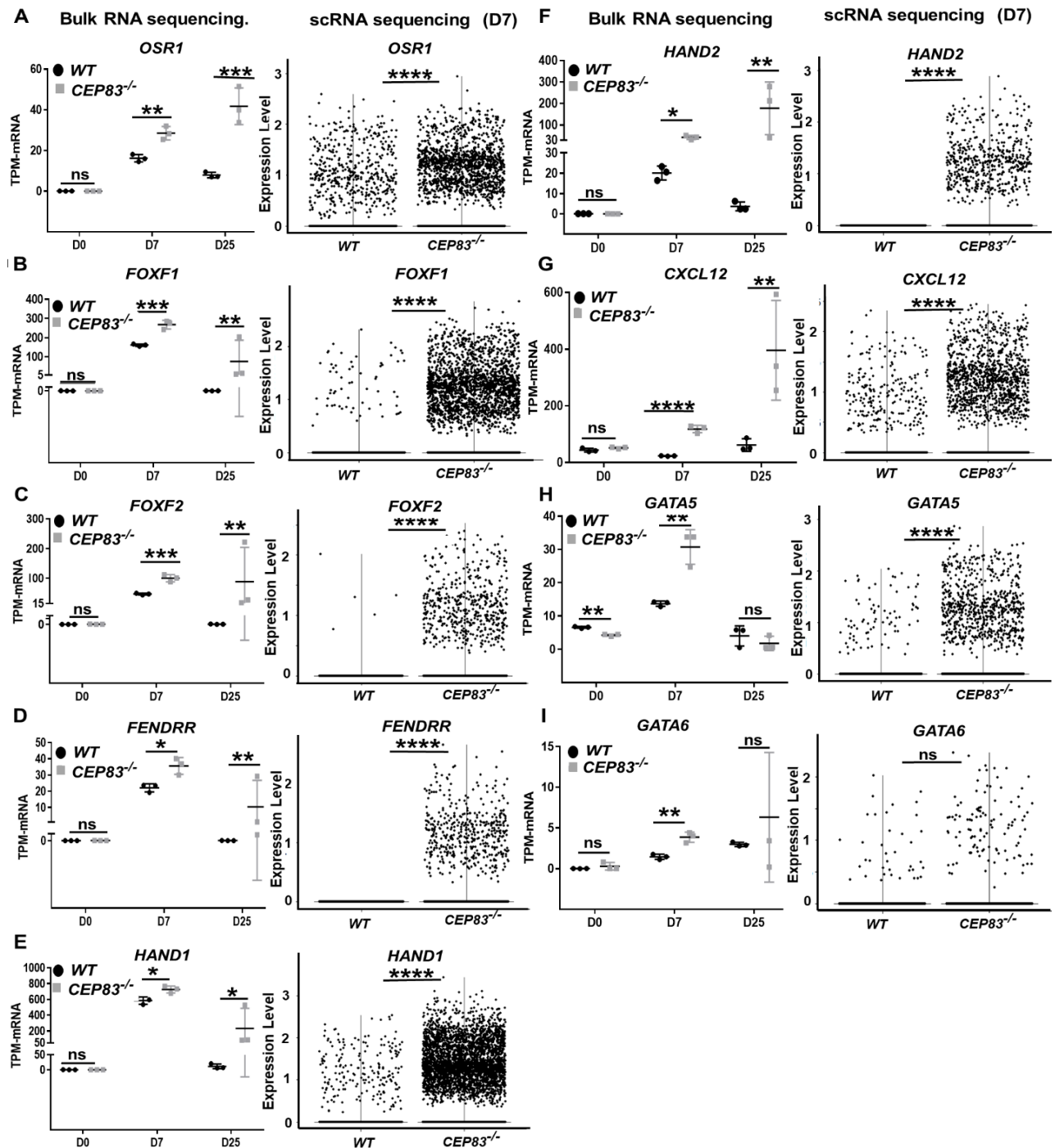
Figure 12: Differential expression analysis shows upregulated expression of early lateral plate mesoderm (LPM) genes in *CEP83*⁻/⁻ cells. (A-I) Plots show the expression of LPM markers (A) Odd-skipped-related 1 (*OSR1*), (B) the forkhead box F1 (*FOXF1*), (C) the forkhead box F2 (*FOXF2*), (D) The *FOXF1* Adjacent Noncoding Developmental Regulatory RNA *(FENDRR)*, (E) Heart And Neural Crest Derivatives Expressed 1 *(HAND1)*, (F) Heart And Neural Crest Derivatives Expressed 2 **(*HAND2*)**, (G) C-X-C motif chemokine 12 *(CXCL12)*, and the transcription factors (H) *GATA5*, and (I) *GATA6* at different time points of the differentiation including day 0 (D0), day 7 (D7) and day 25 (D25). The data are shown by the bulk RNA-sequencing (left panels) and by the single cell RNA sequencing (right panels) at day 7 (D7) between *WT* and *CEP83*⁻/⁻ cells. N = 3 clones per group for bulk RNA seq. N = 2 clones per group for scRNA-seq. Expression units are mean transcripts per million (TPM) ± SD. *P < 0.05, **P < 0.01, ***P < 0.001 and ****P < 0.0001. ns= not significant. The figure is adapted from Mansour *et al.*,2022[67].
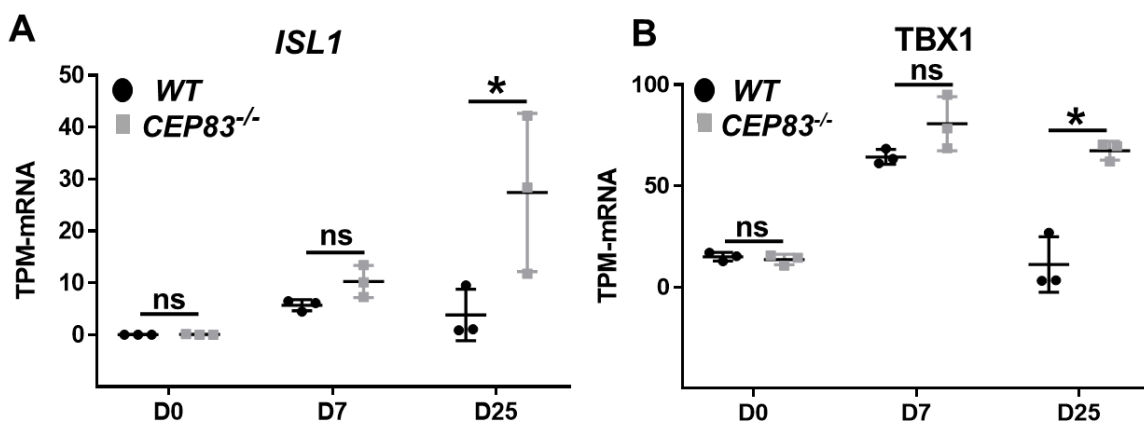
Figure 13: *CEP83*⁻/⁻ cells upregulate expression of cardiomyocyte progenitors at day 25. (A-B) Expression of cardiomyocyte markers (A) *ISL1*, and (B) *TBX1* at day 0 (D0), day 7 (D7), and day 25 (D25) according to bulk RNA-sequencing in *WT* and *CEP83*⁻/⁻ cells. N = 3 clones per group for bulk RNA seq. N = 2 clones per group for scRNA-seq. Expression units are mean transcripts per million (TPM) ± SD. *P < 0.05. ns= not significant. The figure is adapted from Mansour *et al.,*2022[67].

4. Discussion

4.1. Summary of results

Our study showed that *CEP83* plays an essential role in hiPSC differentiation towards intermediate mesoderm (IM) and kidney organoids. CEP83^{-/-} differentiated IM cells downregulated specific nephron progenitor genes including PAX8, EYA1, and HOXB7. Instead, *CEP83^{-/-}* cells upregulated early LPM genes including OSR1, FOXF1, FOXF2, FENDRR, HAND1, HAND2, CXCL12, GATA5, and GATA6. Similarly, *CEP83^{-/-}* organoids failed to develop nephron structures, downregulated expression of different renal epithelial cells marker genes, and massively upregulated LPM marker genes. Our findings indicate a novel role for CEP83 in the differentiation of IM cells and kidney progenitors, and demonstrate that a loss of CEP83 results in the mis-differentiation of hiPSCs to LPM instead of IM, and thus leads to improper kidney development.

4.2. Interpretation of results

Our study provides new insights into the cellular and molecular functions of CEP83 in kidney disease development. Different mutations in CEP83 in human patients have been associated with infantile nephronophthisis with end-stage renal disease (ESRD) at an average age of one to three years[38,126,127]. All of those mutations have been shown to preserve the function of the CEP83 protein either completely or partially. The only patient with a homozygous mutation of CEP83 and a complete loss of CEP83 protein exhibited severe phenotypes including triple X syndrome, facial dysmorphism, heart anomalies, and ESRD at 1 year old[38]. Future studies investigating additional mutations in *CEP83* in humans are required to determine whether a complete loss of function of both CEP83 alleles will result in defective mesodermal differentiation or renal agenesis.

Consistent with our findings, global knockout mice of *Cep83* display mid-embryonic lethality (at E12.5), and no homozygous mutants recovered at weaning. These mice displayed a range of early embryonic phenotypes at E 9.5, but kidney development in these mice has not been characterized (https://www.mousepheno-type.org/data/genes/MGI:1924298). This phenotype reflects the defective differentiation

of the early mesodermal germ layers in *Cep83* knockout mice. However, additional studies are still required to characterize the differentiation pattern of the mesodermal cells in *Cep83* knockout mice.

CEP83 has been identified as one of the distal appendage proteins (DAPs) that plays an essential role in the primary ciliary assembly. Loss of *CEP83* in several cell types resulted in defective ciliogenesis[2,34,38,82,128]. Our study reported defective ciliogenesis in both *KO* IM cells (day 7) and *KO* organoids (day 25), that showed a decreased number of cilia with longer cilia formation (**Fig. 10**). The downregulated expression of nephron progenitor marker genes in *CEP83*^{-/-} cells in the nascent nephron clusters could explain the failed differentiation of *KO* cells to kidney organoids at day 25, as those genes (**Fig. 13**) have been reported to play essential roles in kidney development[90,129-131].

Previous studies showed that disruption in centriolar components or primary cilia assembly and function, resulted in severe disruption of kidney development, resulting in dysplastic developmental defects[132-135]. The loss of function mutation of the ciliary protein, KIF14, resulted in bilateral renal agenesis in human and zebrafish[19,20]. Interestingly, KI14 has been identified recently as a necessary protein for the assembly of the distal appendages proteins[136]. Furthermore, the ciliary protein *Kif3a* that is involved in the intraflagellar transport is essential for normal mesoderm formation in mice. A loss of *Kif3a* in kidney progenitors resulted in reduced nephron numbers[23,24]. Additionally, mutations in the ciliary genes Ift25 and Ift27, which encode intraflagellar transport proteins in mice, resulted in renal agenesis or renal hypoplasia[21,22]. Combined, these studies show the essential role of the primary cilium in the early differentiation of the kidney progenitors in the mesoderm and kidney development. This suggests that CEP83 as an essential protein for the initiation of ciliogenesis plays a role in early kidney progenitors' differentiation and kidney development.

In contrast, *CEP83*^{-/-} cells upregulated the expression of other early LPM genes, including at day 7, and the expression of most genes was extremely upregulated at day 25, indicating proliferative differentiation of *CEP83*^{-/-} cells toward LPM. A previous study in zebrafish showed an interaction between LPM and IM, whereby the overexpression of LPM transcription factors Scl/Tal1 and Lmo2 inhibits IM formation and results in ectopic

vessel induction[137]. Moreover, the LPM transcription factor, *hand2*, is critical in determining the size of the IM[106,138] in zebrafish. Loss of hand2 results in an expanded IM, while overexpression of *hand2* results in reduced or abolished IM.

Consistent with the previously defined developmental role of Hand2 in IM formation, our study showed that *CEP83*^{-/-} cells strongly upregulated the expression of HAND2 at day 7, suggesting that HAND2 expression in *CEP83*^{-/-} cells may have played a central role in reducing IM differentiation, and later in nephron progenitor cell differentiation at the organoid stage. Additionally, *CEP83*^{-/-} cells at day 25 upregulated the expression of the LPM genes that are expressed in the mesothelium including *OSR1*, *CXCL12*, and *HAND1/2* , and cardiomyocyte progenitors including *ISL1* and *TBX1*[108,138].

4.3. Conclusions

In conclusion, our study shows a novel role for the CEP83 protein in controlling the differentiation of IM nephron progenitors, via direct inhibition of the nephron progenitor differentiation in the IM, and indirect expansion of the LPM at the same stage. Future studies are necessary to define the molecular and cellular mechanisms induced by CEP83 function in specifying the IM and LPM differentiation.

Due to lacking kidney phenotype characterization in the mouse model that expresses a complete loss of CEP83 protein, we would recommend additional investigations on the differentiation of the kidney progenitors in the early intermediate mesodermal cells in those mice would provide more information on the functional role of CEP83 protein in kidney development. We also recommend additional studies that investigate the functional role of all the distal appendage proteins (DAPs) in early embryonic development and kidney development, which will help in understanding the molecular defects of the genetic diseases associated with mutations in the genes encode to these proteins. Due to the essential role of the DAPs in primary cilium formation, understanding the functional role of the DAPs proteins in development will help to understand the developmental defects associated with ciliopathic diseases.

5. Reference list

1   Sreekumar, V. & Norris, D. P. Cilia and development. *Current Opinion in Genetics & Development* **56**, 15-21, doi:https://doi.org/10.1016/j.gde.2019.05.002 (2019).

2   Anvarian, Z., Mykytyn, K., Mukhopadhyay, S., Pedersen, L. B. & Christensen, S. T. Cellular signalling by primary cilia in development, organ function and disease. *Nature Reviews Nephrology* **15**, 199-219, doi:10.1038/s41581-019-0116-9 (2019).

3   Davenport, J. R. & Yoder, B. K. An incredible decade for the primary cilium: a look at a once-forgotten organelle. *Am J Physiol Renal Physiol* **289**, F1159-1169, doi:10.1152/ajprenal.00118.2005 (2005).

4   Nager, A. R., Goldstein, J. S., Herranz-Pérez, V., Portran, D., Ye, F., Garcia-Verdugo, J. M. & Nachury, M. V. An actin network dispatches ciliary GPCRs into extracellular vesicles to modulate signaling. *Cell* **168**, 252-263. e214 (2017).

5   Labour, M.-N., Riffault, M., Christensen, S. T. & Hoey, D. A. TGFβ1–induced recruitment of human bone mesenchymal stem cells is mediated by the primary cilium in a SMAD3-dependent manner. *Scientific reports* **6**, 1-13 (2016).

6   Christensen, S. T., Morthorst, S. K., Mogensen, J. B. & Pedersen, L. B. Primary cilia and coordination of receptor tyrosine kinase (RTK) and transforming growth factor β (TGF-β) signaling. *Cold Spring Harbor perspectives in biology* **9**, a028167 (2017).

7   Wheway, G., Nazlamova, L. & Hancock, J. T. Signaling through the primary cilium. *Frontiers in cell and developmental biology* **6**, 8 (2018).

8   Haycraft, C. J., Banizs, B., Aydin-Son, Y., Zhang, Q., Michaud, E. J. & Yoder, B. K. Gli2 and Gli3 localize to cilia and require the intraflagellar transport protein polaris for processing and function. *PLoS Genet* **1**, e53, doi:10.1371/journal.pgen.0010053 (2005).

9   Pala, R., Alomari, N. & Nauli, S. M. Primary Cilium-Dependent Signaling Mechanisms. *Int J Mol Sci* **18**, doi:10.3390/ijms18112272 (2017).

10   Christensen, S. T., Clement, C. A., Satir, P. & Pedersen, L. B. Primary cilia and coordination of receptor tyrosine kinase (RTK) signalling. *J Pathol* **226**, 172-184, doi:10.1002/path.3004 (2012).

11   Schneider, L., Clement, C. A., Teilmann, S. C., Pazour, G. J., Hoffmann, E. K., Satir, P. & Christensen, S. T. PDGFRalphaalpha signaling is regulated through the

primary cilium in fibroblasts. *Curr Biol* **15**, 1861-1866, doi:10.1016/j.cub.2005.09.012 (2005).

12   Guruharsha, K. G., Kankel, M. W. & Artavanis-Tsakonas, S. The Notch signalling system: recent insights into the complexity of a conserved pathway. *Nat Rev Genet* **13**, 654-666, doi:10.1038/nrg3272 (2012).

13   Bellavia, S., Dahan, K., Terryn, S., Cosyns, J. P., Devuyst, O. & Pirson, Y. A homozygous mutation in INVS causing juvenile nephronophthisis with abnormal reactivity of the Wnt/beta-catenin pathway. *Nephrol Dial Transplant* **25**, 4097-4102, doi:10.1093/ndt/gfq519 (2010).

14   Snoek, R., van Setten, J., Keating, B. J., Israni, A. K., Jacobson, P. A., Oetting, W. S., Matas, A. J., Mannon, R. B., Zhang, Z., Zhang, W., Hao, K., Murphy, B., Reindl-Schwaighofer, R., Heinzl, A., Oberbauer, R., Viklicky, O., Conlon, P. J., Stapleton, C. P., Bakker, S. J. L., Snieder, H., Peters, E. D. J., van der Zwaag, B., Knoers, N., de Borst, M. H. & van Eerde, A. M. NPHP1 (Nephrocystin-1) Gene Deletions Cause Adult-Onset ESRD. *J Am Soc Nephrol* **29**, 1772-1779, doi:10.1681/asn.2017111200 (2018).

15   Srivastava, S., Molinari, E., Raman, S. & Sayer, J. A. Many genes—one disease? Genetics of Nephronophthisis (NPHP) and NPHP-associated disorders. *Frontiers in pediatrics* **5**, 287 (2018).

16   Tory, K., Rousset-Rouvière, C., Gubler, M.-C., Morinière, V., Pawtowski, A., Becker, C., Guyot, C., Gié, S., Frishberg, Y., Nivet, H., Deschênes, G., Cochat, P., Gagnadoux, M.-F., Saunier, S., Antignac, C. & Salomon, R. Mutations of NPHP2 and NPHP3 in infantile nephronophthisis. *Kidney International* **75**, 839-847, doi:https://doi.org/10.1038/ki.2008.662 (2009).

17   Helou, J., Otto, E. A., Attanasio, M., Allen, S. J., Parisi, M. A., Glass, I., Utsch, B., Hashmi, S., Fazzi, E. & Omran, H. Mutation analysis of NPHP6/CEP290 in patients with Joubert syndrome and Senior–Løken syndrome. *Journal of medical genetics* **44**, 657-663 (2007).

18   Li, J., Lu, D., Liu, H., Williams, B. O., Overbeek, P. A., Lee, B., Zheng, L. & Yang, T. Sclt1 deficiency causes cystic kidney by activating ERK and STAT3 signaling. *Human Molecular Genetics* **26**, 2949-2960, doi:10.1093/hmg/ddx183 (2017).

19   Filges, I., Nosova, E., Bruder, E., Tercanli, S., Townsend, K., Gibson, W., Röthlisberger, B., Heinimann, K., Hall, J. & Gregory-Evans, C. Exome sequencing

identifies mutations in KIF14 as a novel cause of an autosomal recessive lethal fetal ciliopathy phenotype. *Clinical genetics* **86**, 220-228 (2014).

20   Reilly, M. L., Stokman, M. F., Magry, V., Jeanpierre, C., Alves, M., Paydar, M., Hellinga, J., Delous, M., Pouly, D. & Failler, M. Loss-of-function mutations in KIF14 cause severe microcephaly and kidney development defects in humans and zebrafish. *Human molecular genetics* **28**, 778-795 (2019).

21   Desai, P. B., San Agustin, J. T., Stuck, M. W., Jonassen, J. A., Bates, C. M. & Pazour, G. J. Ift25 is not a cystic kidney disease gene but is required for early steps of kidney development. *Mechanisms of development* **151**, 10-17, doi:10.1016/j.mod.2018.04.001 (2018).

22   Quélin, C., Loget, P., Boutaud, L., Elkhartoufi, N., Milon, J., Odent, S., Fradin, M., Demurger, F., Pasquier, L., Thomas, S. & Attié-Bitach, T. Loss of function IFT27 variants associated with an unclassified lethal fetal ciliopathy with renal agenesis. *American journal of medical genetics. Part A* **176**, 1610-1613, doi:10.1002/ajmg.a.38685 (2018).

23   Takeda, S., Yonekawa, Y., Tanaka, Y., Okada, Y., Nonaka, S. & Hirokawa, N. Left-Right Asymmetry and Kinesin Superfamily Protein KIF3A: New Insights in Determination of Laterality and Mesoderm Induction by kif3A−/− Mice Analysis. *Journal of Cell Biology* **145**, 825-836, doi:10.1083/jcb.145.4.825 (1999).

24   Chi, L., Galtseva, A., Chen, L., Mo, R., Hui, C. C. & Rosenblum, N. D. Kif3a controls murine nephron number via GLI3 repressor, cell survival, and gene expression in a lineage-specific manner. *PloS one* **8**, e65448, doi:10.1371/journal.pone.0065448 (2013).

25   Nonaka, S., Tanaka, Y., Okada, Y., Takeda, S., Harada, A., Kanai, Y., Kido, M. & Hirokawa, N. Randomization of left–right asymmetry due to loss of nodal cilia generating leftward flow of extraembryonic fluid in mice lacking KIF3B motor protein. *Cell* **95**, 829-837 (1998).

26   Siller, S. S., Sharma, H., Li, S., Yang, J., Zhang, Y., Holtzman, M. J., Winuthayanon, W., Colognato, H., Holdener, B. C. & Li, F.-Q. Conditional knockout mice for the distal appendage protein CEP164 reveal its essential roles in airway multiciliated cell differentiation. *PLoS genetics* **13**, e1007128 (2017).

27   Kurtulmus, B., Yuan, C., Schuy, J., Neuner, A., Hata, S., Kalamakis, G., Martin-Villalba, A. & Pereira, G. LRRC45 contributes to early steps of axoneme extension. *Journal of cell science* **131** (2018).

28   Yang, T. T., Chong, W. M., Wang, W.-J., Mazo, G., Tanos, B., Chen, Z., Tran, T. M. N., Chen, Y.-D., Weng, R. R. & Huang, C.-E. Super-resolution architecture of mammalian centriole distal appendages reveals distinct blade and matrix functional components. *Nature communications* **9**, 1-11 (2018).

29   Joukov, V. & De Nicolo, A. The centrosome and the primary cilium: the Yin and Yang of a hybrid organelle. *Cells* **8**, 701 (2019).

30   Jana, S. C., Mendonça, S., Machado, P., Werner, S., Rocha, J., Pereira, A., Maiato, H. & Bettencourt-Dias, M. Differential regulation of transition zone and centriole proteins contributes to ciliary base diversity. *Nature cell biology* **20**, 928-941 (2018).

31   Gonçalves, J. & Pelletier, L. The ciliary transition zone: finding the pieces and assembling the gate. *Molecules and cells* **40**, 243 (2017).

32   Reiter, J. F. & Leroux, M. R. Genes and molecular pathways underpinning ciliopathies. *Nature reviews Molecular cell biology* **18**, 533-547 (2017).

33   Deane, J. A., Cole, D. G., Seeley, E. S., Diener, D. R. & Rosenbaum, J. L. Localization of intraflagellar transport protein IFT52 identifies basal body transitional fibers as the docking site for IFT particles. *Curr Biol* **11**, 1586-1590, doi:10.1016/s0960-9822(01)00484-5 (2001).

34   Tanos, B. E., Yang, H.-J., Soni, R., Wang, W.-J., Macaluso, F. P., Asara, J. M. & Tsou, M.-F. B. Centriole distal appendages promote membrane docking, leading to cilia initiation. *Genes & development* **27**, 163-168 (2013).

35   Bowler, M., Kong, D., Sun, S., Nanjundappa, R., Evans, L., Farmer, V., Holland, A., Mahjoub, M. R., Sui, H. & Loncarek, J. High-resolution characterization of centriole distal appendage morphology and dynamics by correlative STORM and electron microscopy. *Nature Communications* **10**, 993, doi:10.1038/s41467-018-08216-4 (2019).

36   Yang, T. T., Chong, W. M., Wang, W.-J., Mazo, G., Tanos, B., Chen, Z., Tran, T. M. N., Chen, Y.-D., Weng, R. R., Huang, C.-E., Jane, W.-N., Tsou, M.-F. B. & Liao, J.-C. Super-resolution architecture of mammalian centriole distal appendages

reveals distinct blade and matrix functional components. *Nature Communications* **9**, 2023, doi:10.1038/s41467-018-04469-1 (2018).

37 Mansour, F., Boivin, F. J., Shaheed, I. B., Schueler, M. & Schmidt-Ott, K. M. The Role of Centrosome Distal Appendage Proteins (DAPs) in Nephronophthisis and Ciliogenesis. *International journal of molecular sciences* **22**, doi:10.3390/ijms222212253 (2021).

38 Failler, M., Gee, H. Y., Krug, P., Joo, K., Halbritter, J., Belkacem, L., Filhol, E., Porath, J. D., Braun, D. A. & Schueler, M. Mutations of CEP83 cause infantile nephronophthisis and intellectual disability. *The American Journal of Human Genetics* **94**, 905-914 (2014).

39 Chaki, M., Airik, R., Ghosh, A. K., Giles, R. H., Chen, R., Slaats, G. G., Wang, H., Hurd, T. W., Zhou, W., Cluckey, A., Gee, H. Y., Ramaswami, G., Hong, C.-J., Hamilton, B. A., Cervenka, I., Ganji, R. S., Bryja, V., Arts, H. H., van Reeuwijk, J., Oud, M. M., Letteboer, S. J. F., Roepman, R., Husson, H., Ibraghimov-Beskrovnaya, O., Yasunaga, T., Walz, G., Eley, L., Sayer, J. A., Schermer, B., Liebau, M. C., Benzing, T., Le Corre, S., Drummond, I., Janssen, S., Allen, S. J., Natarajan, S., O'Toole, J. F., Attanasio, M., Saunier, S., Antignac, C., Koenekoop, R. K., Ren, H., Lopez, I., Nayir, A., Stoetzel, C., Dollfus, H., Massoudi, R., Gleeson, J. G., Andreoli, S. P., Doherty, D. G., Lindstrad, A., Golzio, C., Katsanis, N., Pape, L., Abboud, E. B., Al-Rajhi, A. A., Lewis, R. A., Omran, H., Lee, E. Y. H. P., Wang, S., Sekiguchi, J. M., Saunders, R., Johnson, C. A., Garner, E., Vanselow, K., Andersen, J. S., Shlomai, J., Nurnberg, G., Nurnberg, P., Levy, S., Smogorzewska, A., Otto, E. A. & Hildebrandt, F. Exome capture reveals ZNF423 and CEP164 mutations, linking renal ciliopathies to DNA damage response signaling. *Cell* **150**, 533-548, doi:10.1016/j.cell.2012.06.028 (2012).

40 Airik, R., Airik, M., Schueler, M., Bates, C. M. & Hildebrandt, F. Roscovitine blocks collecting duct cyst growth in Cep164-deficient kidneys. *Kidney international* **96**, 320-326 (2019).

41 Katagiri, S., Hayashi, T., Yoshitake, K., Murai, N., Matsui, Z., Kubo, H., Satoh, H., Matsufuji, S., Takamura, T. & Yokoo, T. Compound heterozygous splice site variants in the SCLT1 gene highlight an additional candidate locus for Senior-Løken syndrome. *Scientific reports* **8**, 1-10 (2018).

42   Slaats, G. G., Ghosh, A. K., Falke, L. L., Le Corre, S., Shaltiel, I. A., van de Hoek, G., Klasson, T. D., Stokman, M. F., Logister, I. & Verhaar, M. C. Nephronophthisis-associated CEP164 regulates cell cycle progression, apoptosis and epithelial-to-mesenchymal transition. *PLoS genetics* **10** (2014).

43   Airik, R., Airik, M., Schueler, M., Bates, C. M. & Hildebrandt, F. Roscovitine blocks collecting duct cyst growth in Cep164-deficient kidneys. *Kidney International* **96**, 320-326, doi:10.1016/j.kint.2019.04.014 (2019).

44   Hildebrandt, F., Attanasio, M. & Otto, E. Nephronophthisis: Disease Mechanisms of a Ciliopathy. *Journal of the American Society of Nephrology* **20**, 23-35, doi:10.1681/asn.2008050456 (2009).

45   Luo, F. & Tao, Y. H. Nephronophthisis: a review of genotype–phenotype correlation. *Nephrology* **23**, 904-911 (2018).

46   Stokman, M., Lilien, M. & Knoers, N. Nephronophthisis. *GeneReviews®[Internet]* (2016).

47   Oud, M. M., van Bon, B. W., Bongers, E. M. H. F., Hoischen, A., Marcelis, C. L., de Leeuw, N., Mol, S. J. J., Mortier, G., Knoers, N. V. A. M., Brunner, H. G., Roepman, R. & Arts, H. H. Early presentation of cystic kidneys in a family with a homozygous INVS mutation. *American Journal of Medical Genetics Part A* **164**, 1627-1634, doi:10.1002/ajmg.a.36501 (2014).

48   Salomon, R., Saunier, S. & Niaudet, P. Nephronophthisis. *Pediatric Nephrology* **24**, 2333-2344, doi:10.1007/s00467-008-0840-z (2009).

49   Chung, E. M., Conran, R. M., Schroeder, J. W., Rohena-Quinquilla, I. R. & Rooks, V. J. From the Radiologic Pathology Archives: Pediatric Polycystic Kidney Disease and Other Ciliopathies: Radiologic-Pathologic Correlation. *RadioGraphics* **34**, 155-178, doi:10.1148/rg.341135179 (2014).

50   Hildebrandt, F. & Zhou, W. Nephronophthisis-associated ciliopathies. *Journal of the American Society of Nephrology* **18**, 1855-1871 (2007).

51   Schaefer, E., Zaloszyc, A., Lauer, J., Durand, M., Stutzmann, F., Perdomo-Trujillo, Y., Redin, C., Bennouna Greene, V., Toutain, A., Perrin, L., Gérard, M., Caillard, S., Bei, X., Lewis, R. A., Christmann, D., Letsch, J., Kribs, M., Mutter, C., Muller, J., Stoetzel, C., Fischbach, M., Marion, V., Katsanis, N. & Dollfus, H. Mutations in SDCCAG8/NPHP10 Cause Bardet-Biedl Syndrome and Are Associated with

Penetrant Renal Disease and Absent Polydactyly. *Molecular syndromology* **1**, 273-281, doi:10.1159/000331268 (2011).

52   Hartill, V., Szymanska, K., Sharif, S. M., Wheway, G. & Johnson, C. A. Meckel-Gruber Syndrome: An Update on Diagnosis, Clinical Management, and Research Advances. *Frontiers in pediatrics* **5**, 244-244, doi:10.3389/fped.2017.00244 (2017).

53   Otto, E. A., Loeys, B., Khanna, H., Hellemans, J., Sudbrak, R., Fan, S., Muerb, U., O'Toole, J. F., Helou, J. & Attanasio, M. Nephrocystin-5, a ciliary IQ domain protein, is mutated in Senior-Loken syndrome and interacts with RPGR and calmodulin. *Nature genetics* **37**, 282-288 (2005).

54   Takahashi, K., Tanabe, K., Ohnuki, M., Narita, M., Ichisaka, T., Tomoda, K. & Yamanaka, S. Induction of pluripotent stem cells from adult human fibroblasts by defined factors. *cell* **131**, 861-872 (2007).

55   Morizane, R., Lam, A. Q., Freedman, B. S., Kishi, S., Valerius, M. T. & Bonventre, J. V. Nephron organoids derived from human pluripotent stem cells model kidney development and injury. *Nature Biotechnology* **33**, 1193-1200, doi:10.1038/nbt.3392 (2015).

56   Taguchi, A., Kaku, Y., Ohmori, T., Sharmin, S., Ogawa, M., Sasaki, H. & Nishinakamura, R. Redefining the in vivo origin of metanephric nephron progenitors enables generation of complex kidney structures from pluripotent stem cells. *Cell stem cell* **14**, 53-67 (2014).

57   Takasato, M., Er, P. X., Chiu, H. S., Maier, B., Baillie, G. J., Ferguson, C., Parton, R. G., Wolvetang, E. J., Roost, M. S., Chuva de Sousa Lopes, S. M. & Little, M. H. Kidney organoids from human iPS cells contain multiple lineages and model human nephrogenesis. *Nature* **526**, 564-568, doi:10.1038/nature15695 (2015).

58   Freedman, B. S., Brooks, C. R., Lam, A. Q., Fu, H., Morizane, R., Agrawal, V., Saad, A. F., Li, M. K., Hughes, M. R. & Vander Werff, R. Modelling kidney disease with CRISPR-mutant kidney organoids derived from human pluripotent epiblast spheroids. *Nature communications* **6**, 8715 (2015).

59   Kumar, S. V., Er, P. X., Lawlor, K. T., Motazedian, A., Scurr, M., Ghobrial, I., Combes, A. N., Zappia, L., Oshlack, A., Stanley, E. G. & Little, M. H. Kidney micro-organoids in suspension culture as a scalable source of human pluripotent stem

cell-derived kidney cells. *Development (Cambridge, England)* **146**, dev172361, doi:10.1242/dev.172361 (2019).

60   Tan, Z., Shan, J., Rak-Raszewska, A. & Vainio, S. J. Embryonic stem cells derived kidney organoids as faithful models to target programmed nephrogenesis. *Scientific reports* **8**, 1-10 (2018).

61   Boyle, S., Misfeldt, A., Chandler, K. J., Deal, K. K., Southard-Smith, E. M., Mortlock, D. P., Baldwin, H. S. & de Caestecker, M. Fate mapping using Cited1-CreERT2 mice demonstrates that the cap mesenchyme contains self-renewing progenitor cells and gives rise exclusively to nephronic epithelia. *Developmental biology* **313**, 234-245 (2008).

62   Kobayashi, A., Valerius, M. T., Mugford, J. W., Carroll, T. J., Self, M., Oliver, G. & McMahon, A. P. Six2 defines and regulates a multipotent self-renewing nephron progenitor population throughout mammalian kidney development. *Cell stem cell* **3**, 169-181 (2008).

63   Howden, S. E., Vanslambrouck, J. M., Wilson, S. B., Tan, K. S. & Little, M. H. Reporter-based fate mapping in human kidney organoids confirms nephron lineage relationships and reveals synchronous nephron formation. *EMBO reports* **20**, e47483 (2019).

64   Kuraoka, S., Tanigawa, S., Taguchi, A., Hotta, A., Nakazato, H., Osafune, K., Kobayashi, A. & Nishinakamura, R. PKD1-Dependent Renal Cystogenesis in Human Induced Pluripotent Stem Cell-Derived Ureteric Bud/Collecting Duct Organoids. *Journal of the American Society of Nephrology* **31**, 2355-2371 (2020).

65   Concordet, J.-P. & Haeussler, M. CRISPOR: intuitive guide selection for CRISPR/Cas9 genome editing experiments and screens. *Nucleic Acids Research* **46**, W242-W245, doi:10.1093/nar/gky354 (2018).

66   Yumlu, S., Stumm, J., Bashir, S., Dreyer, A.-K., Lisowski, P., Danner, E. & Kühn, R. Gene editing and clonal isolation of human induced pluripotent stem cells using CRISPR/Cas9. *Methods* **121-122**, 29-44, doi:https://doi.org/10.1016/j.ymeth.2017.05.009 (2017).

67   Mansour, F., Hinze, C., Telugu, N. S., Kresoja, J., Shaheed, I. B., Mosimann, C., Diecke, S. & Schmidt-Ott, K. M. The centrosomal protein 83 (CEP83) regulates human pluripotent stem cell differentiation towards the kidney lineage. *eLife* **11**, e80165, doi:10.7554/eLife.80165 (2022).

68   Hinze, C., Karaiskos, N., Boltengagen, A., Walentin, K., Redo, K., Himmerkus, N., Bleich, M., Potter, S. S., Potter, A. S. & Eckardt, K.-U. Kidney single-cell transcriptomes predict spatial corticomedullary gene expression and tissue osmolality gradients. *Journal of the American Society of Nephrology* **32**, 291-306 (2021).

69   Liao, Y., Smyth, G. K. & Shi, W. featureCounts: an efficient general purpose program for assigning sequence reads to genomic features. *Bioinformatics (Oxford, England)* **30**, 923-930, doi:10.1093/bioinformatics/btt656 (2014).

70   Robinson, J. T., Thorvaldsdóttir, H., Winckler, W., Guttman, M., Lander, E. S., Getz, G. & Mesirov, J. P. Integrative genomics viewer. *Nature biotechnology* **29**, 24-26 (2011).

71   Wagner, G. P., Kin, K. & Lynch, V. J. Measurement of mRNA abundance using RNA-seq data: RPKM measure is inconsistent among samples. *Theory in biosciences = Theorie in den Biowissenschaften* **131**, 281-285, doi:10.1007/s12064-012-0162-3 (2012).

72   Alles, J., Karaiskos, N., Praktiknjo, S. D., Grosswendt, S., Wahle, P., Ruffault, P.-L., Ayoub, S., Schreyer, L., Boltengagen, A. & Birchmeier, C. Cell fixation and preservation for droplet-based single-cell transcriptomics. *BMC biology* **15**, 1-14 (2017).

73   Stuart, T., Butler, A., Hoffman, P., Hafemeister, C., Papalexi, E., Mauck III, W. M., Hao, Y., Stoeckius, M., Smibert, P. & Satija, R. Comprehensive integration of single-cell data. *Cell* **177**, 1888-1902. e1821 (2019).

74   Vigolo, E., Markó, L., Hinze, C., Müller, D. N., Schmidt-Ullrich, R. & Schmidt-Ott, K. M. Canonical BMP signaling in tubular cells mediates recovery after acute kidney injury. *Kidney international* **95**, 108-122 (2019).

75   Davies, J. A. Morphogenesis of the metanephric kidney. *TheScientificWorldJournal* **2** (2002).

76   Faa, G., Gerosa, C., Fanni, D., Monga, G., Zaffanello, M., Van Eyken, P. & Fanos, V. Morphogenesis and molecular mechanisms involved in human kidney development. *Journal of cellular physiology* **227**, 1257-1268 (2012).

77   Little, M. H. & McMahon, A. P. Mammalian kidney development: principles, progress, and projections. *Cold Spring Harbor perspectives in biology* **4**, a008300 (2012).

78 Michos, O. Kidney development: from ureteric bud formation to branching morphogenesis. *Current opinion in genetics & development* **19**, 484-490 (2009).

79 Hariharan, K., Kurtz, A. & Schmidt-Ott, K. M. Assembling kidney tissues from cells: the long road from organoids to organs. *Frontiers in Cell and Developmental Biology* **3**, 70 (2015).

80 Schmidt-Ott, K. M. How to grow a kidney: patient-specific kidney organoids come of age. *Nephrology Dialysis Transplantation* **32**, 17-23, doi:10.1093/ndt/gfw256 (2016).

81 Qiao, J., Cohen, D. & Herzlinger, D. The metanephric blastema differentiates into collecting system and nephron epithelia in vitro. *Development (Cambridge, England)* **121**, 3207-3214 (1995).

82 Shao, W., Yang, J., He, M., Yu, X.-Y., Lee, C. H., Yang, Z., Joyner, A. L., Anderson, K. V., Zhang, J., Tsou, M.-F. B., Shi, H. & Shi, S.-H. Centrosome anchoring regulates progenitor properties and cortical formation. *Nature* **580**, 106-112, doi:10.1038/s41586-020-2139-6 (2020).

83 Bilous, R. W., Murty, G., Parkinson, D. B., Thakker, R. V., Coulthard, M. G., Burn, J., Mathias, D. & Kendall-Taylor, P. Autosomal dominant familial hypoparathyroidism, sensorineural deafness, and renal dysplasia. *New England Journal of Medicine* **327**, 1069-1074 (1992).

84 Grote, D., Souabni, A., Busslinger, M. & Bouchard, M. Pax2/8-regulated Gata3 expression is necessary for morphogenesis and guidance of the nephric duct in the developing kidney. *Development (Cambridge, England)* **133**, 53-61, doi:10.1242/dev.02184 (2006).

85 Kress, C., Vogels, R., De Graaff, W., Bonnerot, C., Meijlink, F., Nicolas, J.-F. & Deschamps, J. Hox-2.3 upstream sequences mediate lacZ expression in intermediate mesoderm derivatives of transgenic mice. *Development (Cambridge, England)* **109**, 775-786 (1990).

86 Srinivas, S., Wu, Z., Chen, C.-M., D'Agati, V. & Costantini, F. Dominant effects of RET receptor misexpression and ligand-independent RET signaling on ureteric bud development. *Development (Cambridge, England)* **126**, 1375-1386 (1999).

87 Wellik, D. M., Hawkes, P. J. & Capecchi, M. R. Hox11 paralogous genes are essential for metanephric kidney induction. *Genes & development* **16**, 1423-1432 (2002).

88   Mugford, J. W., Sipilä, P., Kobayashi, A., Behringer, R. R. & McMahon, A. P. Hoxd11 specifies a program of metanephric kidney development within the intermediate mesoderm of the mouse embryo. *Developmental biology* **319**, 396-405, doi:10.1016/j.ydbio.2008.03.044 (2008).

89   Ruf, R. G., Xu, P.-X., Silvius, D., Otto, E. A., Beekmann, F., Muerb, U. T., Kumar, S., Neuhaus, T. J., Kemper, M. J. & Raymond, R. M. SIX1 mutations cause branchio-oto-renal syndrome by disruption of EYA1–SIX1–DNA complexes. *Proceedings of the National Academy of Sciences* **101**, 8090-8095 (2004).

90   Sajithlal, G., Zou, D., Silvius, D. & Xu, P.-X. Eya1 acts as a critical regulator for specifying the metanephric mesenchyme. *Developmental Biology* **284**, 323-336, doi:https://doi.org/10.1016/j.ydbio.2005.05.029 (2005).

91   Subramanian, A., Sidhom, E.-H., Emani, M., Vernon, K., Sahakian, N., Zhou, Y., Kost-Alimova, M., Slyper, M., Waldman, J., Dionne, D., Nguyen, L. T., Weins, A., Marshall, J. L., Rosenblatt-Rosen, O., Regev, A. & Greka, A. Single cell census of human kidney organoids shows reproducibility and diminished off-target cells after transplantation. *Nature Communications* **10**, 5462, doi:10.1038/s41467-019-13382-0 (2019).

92   Low, J. H., Li, P., Chew, E. G. Y., Zhou, B., Suzuki, K., Zhang, T., Lian, M. M., Liu, M., Aizawa, E. & Esteban, C. R. Generation of human PSC-derived kidney organoids with patterned nephron segments and a de novo vascular network. *Cell Stem Cell* **25**, 373-387. e379 (2019).

93   Mugford, J. W., Sipilä, P., McMahon, J. A. & McMahon, A. P. Osr1 expression demarcates a multi-potent population of intermediate mesoderm that undergoes progressive restriction to an Osr1-dependent nephron progenitor compartment within the mammalian kidney. *Developmental biology* **324**, 88-98 (2008).

94   Mae, S.-I., Shono, A., Shiota, F., Yasuno, T., Kajiwara, M., Gotoda-Nishimura, N., Arai, S., Sato-Otubo, A., Toyoda, T., Takahashi, K., Nakayama, N., Cowan, C. A., Aoi, T., Ogawa, S., McMahon, A. P., Yamanaka, S. & Osafune, K. Monitoring and robust induction of nephrogenic intermediate mesoderm from human pluripotent stem cells. *Nature Communications* **4**, 1367, doi:10.1038/ncomms2378 (2013).

95   Mahlapuu, M., Ormestad, M., Enerbäck, S. & Carlsson, P. The forkhead transcription factor Foxf1 is required for differentiation of extra-embryonic and lateral plate mesoderm. *Development* **128**, 155-166 (2001).

96   Ormestad, M., Astorga, J. & Carlsson, P. Differences in the embryonic expression patterns of mouse Foxf1 and -2 match their distinct mutant phenotypes. *Dev Dyn* **229**, 328-333, doi:10.1002/dvdy.10426 (2004).

97   Wilm, B., James, R. G., Schultheiss, T. M. & Hogan, B. L. M. The forkhead genes, Foxc1 and Foxc2, regulate paraxial versus intermediate mesoderm cell fate. *Developmental Biology* **271**, 176-189, doi:https://doi.org/10.1016/j.ydbio.2004.03.034 (2004).

98   Wotton, K. R., Mazet, F. & Shimeld, S. M. Expression of FoxC, FoxF, FoxL1, and FoxQ1 genes in the dogfish Scyliorhinus canicula defines ancient and derived roles for Fox genes in vertebrate development. *Developmental dynamics: an official publication of the American Association of Anatomists* **237**, 1590-1603 (2008).

99   Grote, P., Wittler, L., Hendrix, D., Koch, F., Währisch, S., Beisaw, A., Macura, K., Bläss, G., Kellis, M., Werber, M. & Herrmann, B. G. The tissue-specific lncRNA Fendrr is an essential regulator of heart and body wall development in the mouse. *Developmental cell* **24**, 206-214, doi:10.1016/j.devcel.2012.12.012 (2013).

100   Schindler, Y. L., Garske, K. M., Wang, J., Firulli, B. A., Firulli, A. B., Poss, K. D. & Yelon, D. Hand2 elevates cardiomyocyte production during zebrafish heart development and regeneration. *Development (Cambridge, England)* **141**, 3112-3122, doi:10.1242/dev.106336 (2014).

101   Tsuchihashi, T., Maeda, J., Shin, C. H., Ivey, K. N., Black, B. L., Olson, E. N., Yamagishi, H. & Srivastava, D. Hand2 function in second heart field progenitors is essential for cardiogenesis. *Developmental biology* **351**, 62-69, doi:10.1016/j.ydbio.2010.12.023 (2011).

102   McFadden, D. G., Barbosa, A. C., Richardson, J. A., Schneider, M. D., Srivastava, D. & Olson, E. N. The Hand1 and Hand2 transcription factors regulate expansion of the embryonic cardiac ventricles in a gene dosage-dependent manner. (2005).

103   Firulli, A. B., McFadden, D. G., Lin, Q., Srivastava, D. & Olson, E. N. Heart and extra-embryonic mesodermal defects in mouse embryos lacking the bHLH transcription factor Hand1. *Nat Genet* **18**, 266-270, doi:10.1038/ng0398-266 (1998).

104   Risebro, C. A., Smart, N., Dupays, L., Breckenridge, R., Mohun, T. J. & Riley, P. R. Hand1 regulates cardiomyocyte proliferation versus differentiation in the

developing heart. *Development (Cambridge, England)* **133**, 4595-4606, doi:10.1242/dev.02625 (2006).

105   Angelo, S., Lohr, J., Lee, K. H., Ticho, B. S., Breitbart, R. E., Hill, S., Yost, H. J. & Srivastava, D. Conservation of sequence and expression of Xenopus and zebrafish dHAND during cardiac, branchial arch and lateral mesoderm development. *Mechanisms of development* **95**, 231-237 (2000).

106   Perens, E. A., Garavito-Aguilar, Z. V., Guio-Vega, G. P., Peña, K. T., Schindler, Y. L. & Yelon, D. Hand2 Inhibits Kidney Specification While Promoting Vein Formation Within the Posterior Mesoderm. *bioRxiv*, 075036, doi:10.1101/075036 (2016).

107   Prummel, K. D., Crowell, H. L., Nieuwenhuize, S., Brombacher, E. C., Daetwyler, S., Soneson, C., Kresoja-Rakic, J., Ronner, M., Kocere, A. & Ernst, A. Hand2 delineates mesothelium progenitors and is reactivated in mesothelioma. *bioRxiv*, 2020.2011. 2011.355693 (2021).

108   Prummel, K. D., Nieuwenhuize, S. & Mosimann, C. The lateral plate mesoderm. *Development (Cambridge, England)* **147**, dev175059 (2020).

109   Salcedo, R. & Oppenheim, J. J. Role of chemokines in angiogenesis: CXCL12/SDF-1 and CXCR4 interaction, a key regulator of endothelial cell responses. *Microcirculation* **10**, 359-370 (2003).

110   Liekens, S., Schols, D. & Hatse, S. CXCL12-CXCR4 axis in angiogenesis, metastasis and stem cell mobilization. *Current pharmaceutical design* **16**, 3903-3920 (2010).

111   Loh, K. M., Chen, A., Koh, P. W., Deng, T. Z., Sinha, R., Tsai, J. M., Barkal, A. A., Shen, K. Y., Jain, R., Morganti, R. M., Shyh-Chang, N., Fernhoff, N. B., George, B. M., Wernig, G., Salomon, R. E. A., Chen, Z., Vogel, H., Epstein, J. A., Kundaje, A., Talbot, W. S., Beachy, P. A., Ang, L. T. & Weissman, I. L. Mapping the Pairwise Choices Leading from Pluripotency to Human Bone, Heart, and Other Mesoderm Cell Types. *Cell* **166**, 451-467, doi:10.1016/j.cell.2016.06.011 (2016).

112   Koutsourakis, M., Langeveld, A., Patient, R., Beddington, R. & Grosveld, F. The transcription factor GATA6 is essential for early extraembryonic development. *Development (Cambridge, England)* **126**, 723-732 (1999).

113   Holtzinger, A. & Evans, T. Gata5 and Gata6 are functionally redundant in zebrafish for specification of cardiomyocytes. *Developmental biology* **312**, 613-622 (2007).

114   Reiter, J. F., Alexander, J., Rodaway, A., Yelon, D., Patient, R., Holder, N. & Stainier, D. Y. Gata5 is required for the development of the heart and endoderm in zebrafish. *Genes & development* **13**, 2983-2995 (1999).

115   Pikkarainen, S., Tokola, H., Kerkelä, R. & Ruskoaho, H. GATA transcription factors in the developing and adult heart. *Cardiovascular research* **63**, 196-207 (2004).

116   Laverriere, A. C., MacNeill, C., Mueller, C., Poelmann, R. E., Burch, J. & Evans, T. GATA-4/5/6, a subfamily of three transcription factors transcribed in developing heart and gut. *Journal of Biological Chemistry* **269**, 23177-23184 (1994).

117   Zhao, R., Watt, A. J., Battle, M. A., Li, J., Bondow, B. J. & Duncan, S. A. Loss of both GATA4 and GATA6 blocks cardiac myocyte differentiation and results in acardia in mice. *Developmental Biology* **317**, 614-619, doi:https://doi.org/10.1016/j.ydbio.2008.03.013 (2008).

118   Cai, C.-L., Liang, X., Shi, Y., Chu, P.-H., Pfaff, S. L., Chen, J. & Evans, S. Isl1 identifies a cardiac progenitor population that proliferates prior to differentiation and contributes a majority of cells to the heart. *Developmental cell* **5**, 877-889 (2003).

119   Kwon, C., Qian, L., Cheng, P., Nigam, V., Arnold, J. & Srivastava, D. A regulatory pathway involving Notch1/β-catenin/Isl1 determines cardiac progenitor cell fate. *Nature cell biology* **11**, 951-957 (2009).

120   Laugwitz, K.-L., Moretti, A., Lam, J., Gruber, P., Chen, Y., Woodard, S., Lin, L.-Z., Cai, C.-L., Lu, M. M. & Reth, M. Postnatal isl1+ cardioblasts enter fully differentiated cardiomyocyte lineages. *Nature* **433**, 647-653 (2005).

121   Moretti, A., Caron, L., Nakano, A., Lam, J. T., Bernshausen, A., Chen, Y., Qyang, Y., Bu, L., Sasaki, M. & Martin-Puig, S. Multipotent embryonic isl1+ progenitor cells lead to cardiac, smooth muscle, and endothelial cell diversification. *Cell* **127**, 1151-1165 (2006).

122   Gao, R., Liang, X., Cheedipudi, S., Cordero, J., Jiang, X., Zhang, Q., Caputo, L., Günther, S., Kuenne, C., Ren, Y., Bhattacharya, S., Yuan, X., Barreto, G., Chen, Y., Braun, T., Evans, S. M., Sun, Y. & Dobreva, G. Pioneering function of Isl1 in the epigenetic control of cardiomyocyte cell fate. *Cell Research* **29**, 486-501, doi:10.1038/s41422-019-0168-1 (2019).

123 Stennard, F. A. & Harvey, R. P. T-box transcription factors and their roles in regulatory hierarchies in the developing heart. *Development (Cambridge, England)* **132**, 4897-4910, doi:10.1242/dev.02099 (2005).

124 Baldini, A. Dissecting contiguous gene defects: TBX1. *Current opinion in genetics & development* **15**, 279-284, doi:10.1016/j.gde.2005.03.001 (2005).

125 Chen, L., Fulcoli, F. G., Tang, S. & Baldini, A. Tbx1 regulates proliferation and differentiation of multipotent heart progenitors. *Circ Res* **105**, 842-851, doi:10.1161/CIRCRESAHA.109.200295 (2009).

126 Veldman, B. C. F., Kuper, W. F. E., Lilien, M., Schuurs-Hoeijmakers, J. H. M., Marcelis, C., Phan, M., Hettinga, Y., Talsma, H. E., van Hasselt, P. M. & Haijes, H. A. Beyond nephronophthisis: Retinal dystrophy in the absence of kidney dysfunction in childhood expands the clinical spectrum of CEP83 deficiency. *American journal of medical genetics. Part A* **185**, 2204-2210, doi:10.1002/ajmg.a.62225 (2021).

127 Haer-Wigman, L., van Zelst-Stams, W. A. G., Pfundt, R., van den Born, L. I., Klaver, C. C. W., Verheij, J. B. G. M., Hoyng, C. B., Breuning, M. H., Boon, C. J. F., Kievit, A. J., Verhoeven, V. J. M., Pott, J. W. R., Sallevelt, S. C. E. H., van Hagen, J. M., Plomp, A. S., Kroes, H. Y., Lelieveld, S. H., Hehir-Kwa, J. Y., Castelein, S., Nelen, M., Scheffer, H., Lugtenberg, D., Cremers, F. P. M., Hoefsloot, L. & Yntema, H. G. Diagnostic exome sequencing in 266 Dutch patients with visual impairment. *European Journal of Human Genetics* **25**, 591-599, doi:10.1038/ejhg.2017.9 (2017).

128 Lo, C.-H., Lin, I., Yang, T. T., Huang, Y.-C., Tanos, B. E., Chou, P.-C., Chang, C.-W., Tsay, Y.-G., Liao, J.-C. & Wang, W.-J. Phosphorylation of CEP83 by TTBK2 is necessary for cilia initiation. *Journal of Cell Biology* **218**, 3489-3505 (2019).

129 Bouchard, M., Souabni, A., Mandler, M., Neubüser, A. & Busslinger, M. Nephric lineage specification by Pax2 and Pax8. *Genes & development* **16**, 2958-2970 (2002).

130 Xu, P.-X., Adams, J., Peters, H., Brown, M. C., Heaney, S. & Maas, R. Eya1-deficient mice lack ears and kidneys and show abnormal apoptosis of organ primordia. *Nature Genetics* **23**, 113-117, doi:10.1038/12722 (1999).

131   Patterson, L. T. & Potter, S. S. Atlas of Hox gene expression in the developing kidney. *Developmental Dynamics* **229**, 771-779, doi:https://doi.org/10.1002/dvdy.10474 (2004).

132   Gerdes, J. M., Davis, E. E. & Katsanis, N. The vertebrate primary cilium in development, homeostasis, and disease. *Cell* **137**, 32-45 (2009).

133   Hildebrandt, F., Benzing, T. & Katsanis, N. Ciliopathies. *New England Journal of Medicine* **364**, 1533-1543 (2011).

134   Oh, E. C. & Katsanis, N. Cilia in vertebrate development and disease. *Development (Cambridge, England)* **139**, 443-448 (2012).

135   Fry, A. M., Leaper, M. J. & Bayliss, R. The primary cilium: guardian of organ development and homeostasis. *Organogenesis* **10**, 62-68, doi:10.4161/org.28910 (2014).

136   Pejskova, P., Reilly, M. L., Bino, L., Bernatik, O., Dolanska, L., Ganji, R. S., Zdrahal, Z., Benmerah, A. & Cajanek, L. KIF14 controls ciliogenesis via regulation of Aurora A and is important for Hedgehog signaling. *J Cell Biol* **219**, doi:10.1083/jcb.201904107 (2020).

137   Gering, M., Yamada, Y., Rabbitts, T. H. & Patient, R. K. Lmo2 and Scl/Tal1 convert non-axial mesoderm into haemangioblasts which differentiate into endothelial cells in the absence of Gata1. *Development (Cambridge, England)* **130**, 6187-6199, doi:10.1242/dev.00875 (2003).

138   Prummel, K. D., Crowell, H. L., Nieuwenhuize, S., Brombacher, E. C., Daetwyler, S., Soneson, C., Kresoja-Rakic, J., Kocere, A., Ronner, M., Ernst, A., Labbaf, Z., Clouthier, D. E., Firulli, A. B., Sánchez-Iranzo, H., Naganathan, S. R., O'Rourke, R., Raz, E., Mercader, N., Burger, A., Felley-Bosco, E., Huisken, J., Robinson, M. D. & Mosimann, C. Hand2 delineates mesothelium progenitors and is reactivated in mesothelioma. *Nature Communications* **13**, 1677, doi:10.1038/s41467-022-29311-7 (2022).

6. Statutory Declaration

"I, Fatma Mansour, by personally signing this document in lieu of an oath, hereby affirm that I prepared the submitted dissertation on the topic [The role of Centrosomal protein 83 (CEP83) in kidney progenitor differentiation from human induced pluripotent stem cells (hiPSCs)], independently and without the support of third parties, and that I used no other sources and aids than those stated.

All parts, which are based on the publications or presentations of other authors, either in letter or in spirit, are specified as such in accordance with the citing guidelines. The sections on methodology (in particular regarding practical work, laboratory regulations, statistical processing) and results (in particular regarding figures, charts and tables) are exclusively my responsibility.

Furthermore, I declare that I have correctly marked all of the data, the analyses, and the conclusions generated from data obtained in collaboration with other persons and that I have correctly marked my own contribution and the contributions of other persons (cf. declaration of contribution). I have correctly marked all texts or parts of texts that were generated in collaboration with other persons.

My contributions to any publications to this dissertation correspond to those stated in the below joint declaration made together with the supervisor. The publication created within the scope of the dissertation complies with the guidelines of the ICMJE (International Committee of Medical Journal Editors; www.icmje.org) on authorship. In addition, I declare that I shall comply with the regulations of Charité – Universitätsmedizin Berlin on ensuring good scientific practice.

I declare that I have not yet submitted this dissertation in an identical or similar form to another Faculty.

The significance of this statutory declaration and the consequences of a false statutory declaration under criminal law (Sections 156, 161 of the German Criminal Code) are known to me."

Date   Signature   Fatma Mansour

7. Declaration of your own contribution to the publications

Fatma Mansour contributed the following to the below listed publication:

Fatma Mansour; Christian Hinze; Narasimha Swamy Telugu; Jelena Kresoja; Iman B. Shaheed; Christian Mosimann; Sebastian Diecke; Kai M. Schmidt-Ott. **The centrosomal protein 83 (CEP83) regulates human pluripotent stem cell differentiation towards the kidney lineage**. eLife 11:e80165, Oct 12, 2022. https://doi.org/10.7554/eLife.80165.

I, Fatma Mansour, by personally signing this document, hereby affirm that I contributed to all experiments. I differentiated the cells toward kidney organoids. I prepared the samples from the different time points for all the experiments. I did all the PCR, histology staining, immunostaining, and immunoblotting experiments. For the Bulk RNA sequencing experiments, I extracted the RNA and prepared for the sequencing by NOVOGENE. For the single cell RNA sequencing experiments, I prepared the single cell suspension, and I prepared the libraries to be sequenced by the Genomics Facility (Berlin Institute for Medical Systems Biology (BIMSB) at the Max Delbrück Center for Molecular Medicine (MDC), Berlin, Germany). I analysed the respective data obtained from my experiments, performed the statistical tests. All the figures 1-8 were created by me and were based on my statistical evaluations. Finally, I and wrote the first draft of the paper

Prof. Dr. med. Kai M. Schmidt-Ott

_____

Signature, date and stamp of first supervising university professor / lecturer

Fatma Mansour

_____

Signature of doctoral candidate

8. Excerpt from Journal Summary List

Journal Data Filtered By: **Selected JCR Year: 2020** Selected Editions: SCIE,SSCI
Selected Categories: **"BIOLOGY"** Selected Category Scheme: WoS
Gesamtanzahl: 93 Journale

Rank	Full Journal Title	Total Cites	Journal Impact Factor	Eigenfactor Score
1	BIOLOGICAL REVIEWS	17,047	12.820	0.019750
2	Physics of Life Reviews	1,942	11.025	0.003280
3	CURRENT BIOLOGY	78,289	10.834	0.116100
4	BIOSCIENCE	22,560	8.589	0.012470
5	eLife	68,113	8.140	0.287820
6	PLOS BIOLOGY	39,598	8.029	0.059920
7	BMC BIOLOGY	8,577	7.431	0.015750
8	Communications Biology	4,996	6.268	0.016030
9	PHILOSOPHICAL TRANSACTIONS OF THE ROYAL SOCIETY B-BIOLOGICAL SCIENCES	56,921	6.237	0.055730
10	Science China-Life Sciences	6,307	6.038	0.006960
11	BIOLOGICAL RESEARCH	2,563	5.612	0.002270
12	BIOELECTROCHEMISTRY	6,107	5.373	0.004870
13	PROCEEDINGS OF THE ROYAL SOCIETY B-BIOLOGICAL SCIENCES	64,652	5.349	0.061070
14	FASEB JOURNAL	54,279	5.191	0.044390
15	Current Opinion in Insect Science	3,455	5.186	0.008610
16	Biology-Basel	2,726	5.079	0.003990
17	QUARTERLY REVIEW OF BIOLOGY	4,781	4.875	0.000920
18	Life Science Alliance	1,208	4.591	0.004260
19	COMPUTERS IN BIOLOGY AND MEDICINE	9,751	4.589	0.011860
20	Biology Direct	2,265	4.540	0.002430
21	Geobiology	2,793	4.407	0.003600
22	BIOESSAYS	11,559	4.345	0.011680
23	ASTROBIOLOGY	4,963	4.335	0.005570
24	SAUDI JOURNAL OF BIOLOGICAL SCIENCES	6,487	4.219	0.007240
25	EXCLI Journal	2,642	4.068	0.002870
26	Interface Focus	2,863	3.906	0.004480
27	Life-Basel	1,851	3.817	0.003870
28	Biology Letters	12,880	3.703	0.016230
29	JOURNAL OF EXPERIMENTAL BIOLOGY	40,334	3.312	0.026860
30	JOURNAL OF BIOLOGICAL RHYTHMS	4,128	3.182	0.003270
31	YALE JOURNAL OF BIOLOGY AND MEDICINE	2,938	3.026	0.003300

9. Printing copy of the publication

The centrosomal protein 83 (CEP83) regulates human pluripotent stem cell differentiation toward the kidney lineage

Fatma Mansour[1,2,3], Christian Hinze[1,2,4,5], Narasimha Swamy Telugu[4,6], Jelena Kresoja[7], Iman B Shaheed[3], Christian Mosimann[7], Sebastian Diecke[4,6], Kai M Schmidt-Ott[1,2,5*]

[1]Department of Nephrology and Medical Intensive Care, Charité-Universitätsmedizin Berlin, Berlin, Germany; [2]Molecular and Translational Kidney Research, Max Delbrück Center for Molecular Medicine in the Helmholtz Association, Berlin, Germany; [3]Department of Pathology, Faculty of Veterinary Medicine, Cairo University, Cairo, Egypt; [4]Berlin Institute of Health, Berlin, Germany; [5]Department of Nephrology and Hypertension, Hannover Medical School, Hannover, Germany; [6]Technology Platform Pluripotent Stem Cells, Max Delbrück Center for Molecular Medicine in the Helmholtz Association, Berlin, Germany; [7]Department of Pediatrics, Section of Developmental Biology, University of Colorado School of Medicine, Anschutz Medical Campus, Aurora, United States

*For correspondence:
schmidt-ott.kai@mh-hannover.de

Abstract During embryonic development, the mesoderm undergoes patterning into diverse lineages including axial, paraxial, and lateral plate mesoderm (LPM). Within the LPM, the so-called intermediate mesoderm (IM) forms kidney and urogenital tract progenitor cells, while the remaining LPM forms cardiovascular, hematopoietic, mesothelial, and additional progenitor cells. The signals that regulate these early lineage decisions are incompletely understood. Here, we found that the centrosomal protein 83 (CEP83), a centriolar component necessary for primary cilia formation and mutated in pediatric kidney disease, influences the differentiation of human-induced pluripotent stem cells (hiPSCs) toward IM. We induced inactivating deletions of *CEP83* in hiPSCs and applied a 7-day in vitro protocol of IM kidney progenitor differentiation, based on timed application of WNT and FGF agonists. We characterized induced mesodermal cell populations using single-cell and bulk transcriptomics and tested their ability to form kidney structures in subsequent organoid culture. While hiPSCs with homozygous *CEP83* inactivation were normal regarding morphology and transcriptome, their induced differentiation into IM progenitor cells was perturbed. Mesodermal cells induced after 7 days of monolayer culture of *CEP83*-deficient hiPCS exhibited absent or elongated primary cilia, displayed decreased expression of critical IM genes (*PAX8, EYA1, HOXB7*), and an aberrant induction of LPM markers (e.g. *FOXF1, FOXF2, FENDRR, HAND1, HAND2*). Upon subsequent organoid culture, wildtype cells differentiated to form kidney tubules and glomerular-like structures, whereas *CEP83*-deficient cells failed to generate kidney cell types, instead upregulating cardiomyocyte, vascular, and more general LPM progenitor markers. Our data suggest that *CEP83* regulates the balance of IM and LPM formation from human pluripotent stem cells, identifying a potential link between centriolar or ciliary function and mesodermal lineage induction.

Editor's evaluation

This paper describes a novel role of the centrosomal protein CEP83 in mesoderm patterning. Specifically, CEP83 is shown to be required for the formation of the intermediate mesoderm and

kidney progenitor tissue derived from it. In a CEP83 knockout situation in human pluripotent stem cells, a shift to lateral plate mesoderm at the expense of intermediate mesoderm occurs, which is convincingly demonstrated. This work, therefore, presents important new insights into the processes involved in mesodermal lineage induction and the fine-tuning of kidney differentiation.

Introduction

During mammalian embryonic development, the mesoderm forms axial, paraxial, and lateral plate domains that harbor precursor cells for distinct organ systems. Forming as a major part of the lateral plate mesoderm (LPM), the intermediate mesoderm (IM) harbors progenitor cells of all kidney epithelial cells (*Davidson et al., 2019*), whereas the remaining LPM contributes progenitors of various cell types, including cells of the cardiovascular system (*Prummel et al., 2020*). The molecular and cellular mechanisms that drive induction of the IM and distinct LPM domains during embryonic development are not fully understood.

The centrosomal protein 83 (CEP83) is a component of distal appendages (DAPs) of centrioles. DAPs are involved in the anchoring of the mother centriole to the cell membrane, an early and critical step in ciliogenesis (*Lo et al., 2019*; *Tanos et al., 2013*; *Yang et al., 2018*; *Kurtulmus et al., 2018*; *Wheway et al., 2015*; *Bowler et al., 2019*; *Failler et al., 2014*; *Shao et al., 2020*; *Mansour et al., 2021*). CEP83 recruits other DAP components to the ciliary base, and loss of CEP83 disrupts ciliogenesis (*Tanos et al., 2013*). In radial glial progenitors, removal of CEP83 disrupts DAP assembly and impairs the anchoring of the centrosome to the apical membrane as well as primary ciliogenesis (*Yang et al., 2018*; *Shao et al., 2020*). Mutations of CEP83 in humans have been associated with infantile nephronophthisis (*Failler et al., 2014*), an early onset kidney disease that results in end-stage renal disease before the age of 3 years (*Hildebrandt, 2004*; *Luo and Tao, 2018*) and additional organ anomalies (*Failler et al., 2014*). To date, how the loss of CEP83 function contributes to aberrant kidney development remains unclear.

Human-induced pluripotent stem cells (hiPSCs) provide useful tools to study molecular mechanisms of cellular differentiation. Protocols for the induction of kidney organoids from iPSC have been successfully developed (*Takahashi et al., 2007*; *Morizane et al., 2015*; *Taguchi et al., 2014*; *Takasato et al., 2015*; *Freedman et al., 2015*; *Kumar et al., 2019*). The protocol by Takasato et al. uses stepwise exposure of iPSC to WNT and FGF agonists in a monolayer culture system for a 7-day period, which results in the induction of cells with a transcriptional phenotype resembling kidney progenitors in the IM (*Takasato et al., 2015*). Transfer of these cells to an organoid culture system followed by another series of WNT and FGF signals results in the differentiation of three-dimensional (3D) kidney organoids composed of different kidney cell types, including glomerular and tubular cells. Genome editing studies have previously been used to study the effects of genetic defects associated with kidney diseases on kidney differentiation in human iPSC systems (*Freedman et al., 2015*; *Tan et al., 2018*; *Boyle et al., 2008*; *Kobayashi et al., 2008*; *Howden et al., 2019*; *Kuraoka et al., 2020*). Here, we studied the effect of an induced knockout of *CEP83* in human iPSCs on kidney organoid differentiation. We uncovered a novel role of CEP83 in determining the balance of IM versus LPM differentiation, implicating a centrosomal protein in early mesodermal lineage decisions.

Results

CEP83 is essential for the differentiation of hiPSCs into kidney cells

To investigate the effect of *CEP83* loss on the differentiation of hiPSCs into IM kidney progenitors, we applied CRISPR-Cas9 technology to induce a null mutation in the *CEP83* gene in hiPSCs (*Figure 1A*). Three hiPSCs clones designated *CEP83*$^{-/-}$ (*KO1, KO2,* and *KO3*) carried deletions within *CEP83* exon 7, each of which led to an induction of a premature stop codon resulting in a predicted truncated protein (*Figure 1B–D* and *Figure 1—figure supplement 1A*). These clones exhibited a complete loss of CEP83 protein by immunoblotting (*Figure 1E*). Three wildtype clones were derived as controls (*WT1, WT2,* and *WT3*). All six clones were morphologically indistinguishable (by brightfield microscopy) and had similar overall gene expression profiles (by bulk RNA-seq and qRT-PCR), including pluripotency and lineage marker expression (*Figure 1—figure supplement 1B, C*, and *Figure 1—figure supplement 2A, B*). In KO clones, the anticipated altered transcripts of CEP83 were detectable
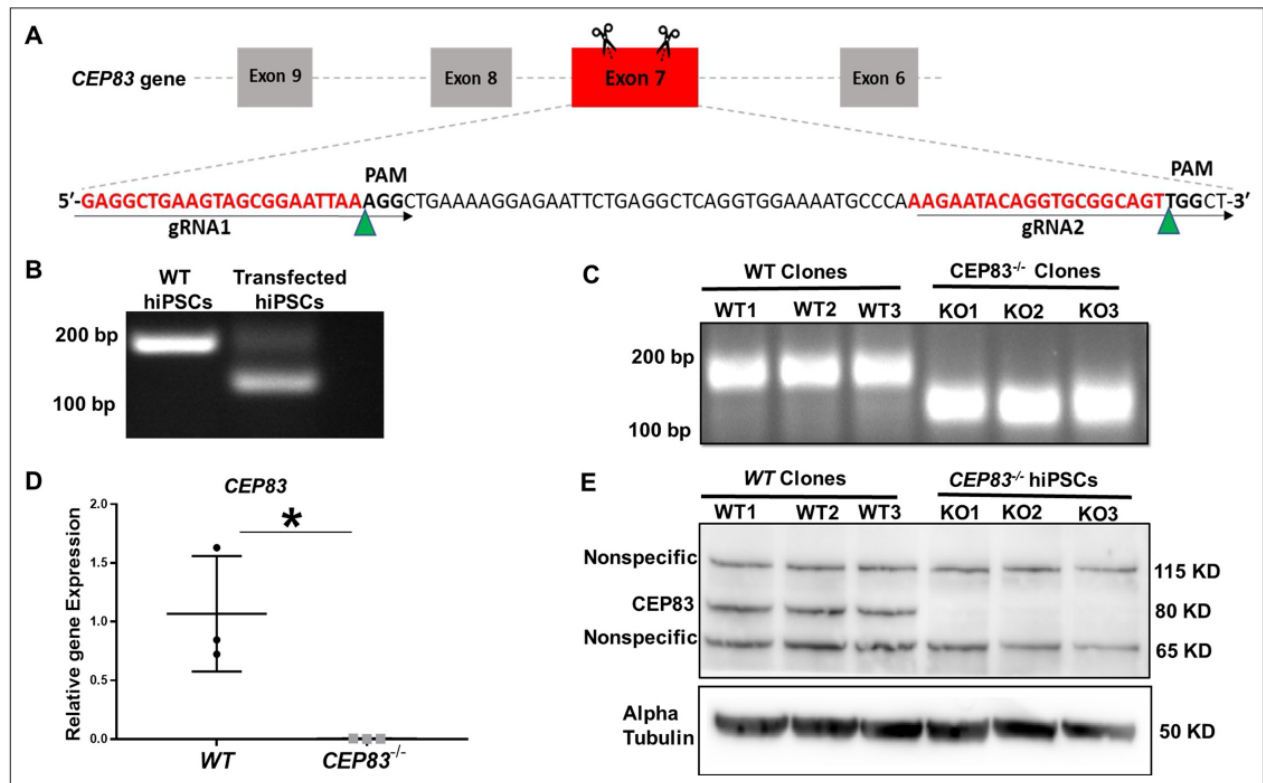
49

Figure 1. Generation of centrosomal protein 83 (CEP83)-deficient human pluripotent stem cells. (**A**) Schematic of the experimental approach to induce a deleting mutation in exon 7 of the *CEP83* gene (as described in the methods section). (**B**) DNA extracted from pooled transfected cells was subjected to PCR, targeting the predicted deletion site in the *CEP83* gene. In addition to the 182 bp fragment present in untransfected wildtype (WT) cells, an approximately 120 bp fragment was detected in transfected cells, corresponding to the induced deletion in exon 7. (**C**) Three clones (*CEP83$^{-/-}$* clones KO1, KO2, KO3) carried 62–74 bp deletions within *CEP83* exon 7, which led to an induction of premature stop codons or frameshift mutation on both alleles of *CEP83*. Three wildtype clones (*WT1, WT2,* and *WT3*) were used as controls. (**D**) Quantitative RT-PCR for a fragment corresponding to the deleted region in *CEP83* exon 7 produced a detectable signal in RNA extracts from WT clones but not *CEP83$^{-/-}$* clones. (**E**) Immunoblotting of *WT* and *CEP83$^{-/-}$* clones using a CEP83 antibody targeting the C-terminal region of the protein (see Methods for details) indicated a complete loss of the 83 KD band corresponding to CEP83 protein in the three *KO* clones compared with the three *WT* clones. Data are mean ± SD.*p<0.05 and **p<0.01 vs. WT. See *Figure 1—source data 1 and 2*. See also *Figure 1—figure supplements 1–2*.

The online version of this article includes the following source data and figure supplement(s) for figure 1:

Source data 1. The file contains detailed original PCR gels and immunoblots.

Source data 2. Excel sheet shows RT-qPCR data for mRNA expression of CEP83 in WT and knockout hiPSCs.

Source data 3. File contains uncropped PCR gels and immunoblots.

Figure supplement 1. *CEP83$^{-/-}$* human-induced pluripotent stem cells (hiPSCs) retain global iPCS cell gene expression signatures and express pluripotency markers.

Figure supplement 2. Phenotypical, molecular, and genetic characterization of *CEP83$^{-/-}$* human-induced pluripotent stem cells (hiPSCs) versus the wildtype hiPSCs.

based on bulk RNA-seq (data not shown). Single nucleotide polymorphism - analysis confirmed identical karyotypes of all six clones (*Figure 1—figure supplement 2C*).

Together, these findings confirmed the successful deletion of CEP83 in iPSCs without any overt direct cellular phenotypic consequences. We applied a 7-day monolayer protocol using timed application of WNT and FGF agonists as reported by *Takasato et al., 2015* to differentiate *WT* and *KO* hiPSCs into IM kidney progenitors (*Takahashi et al., 2007*; *Morizane et al., 2015*; *Taguchi et al., 2014*; *Figure 2A*).
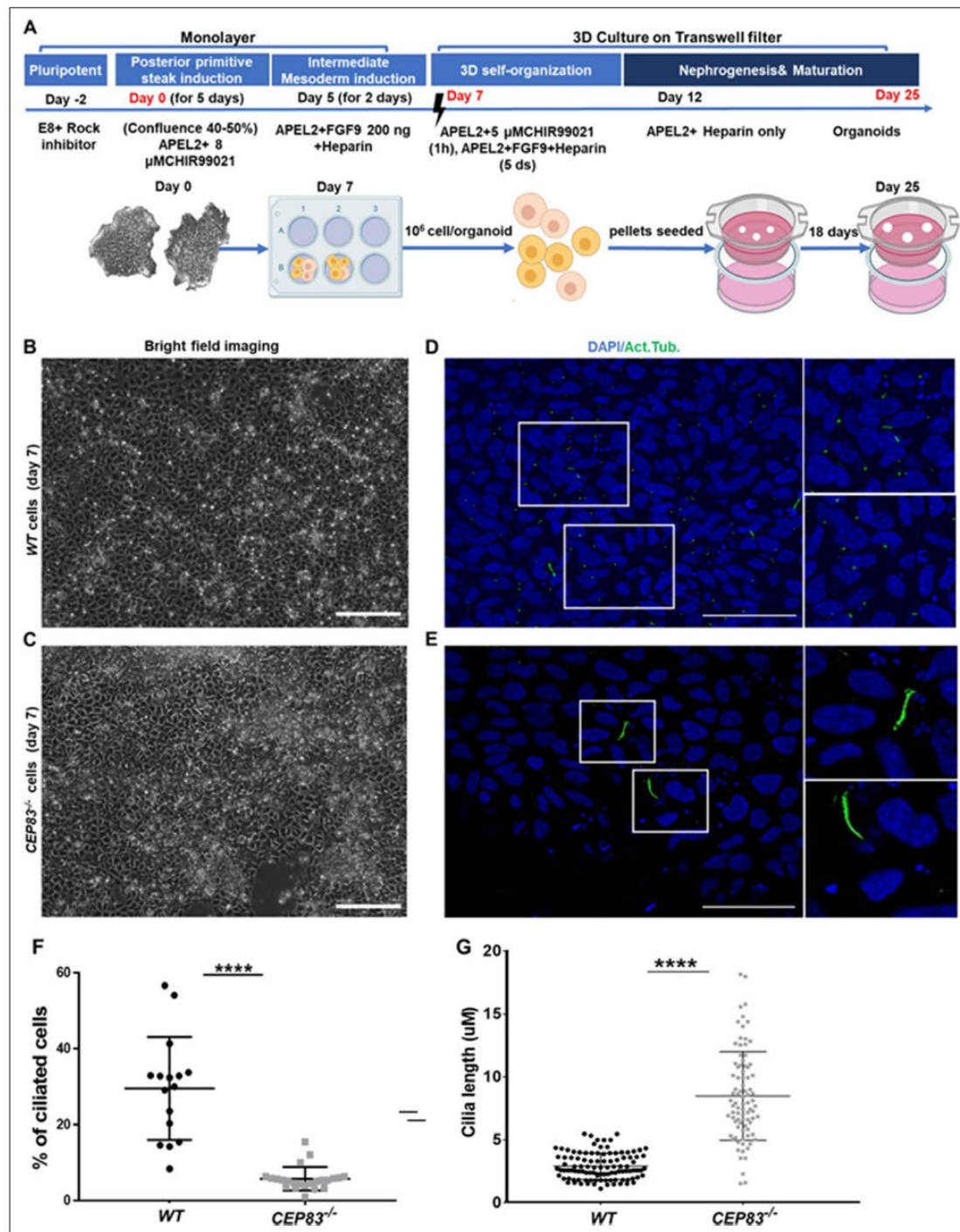
50

Figure 2. Differentiation of CEP83$^{-/-}$ human-induced pluripotent stem cells (hiPSCs) to intermediate mesoderm cells (day 7) is associated with defective ciliogenesis. (**A**) The schematic illustrates the applied differentiation protocol of hiPSCs, as previously described by *Takasato et al., 2015*. (**B–C**) *WT* and *CEP83$^{-/-}$* cells on 7 days of culture (D7) of differentiation did not show overt morphological differences by brighfield microscopy. (**D–E**) Representative images of *WT* and *CEP83$^{-/-}$* cells on D7, immunostained for acetylated tubulin (green) and nuclei (DAPI, blue), revealing fewer and elongated cilia in

Figure 2 continued on next page

51

Figure 2 continued

CEP83$^{-/-}$ cells. (**F**) Quantitative analysis of the percentage of ciliated cells in *WT* and CEP83$^{-/-}$ cells (D7). (**G**) Quantitative analysis of the ciliary length in *WT* and CEP83$^{-/-}$ cells (**D7**). n=3 clones per group. ****p<0.0001. Bar = 50 μm. See *Figure 2—figure supplement 1*.

The online version of this article includes the following figure supplement(s) for figure 2:

Figure supplement 1. Loss of *CEP83* in organoids results in defective ciliogenesis.

After 7 days of culture (D7), *WT* and *KO* cells exhibited an indistinguishable morphology by bright field microscopy (*Figure 2B and C*). Immunostaining for acetylated tubulin, however, indicated abnormal primary cilia formation in *CEP83*-deficient cells (*Figure 2D and E*). The number of ciliated cells was reduced from approximately 30% (in *WT* clones) to less than 10% (in *KO* clones) (*Figure 2F*). Among ciliated cells, the length of cilia was increased from 2 to 5 μm (in *WT* clones) to 5–13 μm (in *KO* clones) (*Figure 2G*). This indicated that CEP83$^{-/-}$ hiPSCs differentiated toward IM progenitors exhibited ciliary abnormalities. To analyze the induced IM kidney progenitor cells functionally, we collected D7 *WT* and CEP83$^{-/-}$ cells and placed them into an organoid culture system again applying timed WNT and FGF agonists to foster differentiation of mature kidney cell types, as previously reported (*Takasato et al., 2015*; *Figure 2A*). Organoids harvested from *WT* clones after a total of 25 days of culture (D25) had formed patterned kidney epithelial-like structures, including NPHS1-positive glomerulus-like structures, *Lotus tetragonolobus* lectin-positive proximal tubule-like, and E-cadherin (CDH1)-positive distal tubule-like structures (*Figure 3A, C and E*, and *Figure 3— figure supplement 1*). In contrast, CEP83$^{-/-}$ organoids at day 25 were composed of monomorphic cells with a mesenchyme-like appearance, which stained negative for an array of kidney cell markers (*Figure 3B, D and F*).

Kidney epithelial-like structures formed only in *WT* but not in CEP83$^{-/-}$ organoids (*Figure 3G*). Similar to the findings in day 7 cells reported above, primary cilia were found in fewer cells of CEP83$^{-/-}$ organoids (<5% of cells) and were abnormally elongated (*Figure 2—figure supplement 1*).

Next, bulk RNA sequencing of *WT* (WT1, WT2, WT3) and CEP83$^{-/-}$ (KO1, KO2, KO3) organoids was carried out to evaluate differential gene expression on a genome-wide level, and RT-PCR was used to validate selected genes. Hierarchical clustering of the samples indicated strong gene expression differences between *WT* and CEP83$^{-/-}$ samples (*Figure 3—figure supplement 2*). Several genes associated with kidney development and kidney epithelial differentiation were differentially expressed with high expression in *WT* organoids but showed comparatively low or absent expression in CEP83$^{-/-}$ organoids: these genes included kidney-specific lineage genes (*PAX2*, *PAX8*), and lineage/differentiation markers of glomerular cells (*NPHS1*, *PODXL*, *WT1*, *PTPRO*), proximal (*HNF1B*, *LRP2*, *CUBN*), and distal (*EMX2*, *MAL2*, *EPCAM*, GATA3) kidney epithelial cells (*Figure 3H–L*, *Figure 3—figure supplement 2*). This indicated that CEP83$^{-/-}$ IM progenitors failed to differentiate into kidney cells, suggesting that *CEP83* function is necessary to complete essential steps in the process of differentiation from pluripotent stem cells to kidney cells.

CEP83 deficiency associates with molecular defects of nephron progenitor cells

We next aimed to gain molecular insights into the lineage impact of *CEP83* deficiency during the course of kidney epithelial differentiation. Since no global transcriptomic differences were detectable between *WT* and CEP83$^{-/-}$ hiPSCs prior to differentiation (see above), we focused on mesodermal cell stages induced at D7, which displayed mild overall gene expression differences between *WT*- and *CEP83*-deficient cells as detected by bulk RNA sequencing (*Figure 4—figure supplement 1*).

A marked upregulation of nephron progenitor marker genes (*GATA3*, *HOXB7*, *HOXD11*, *EYA1*) (*Bilous et al., 1992*; *Grote et al., 2006*; *Kress et al., 1990*; *Srinivas et al., 1999*; *Wellik et al., 2002*; *Mugford et al., 2008a*; *Ruf et al., 2004*; *Sajithlal et al., 2005*) was observed in both *WT* and CEP83$^{-/-}$ cells at day 7 (*Figure 4—figure supplement 2*), suggesting that the differentiation path of pluripotent CEP83$^{-/-}$ cells to IM nephron progenitors was largely intact. To understand the potential molecular defects at the IM stage in more detail, we performed single-cell RNA (scRNA) sequencing on D7 *WT* and CEP83$^{-/-}$ cells (representing two different hiPSC clones for each condition differentiated in two separate experiments). We obtained transcriptomes from 27,328 cells, representing clones *WT1* (experiment 1: 3768 cells), *WT2* (experiment 2: 5793 cells), *KO1* (experiment 1: 8503 cells), and *KO2*
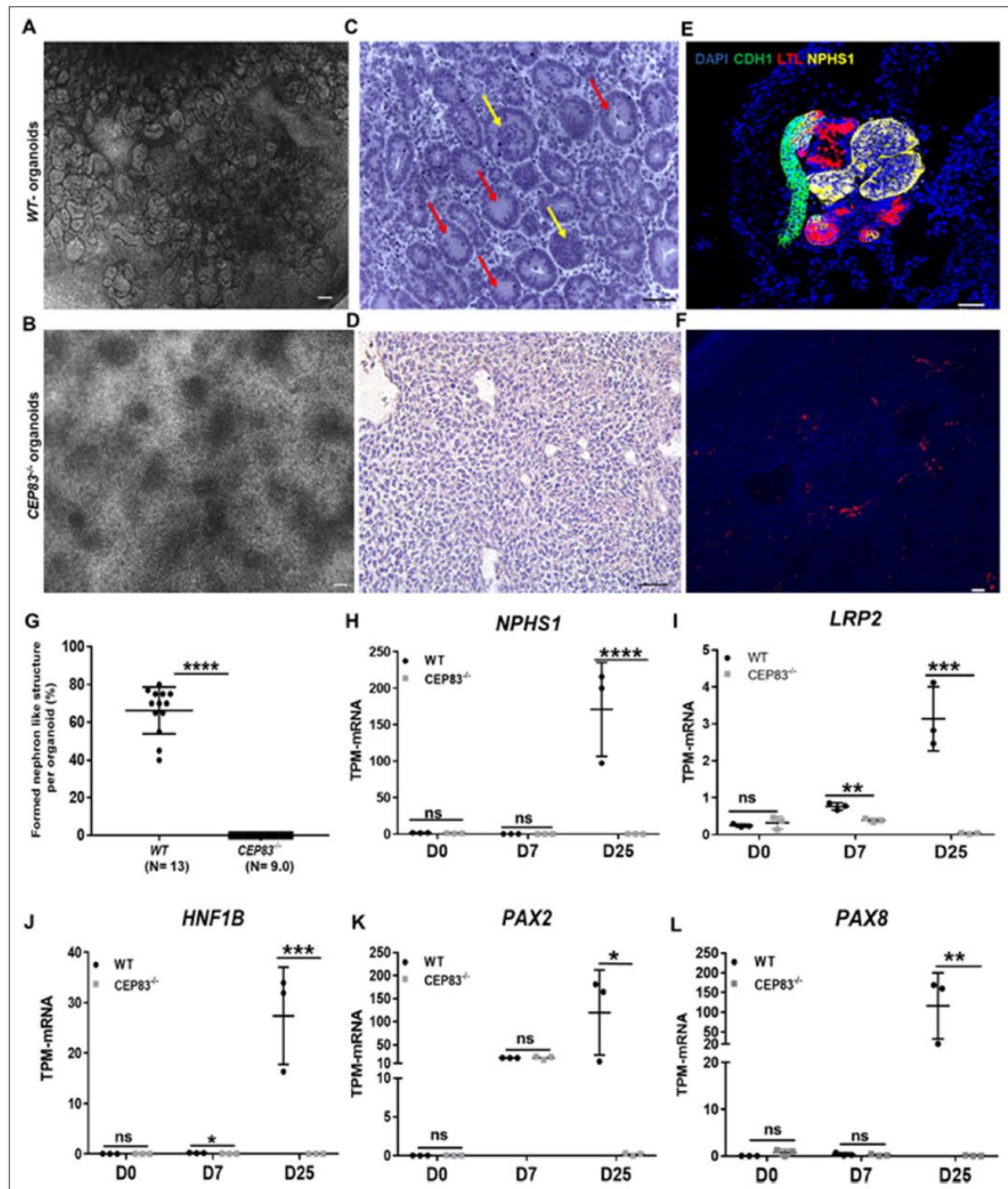
52

Figure 3. Defective kidney organoid differentiation from *CEP83*-deficient pluripotent stem cells. (**A, B**) Brightfield images of organoids after a total of 25 days of culture (**D25**) indicate the formation of multiple kidney-like structures in *WT* organoids (**A**), whereas *CEP83*⁻/⁻ organoids are composed of uniform clusters (**B**). (**C, D**) Representative images of hematoxylin-eosin–stained sections of organoids. *WT* organoids (**C**) display glomerulus-like (yellow arrows) and tubular (red arrow) components, whereas *CEP83*⁻/⁻ organoids (**D**) are composed of monomorphic mesenchymal-like cells.

Figure 3 continued on next page

53

Figure 3 continued

(**E–F**) Whole mounting immunostaining of organoids for NPHS1 (podocyte marker), LTL (proximal tubule marker), and CDH1 (distal tubule marker) indicates segmented nephron-like structures in *WT* organoids (**E**), and the absence of such structures in *CEP83⁻ᐟ⁻* organoids (**F**). (**G**) Quantitative analysis of brightfield images indicating the estimated percentage of organoid area composed of nephron-like structures, organoids were collected from three different experiments. (**H–L**) Gene expression (transcripts per million [TPM]) of *NPHP1* (**H**), *LRP2* (**I**), *HNF1B* (**J**), *PAX2* (**K**), and *PAX8* (**L**) in *WT* and *CEP83⁻ᐟ⁻* cells at the indicated time points based on bulk RNA sequencing. n=3 clones per group. Data are mean ± SD. *p<0.05, **p<0.01, ***p<0.001, and ****p<0.0001. ns = not significant. Panels A–F: Bar = 50 μm. See *Figure 3—source data 1 and 2*. See also *Figure 3—figure supplements 1–2*.

The online version of this article includes the following source data and figure supplement(s) for figure 3:

Source data 1. The data shows the quantitative analysis of the percent of nephron formation per organoid in knockout organoids versus WT organoids.

Source data 2. The sheet shows the plotted TPM values of mRNA sequencing analysis in *Figure 3L-H* for the expression of renal epithelial marker genes in KO and WT at days 0, 7, and 25 of the differentiation.

Figure supplement 1. Whole mount immunostaining of the wildtype organoids shows positive staining for NPHS1 (podocyte marker), LTL (proximal tubule marker), and CDH1 (distal tubule marker).

Figure supplement 2. mRNA analysis of organoids differentiated for 7+ (18) days indicates marked differences in global gene expression in *CEP83⁻ᐟ⁻* (*KO1–KO3*) compared to wildtype (*WT1–WT3*) organoids.

(experiment 2: 9264 cells). Principal component analysis (PCA) using pseudo-bulk expression data of the top 1000 highly variable genes (HVGs) indicated that the first principal component (dimension 1, explaining 54% of expression variation) was driven by the genotype (*WT* vs. *KO*), while the second principal component (dimension 2, explaining 51% of expression variation) was driven by a batch effect of the two experiments (*Figure 4A*). We combined all cells and generated a uniform manifold approximation and projection plot uncovering 10 different cell states/clusters (0–9; *Figure 4B*). We identified marker genes for each cluster (*Figure 4C*), indicating that clusters 1, 3, and 4 represented kidney progenitors/nascent nephrons (expressing, e.g., *PAX8*, *EYA1*, *HOXB7*) in different phases of the cell cycle. Other clusters represented as-of-yet uncharacterized cell types, which were consistent with previous single-cell transcriptome analyses from iPSC-derived cells induced by the same induction protocol (*Subramanian et al., 2019*; *Low et al., 2019*). Each of the four samples (*WT1, WT2, KO1, and KO2*) contributed to each cluster (*Figure 4D*). However, one cluster representing damaged cells (cluster 5) was observed at numerically higher percentages in *KO* cells compared to *WT* cells. Cluster 5 cells expressed high levels of mitochondrial RNAs, and staining for active caspase 3 demonstrated an increased percentage of apoptotic cells in KO samples compared to controls (*Figure 4—figure supplement 3*). We focused on kidney progenitors (clusters 1, 3, and 4) and found that a numerically lower percentage of *KO* cells (11.9 and 12.5% in KO clones) contributed to cluster 1 when compared with *WT* cells (25.9 and 36.3% in WT clones) (*Figure 5A*). In contrast, similar percentages of *WT* and *KO* cells were represented in kidney progenitor clusters 3 and 4 (*Figure 5B and C*). Differential gene expression analysis in these three clusters indicated significantly lower expression of kidney progenitor markers *PAX8*, *EYA1*, *CITED1*, and *HOXB7* in *KO* cells from clusters 1, 3, and 4 when compared to *WT* cells (*Figure 5D, E and F*; *Figure 5—figure supplements 1–2*). Interestingly, scRNA sequencing data also showed downregulated expression of genes encoding ciliary proteins, including OFD1, PCM1, and RAB11A (*Ferrante et al., 2006*; *Dammermann and Merdes, 2002*; *Knödler et al., 2010*; *Figure 5—figure supplement 3*), consistent with the ciliogenesis defects in CEP83 knockout cells. These results indicate that *CEP83* deficiency remained permissive with initial kidney progenitor induction, but that these cells exhibited mild molecular defects detectable by differential expression of kidney progenitor genes, which potentially contributed to the failure of *CEP83*-deficient cells to further differentiate toward mature kidney cell types.

CEP83 deficiency promotes ectopic induction of lateral plate mesoderm-like cells followed by an expansion of cardiac and vascular progenitors

We next inspected single-cell transcriptomes and bulk RNA sequencing data from D7 cells for genes that were upregulated in *CEP83⁻ᐟ⁻* cells compared to WT cells. From this analysis, we observed a consistent upregulation of genes that are normally expressed in early LPM, including *OSR1*, *FOXF1*,
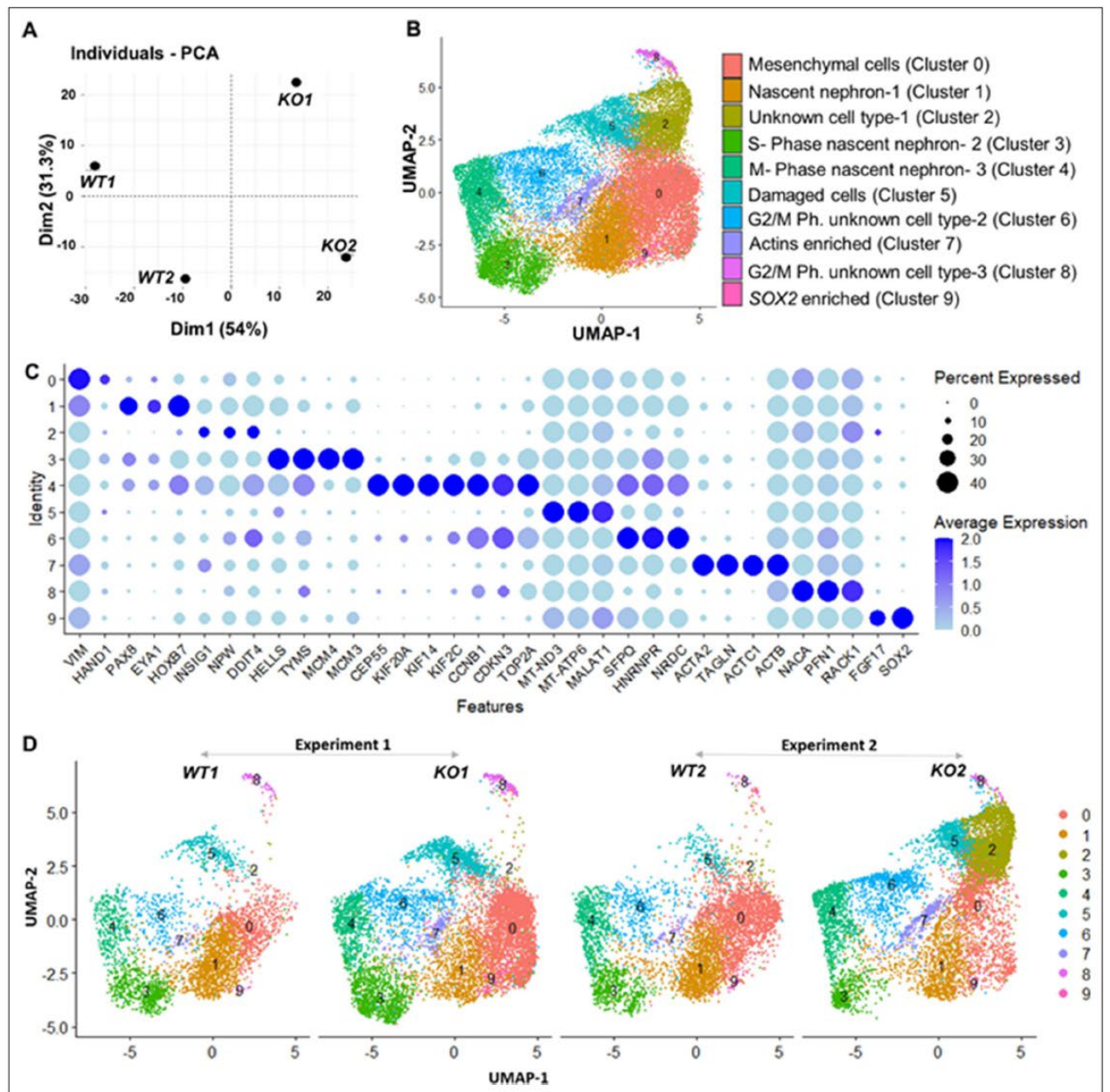
54

Figure 4. Gene expression differences of wildtype (WT) and CEP83⁻/⁻ D7 monolayers based on bulk and single-cell transcriptomics. (**A**) Principal component analysis (PCA) of *WT* (*WT1, WT2*) and *CEP83*⁻/⁻ (*KO1, KO2*) cells at day 7 using the average gene expression of the top highly variable 1000 genes in pseudo-bulk scRNA sequencing data. The % variation explained by each PCA axis is indicated in brackets. (**B**) PCA eigenvalues indicate that the principal components, Dim 1 (54%) and Dim 2 (31.3%), account for 85.3% of the expression differences. Dim 1 separates the WT samples from the KO samples, while Dim 2 separates experiment 1 (*WT1, KO1*) from experiment 2 (*WT2, KO2*). (**B**) Uniform manifold approximation and projection (UMAP) of scRNA-seq profiles from 27,328 cells from two wildtype clones (*WT1, WT2*) and two *CEP83*⁻/⁻ clones (*KO1, KO2*) derived from two separate experiments (experiment 1: *WT1, KO1*; experiment 2: *WT2, KO2*). Unbiased clustering resulted in 10 clusters, and (**C**) dot plots show expression of selected marker genes of each cluster. (**D**) UMAP plots for *WT* and *KO* samples show the distribution of all clusters per sample (N=2 per group) in B–D. See *Figure 4—figure supplements 1–3*. Source data is available as described in section (Data availability).

The online version of this article includes the following figure supplement(s) for figure 4:

Figure 4 continued on next page

55

Figure 4 continued

Figure supplement 1. Bulk RNA sequencing shows mild overall gene expression differences between *WT* and *CEP83*-deficient cells at day 7 of differentiation.

Figure supplement 2. Expression of intermediate mesoderm marker genes in *WT* and *CEP83⁻/⁻* human-induced pluripotent stem cells (hiPSCs) after 7 days of differentiation in a monolayer culture.

Figure supplement 3. *CEP83* loss induces apoptosis at day 7 of differentiation.

FOXF2, FENDRR, HAND1, HAND2, CXCL12, GATA5, and *GATA6* (*Prummel et al., 2020*; *Mugford et al., 2008b*; *Mae et al., 2013*; *Mahlapuu et al., 2001*; *Ormestad et al., 2004*; *Wilm et al., 2004*; *Wotton et al., 2008*; *Grote et al., 2013*; *Schindler et al., 2014*; *Tsuchihashi et al., 2011*; *McFadden et al., 2005*; *Firulli et al., 1998*; *Risebro et al., 2006*; *Angelo et al., 2000*; *Perens et al., 2016*; *Salcedo and Oppenheim, 2003*; *Liekens et al., 2010*; *Loh et al., 2016*; *Koutsourakis et al., 1999*; *Holtzinger and Evans, 2007*; *Reiter et al., 1999*; *Pikkarainen et al., 2004*; *Laverriere et al., 1994*; *Zhao et al., 2008*; *Prummel et al., 2021*; *Figure 6A–I*). This suggested that *CEP83⁻/⁻* cells entered an aberrant differentiation path assuming a phenotype indicative of broader LPM instead of more specific IM. To further substantiate this idea, we restricted the analysis to progenitor cells of clusters 1, 3, and 4 and to cells from cluster 0, which exhibited a mesenchymal transcriptome fingerprint (see *Figure 4C*). Within each cell, we analyzed the expression of LPM markers (*FOXF1, HAND1, HAND2,* and *CXCL12*) and of more restricted IM markers (*PAX8, EYA1, and HOXB7*) (*Figure 6—figure supplement 1*). This analysis indicated that *WT* cells of these clusters exhibited an IM-like phenotype, while *KO* cells were shifted toward an LPM-like phenotype. The common IM/LPM marker *OSR1* was expressed at higher level in *KO* cells comparing to the *WT* cells.

We then inspected RNA-seq data from *WT* and *KO* organoids at day 25 for the expression of LPM genes and markers of LPM derivatives. The expression of several LPM genes (*OSR1, FOXF1, FOXF2, FENDRR, HAND1, HAND2,* and *CXCL12*) was strongly upregulated in *KO* cells compared to *WT* cells suggesting that an LPM-like cell pool persisted in D25 *KO* organoids (*Figure 6A–I*). To further substantiate the potential differentiation of the *CEP83*-mutant cells into broadly LPM-like cells, we compared genes that were upregulated genes in D25 organoids (in total, 397 genes) with LPM genes that were previously identified by single-cell transcriptomics of sorted post-gastrulation LPM cells from developing zebrafish (*Prummel et al., 2021*; *Prummel et al., 2020*; *Prummel et al., 2022*). Our targeted comparison documented that *CEP83⁻/⁻* organoids showed significant enrichment for expression of orthologs of early LPM genes (p=0.006) (*Figure 6—figure supplement 2*), including *OSR1, CXCL12, HAND1/2, KCTD12, PIK3R3,* and *ZBTB2*. A subset of LPM genes enriched for expression in *CEP83*-mutant cells at D25 of differentiation was indicative of cardiac or cardiopharyngeal (*ISL1, TBX1*) as well as vascular progenitor (*SOX7, SOX11, NAP1L3, LMO2, GATA2*) differentiation (*Morikawa and Cserjesi, 2004*; *Cai et al., 2003*; *Kwon et al., 2009*; *Laugwitz et al., 2005*; *Moretti et al., 2006*; *Gao et al., 2019*; *Stennard and Harvey, 2005*; *Baldini, 2005*; *Chen et al., 2009*; *Figure 7A–G*, *Figure 6—figure supplement 2*). Interestingly, three genes of the upregulated LPM genes, namely OSR1, FOXF1, and FOXF2, are downstream genes of hedgehog signaling (*Han et al., 2017*; *Kugler et al., 2015*). In addition, HAND2 is upstream of hedgehog signaling (*Anderson et al., 2012*), essential for early embryonic development and regulated by primary cilium (*Kugler et al., 2015*). Furthermore, bulk RNA sequencing data showed significant upregulation of hedgehog signaling components GLI1 and PTCH1 in CEP83⁻/⁻ cells (*Lee et al., 1997*; *Villavicencio et al., 2000*; *Figure 6—figure supplement 3*).

Taken together, these observations document that hiPSCs deficient in *CEP83* respond to an in vitro differentiation program toward kidney progenitors, yet diverge toward a broader LPM progenitor composition without significant IM instead.

Discussion

This study indicates a novel contribution of CEP83 in regulating the differentiation path from human pluripotent stem cells to kidney progenitors. We pinpoint a stage at day 7 of IM induction where *CEP83* loss of function results in a decreased nephron progenitor pool with downregulation of critical kidney progenitor genes (*PAX8, EYA1, HOXB7*). At the same stage, genes typical of LPM specification (including *FOXF1, FOXF2, FENDRR, HAND1,* and *HAND2*) are upregulated (*Figure 8*). Functionally,
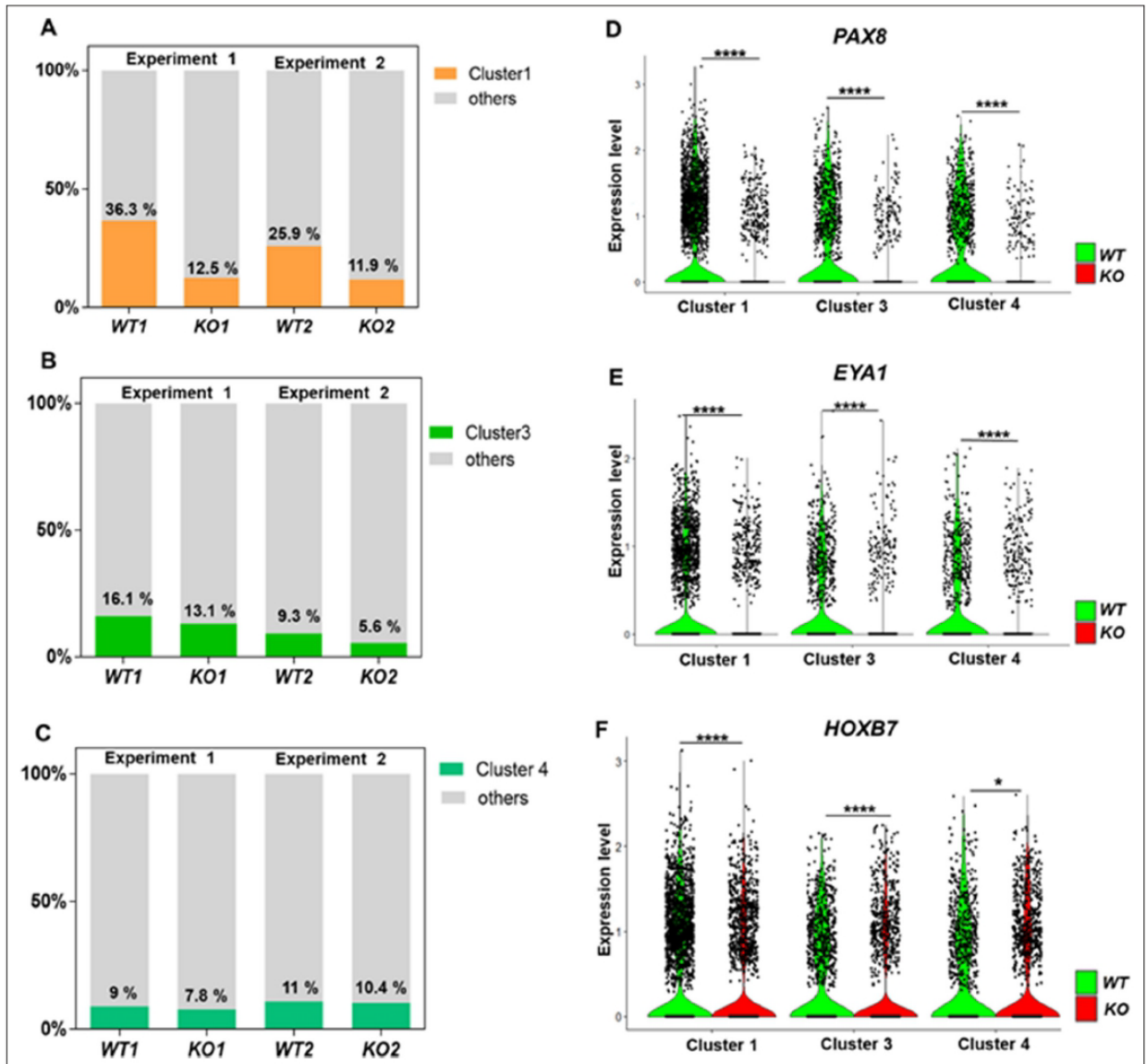
56

Figure 5. Defective kidney progenitor differentiation from *CEP83*$^{-/-}$ cells after 7 days of monolayer induction. (**A, B, C**) Proportions of cells from kidney progenitor clusters 1 (**A**), 3 (**B**), and 4 (**C**) among *wildtype* (*WT1, WT2*) and *CEP83*$^{-/-}$ (*KO1, KO2*) cells. (**D, E, F**) Violin plots of gene expression of kidney progenitor genes *PAX8* (**D**), *EYA1* (**E**), and *HOXB7* (**F**) within kidney progenitor clusters 1, 3, and 4 comparing wildtype (*WT*) and *CEP83*$^{-/-}$ (*KO*) cells. N=2 per group. *p<0.05 and ****p<0.0001. *Figure 5—figure supplements 1–2*. Source data is available as described in section (Data availability).

The online version of this article includes the following figure supplement(s) for figure 5:

Figure supplement 1. Expression of selected genes per cluster and per group (*WT* vs. CEP83$^{-/-}$).

Figure supplement 2. Violin plots of gene expression of kidney progenitor gene *CITED1* within kidney progenitor clusters 1, 3, and 4 comparing wildtype (*WT*) and *CEP83*$^{-/-}$ (*KO*) cells.

Figure supplement 3. Violin plots of single-cell RNA sequencing show downregulated expression of genes encoding ciliary proteins in CEP83$^{-/-}$ cells, including (**A**) the basal body protein oral-facial-digital type I *OFD1*, (**B**) pericentriolar material-1 (*PCM1*), and (**C**) RAS oncogene family 11 A (*RAB11A*).
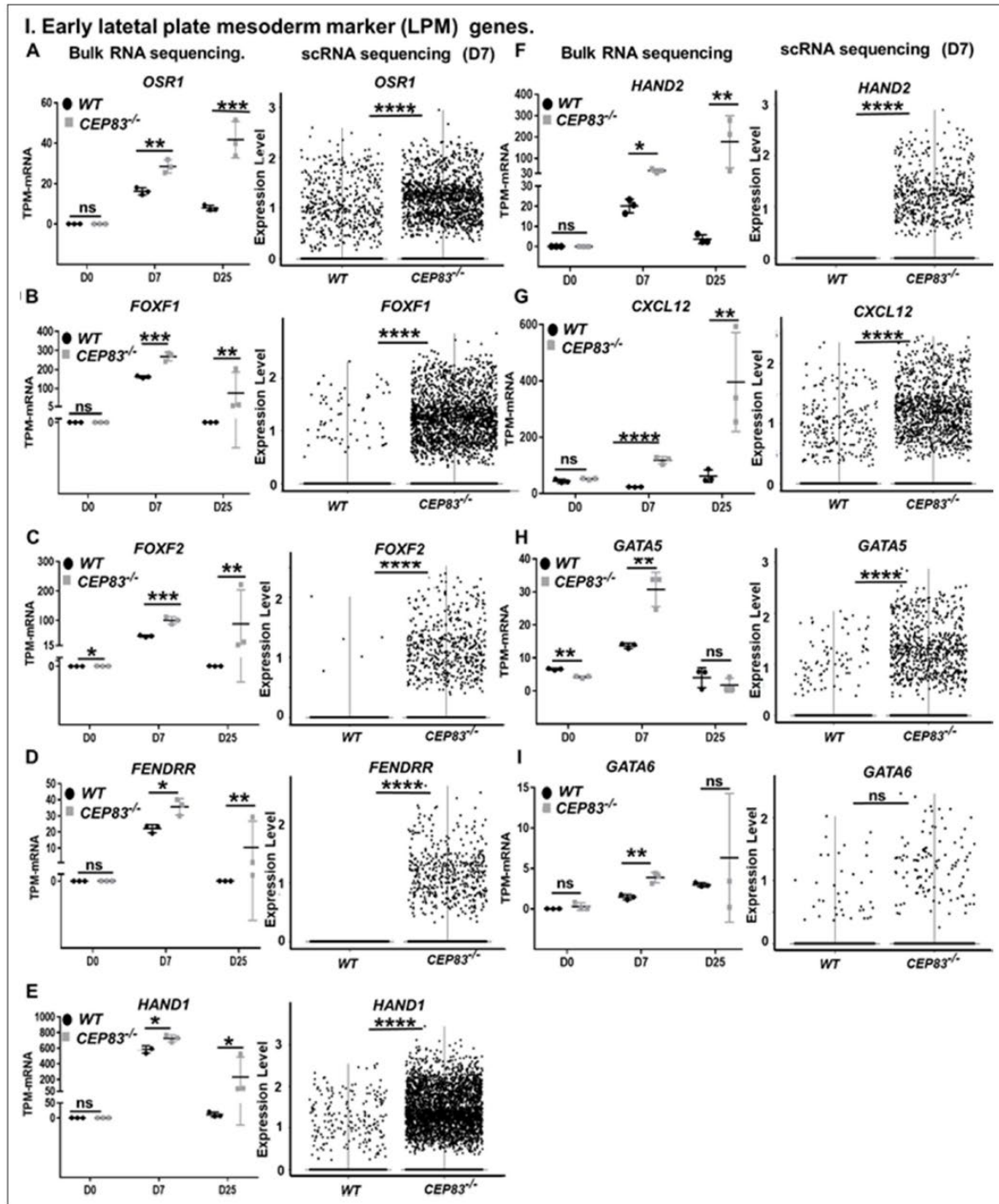
I. Early latetal plate mesoderm marker (LPM) genes.

Figure 6. CEP83^{−/−} cells upregulate expression of genes characteristic of early lateral plate mesoderm (LPM). (**A–I**) Expression of early LPM markers *OSR1* (**A**), *FOXF1* (**B**), *FOXF2* (**C**), *FENDRR* (**D**), *HAND1* (**E**), *HAND2* (**F**), *CXCL12* (**G**), *GATA5* (**H**), and *GATA6* (**I**) in wildtype (*WT*) and CEP83^{−/−} cells at day 0 (D0), day 7 (D7), and day 25 (D25) according to bulk RNA-sequencing (left panels) and at D7 according to single-cell RNA (scRNA) sequencing (right panels). N=3 clones per group for bulk RNA seq. N=2 clones per group for scRNA-seq. Expression units are mean transcripts per million (TPM) ± SD.

Figure 6 continued on next page

58

Figure 6 continued

*p<0.05, **p<0.01, ***p<0.001, and ****p<0.0001. ns = not significant. See *Figure 6—figure supplements 1–3*. See also *Figure 6—source data 1*. Check data availability section for other source data.

The online version of this article includes the following source data and figure supplement(s) for figure 6:

Source data 1. The sheet shows the plotted TPM values of mRNA sequencing analysis in *Figure 6* for the expression of lateral plate mesoderm marker genes between the KO and WT at days 0, 7, and 25 of the differentiation.

Figure supplement 1. *CEP83*$^{-/-}$ cells upregulate lateral plate mesoderm (LPM) genes in mesenchymal cells cluster and nascent nephron progenitor clusters.

Figure supplement 2. CEP83$^{-/-}$ organoids show significant enrichment compared to developmental zebrafish lateral plate mesoderm (LPM) single-cell RNA (scRNA) data.

Figure supplement 3. Upregulation of hedgehog signaling components in CEP83$^{-/-}$ cells.

these alterations are associated with an inability of *CEP83*-deficient cells to form kidney epithelia. Organoids derived from *CEP83*-deficient cells fail to induce any detectable nephron structures, suggesting a novel role for CEP83 during the specification of functional kidney progenitors in the mesoderm.

Our findings are relevant to understanding the cellular and molecular functions of CEP83 and might be relevant to the pathophysiology of human genetic diseases. To date, 11 patients with biallelic mutations of *CEP83* have been reported, 8 of which displayed kidney phenotypes (*Failler et al., 2014*; *Veldman et al., 2021*; *Haer-Wigman et al., 2017*). Available kidney histologies identified microcystic tubular dilatations, tubular atrophy, thickened basement membranes, and interstitial fibrosis.

Extrarenal phenotypes included speech delay, intellectual disability, hydrocephalus, strabismus, retinal degeneration, retinitis pigmentosa, hepatic cytolysis, cholestasis, and portal septal fibrosis with mild thickening of arterial walls and an increase in the number of the biliary canalicules on liver biopsy. Among individuals with *CEP83* mutations, all but one carried at least one missense mutation or short in-frame deletion, suggesting that *CEP83* function may have been partially preserved. One individual with presumed full loss of *CEP83* displayed a more severe phenotype with multiple organ dysfunction. It will be interesting to await future reports of additional *CEP83* mutations in humans and whether complete loss of function alleles will result in broader mesoderm defects or renal agenesis. In this regard, it is interesting that mice with a targeted homozygous loss-of-function mutation of their *CEP83* ortholog (*Cep83*$^{tm1.1(KOMP)Vlcg}$) display midembryonic lethality (at E12.5) with evidence of severe developmental delay as early as E9.5 (https://www.mousephenotype.org/data/genes/MGI:1924298). These phenotypes are potentially consistent with the role of *CEP83* in germ layer patterning and mesoderm development, but a more detailed phenotypical characterization of *Cep83* knockout embryos would be required to substantiate this possibility.

The precise molecular and cellular mechanisms underlying our observations remain to be determined. CEP83 is a protein that is necessary for the assembly of DAPs and primary cilia formation in several cell types (*Tanos et al., 2013*; *Yang et al., 2018*; *Shao et al., 2020*; *Kumar et al., 2021*; *Stinchcombe et al., 2015*; *Joo et al., 2013*). A potential involvement of CEP83-mediated primary cilia formation in the findings reported here is suggested by obvious ciliary defects in CEP83-deficient cells at the D7 and the organoid stage (*Figure 2D–G*, *Figure 2—figure supplement 1*). These defects include reduced percentages of ciliated cells and elongated primary cilia in those cells that continue to form a primary cilium. In addition, CEP83-deficient cells displayed downregulated expression of several transcripts encoding ciliary components (*Figure 5—figure supplement 3*) and evidence of an activation of several hedgehog signaling associated genes. The primary cilium is critically involved in hedgehog signaling (*Ho and Stearns, 2021*). Moreover, Hedgehog signaling is important for mesodermal lineage decisions during gastrulation (*Guzzetta et al., 2020*). This raises the possibility that CEP83 controls mesodermal cell fate decisions by modulating hedgehog signaling in the mesoderm. Nevertheless, additional studies will be necessary to address this possibility. In addition, it remains unknown whether abnormal cilia formation in CEP83-deficient cells causally contributes to the cell fate phenotype.

We observed downregulated expression of the key nephron progenitor genes *PAX8*, *EYA1*, and *HOXB7* in *CEP83*$^{-/-}$ cells at day 7, which might explain their failure to differentiate into kidney cells since each of these genes is essential for normal kidney development (*Vincent et al., 1997*; *Pfeffer*
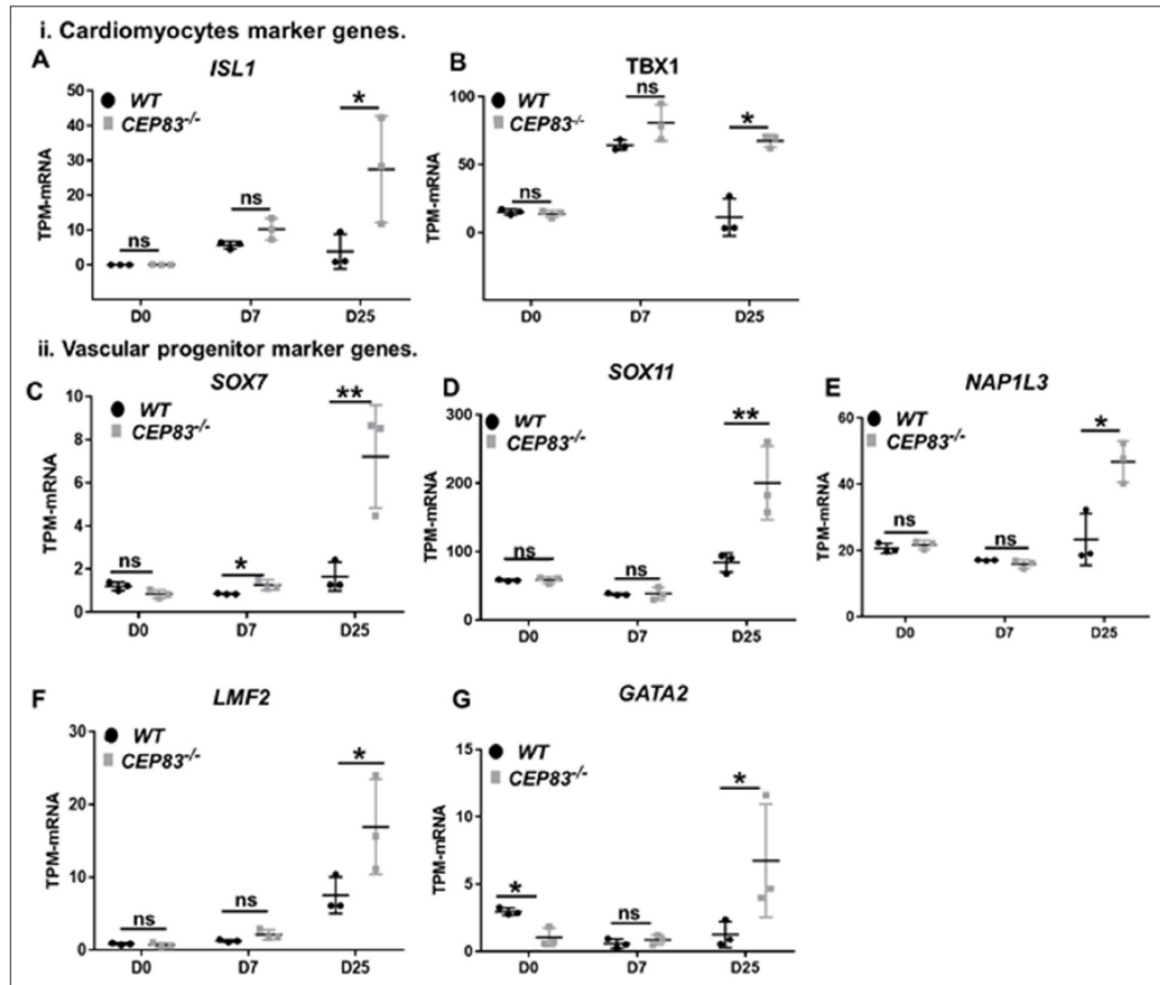
59

Figure 7. CEP83$^{-/-}$ cells upregulate expression of genes characteristic of cardiomyocyte progenitors and vascular progenitors. (**A–G**) Expression of cardiomyocyte markers *ISL1* (**A**), *TBX1* (**B**), and vascular progenitor markers *SOX7* (**C**), *SOX11* (**D**), *NAP1L3* (**E**), *LMO2* (**F**), and *GATA2* (**G**) in wildtype (*WT*) and *CEP83$^{-/-}$* cells at day 0 (D0), day 7 (D7), and day 25 (D25) according to bulk RNA-sequencing. N=3 clones per group for bulk RNA seq. Expression units are mean transcripts per million (TPM) ± SD. *p<0.05, and **p<0.01. ns = not significant. See **Figure 6—figure supplement 2**. See also **Figure 7—source data 1**. Check the data availability section for other source data.

The online version of this article includes the following source data for figure 7:

Source data 1. The sheet shows the plotted TPM values of mRNA sequencing analysis in **Figure 7** for the expression of cardiomyocytes and vascular progenitors marker genes between the KO and WT at days 0, 7, and 25 of the differentiation.

et al., 1998; *Kumar et al., 1998*; *Bouchard et al., 2002*; *Xu et al., 1999*; *Patterson and Potter, 2004*; *Rojek et al., 2006*). Furthermore, inductive signals from HOXB7-positive ureteric bud are known to maintain viability of nephron progenitor cells in the IM (*Barasch et al., 1997*), which may contribute to increased numbers of apoptotic cells we observed in CEP83$^{-/-}$ cells. Defects during nephron progenitor differentiation in the IM would be expected to result in severe kidney phenotypes such as renal agenesis or renal hypodysplasia. Defects of centriolar components or cilia have previously been linked to such phenotypes: in mice, centrosome amplification, i.e., the formation of excess centrosomes per cell severely disrupts kidney development, resulting in depletion of renal progenitors and renal hypoplasia (*Dionne et al., 2018*). In humans, loss of KIF14, a protein necessary for proper DAP assembly and cilium formation, has been associated with kidney malformations, including
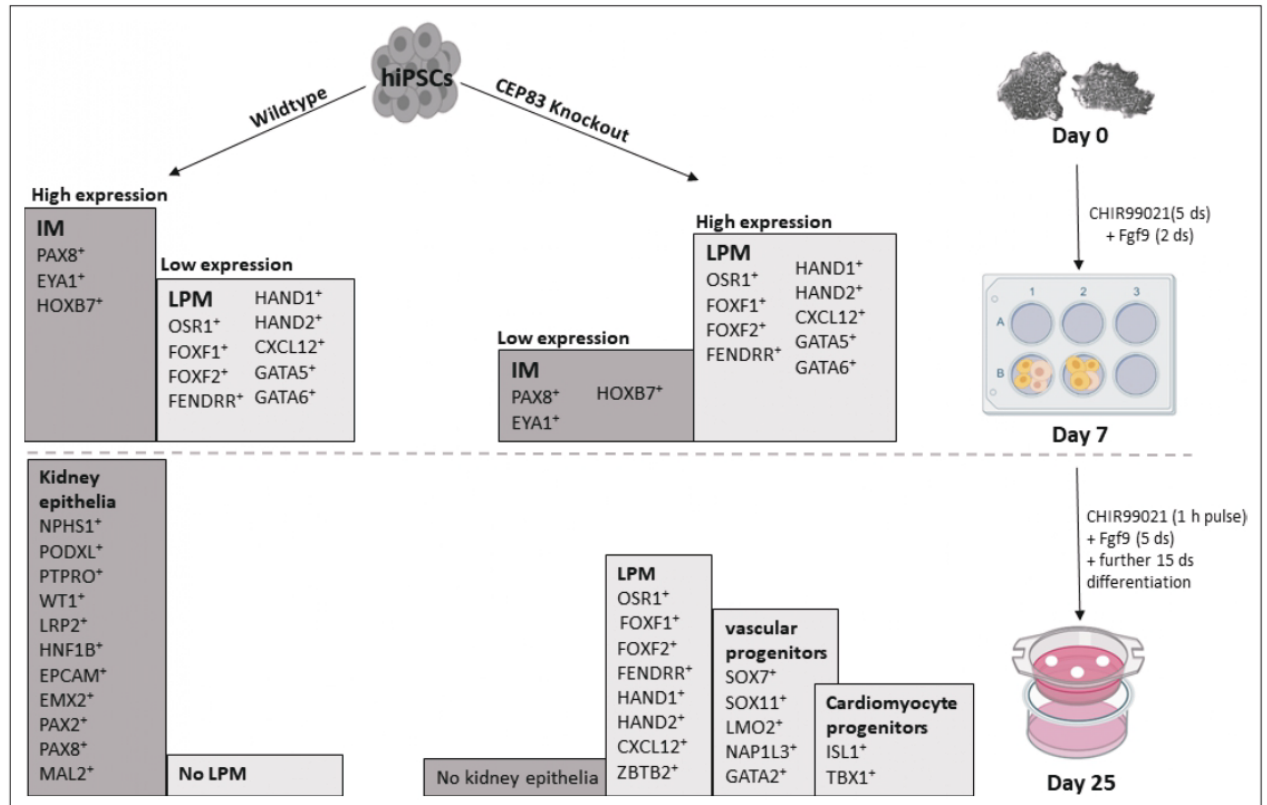
60

Figure 8. Schematic model outlining the functional differences between wildtype and CEP83 knockout cells during the course of differentiation of human pluripotent stem cells toward kidney cells. IM, intermediate mesoderm; LPM, lateral plate mesoderm.

renal agenesis and renal dysplasia (*Filges et al., 2014*; *Reilly et al., 2019*; *Pejskova et al., 2020*). Furthermore, Kif3a, a ciliary protein involved in intraflagellar transport, is necessary for normal mesoderm formation, and kidney progenitor-specific defects of Kif3a have been associated with reduced nephron numbers (*Takeda et al., 1999*; *Chi et al., 2013*). Similarly, mouse genes encoding the ciliary intraflagellar transport proteins IFT25 and IFT27 have been associated with renal agenesis or renal hypoplasia (*Desai et al., 2018*; *Quélin et al., 2018*). Together, these studies highlight the importance of molecules involved in ciliogenesis for mesoderm and kidney progenitor development and suggest that CEP83 contributes to such processes by facilitating an early step of ciliogenesis. Nevertheless, the detailed molecular processes that link CEP83 function, cilia formation, and kidney progenitor specification remain to be determined.

The finding of various upregulated LPM markers in *CEP83*$^{-/-}$ cells starting from day 7 suggests that CEP83 function may be involved in fine-tuning the balance of LPM and IM, thereby contributing to lineage decisions during mesoderm formation. Crosstalk of LPM and IM has been reported previously in zebrafish, overexpression of LPM transcription factors Scl/Tal1 and Lmo2 induces ectopic vessel and blood specification while inhibiting IM formation (*Gering et al., 2003*). Furthermore, the LPM transcription factor Hand2 is critical in determining the size of the IM, while natively expressed in the IM-adjacent LPM progenitors that form mesothelia (*Barbosa et al., 2007Perens et al., 2016*; *Prummel et al., 2022*). Loss of Hand2 in zebrafish results in an expanded IM, whereas Hand2 overexpression reduces or abolishes the IM. Interestingly, HAND2 was among the most strongly induced transcripts in our *CEP83*$^{-/-}$ cells at day 7; connecting with the developmental role of Hand2 in IM formation, these observations suggest that HAND2 expression in CEP83-deficient cells may have contributed to the reduced numbers of nephron progenitor cells at this stage. Of note, CEP83-deficient cells at D25 expressed increased levels of LPM genes expressed in mesothelial (including

OSR1, CXCL12, HAND1/2), cardiopharyngeal (including ISL1, TBX1), and endothelial/hematopoietic (including TAL1, LMO2, GATA2) progenitors (**Prummel et al., 2020**; **Prummel et al., 2022**). In sum, we propose a novel role for CEP83 in regulating the development of IM nephron progenitors, which may involve direct effects of CEP83 in the nephron progenitor differentiation program and indirect LPM-mediated effects on the IM. Future studies are warranted to delineate the molecular and cellular mechanisms underlying CEP83 function in LPM and specifically IM patterning.

Materials and methods

hiPSCs cell line

We used the human iPSC cell line BIHi005-A, which was generated by the Berlin Institute of Health (BIH). The hiPSCs were maintained in six-well plates (Corning, 353046) coated with Matrigel (Corning, 354277) and cultured in Essential 8 medium (E8, A1517001, Gibco-Thermo Fisher Scientific) supplemented with 10 µM Y-27632 (Rocki, Wako, 253–00513). Cells were authenticated and tested for the mycoplasma infection.

CRISPR CAS9 technology to generate CEP83$^{-/-}$ hiPSCs clones

Clustered regularly interspaced short palindromic repeats (CRISPR)-Cas9 technology was used to generate CEP83$^{-/-}$ hiPSCs clones. We designed two CRISPR RNAs (crRNAs) (5'-GGCTGAAG TAGCGGAATTAA-AGG-3' and 5'-AAGAATACAGGTGCGGCAGT-TGG-3') using CRISPOR software (**Concordet and Haeussler, 2018**). The two crRNAs were annealed with trans-activating CRISPR RNA (tracrRNA) to form two guide RNAs (gRNA1 and gRNA2) and then formed a ribonucleoprotein (RNP) complex by incubating gRNA1 and gRNA2 separately with Alt-R S.p. Cas9 Nuclease V3 (1 µM concentration, IDT, 1081058). The hiPSCs were transfected with RNP complexes using Neon transfection system (Thermo Fisher Scientific, MPK5000; **Yumlu et al., 2017**) and Neon transfection 10 µl kit (Thermo Fisher Scientific, MPK10025) according to the manufacturer's instructions. After 48 hr of transfection, we analyzed the editing efficiency in the pool by PCR genotyping.

For PCR genotyping, we isolated genomic DNA from the pool of transfected cells followed by PCR using Phire Tissue Direct PCR Master Mix (Thermo Scientific, F170S) according to the manufacturer's instructions (**Figure 1B**). After confirming the editing efficiency in the pool, we generated single-cell clones by the clonal dilution method. We plated 500 single cells per well of a 6 well plate and picked 24 clones using a picking hood S1 (Max Delbrück Centre Stem Cell Core Facility). Then, clones were screened for homozygous deletions of CEP83 by PCR using Phire Tissue Direct PCR Master Mix. Selected knockout clones were further characterized for CEP83 loss of function on the DNA, RNA, and protein level. CEP83$^{-/-}$ clones (KO1, KO2, and KO3) were registered as (BIHi005-A-71, BIHi005-A-72, and BIHi005-A-73) in the European Human Pluripotent Stem Cell Registry (https://hpscreg.eu).

Single nucleotide polymorphism - karyotype

To assess karyotype integrity, copy number variation (CNV) analysis on the human Illumina OMNI-EXPRESS-8v1.6 BeadChip was used. In brief, genomic DNA was isolated from three WT (WT1, WT2, and WT3) and three KO (KO1, KO2, and KO3) clones using the DNeasy blood and tissue kit (Qiagen, Valencia, CA, United States), hybridized to the human Illumina OMNI-EXPRESS-8v1.6 BeadChip (Illumina), stained, and scanned using the Illumina iScan system according to a standard protocol (**LaFramboise, 2009**; **Arsham et al., 2017**; **Haraksingh et al., 2017**). The genotyping was initially investigated using the GenomeStudio 1 genotyping module (Illumina). Following that, KaryoStudio 1.3 (Illumina) was used to perform automatic normalization and identify genomic aberrations in detected regions by generating B-allele frequency and smoothed Log R ratio plots. To detect CNVs, the stringency parameters were set to 75 kb (loss), 100 kb (gain), and CN-LOH (loss of heterozygosity). KaryoStudio generates reports and displays chromosome, length, list of cytobands, and genes in CNV-affected regions.

Differentiation protocol

We used the protocol of Takasato to differentiate the hiPSCs into nephron organoids (**Takasato et al., 2015**). Briefly, hiPSCs were cultured first in APEL2 medium (Stem Cell Technologies, 05270) supplemented with 5% Protein Free Hybridoma Medium II (PFHMII, GIBCO, 12040077), and 8 µM CHIR99021 (R&D, 4423/10) for 5 days, with medium changes every 2 days. Then, the cells were cultured in APEL2

62

medium supplemented with 200 ng/ml FGF9 (R&D, 273-F9-025) and 1 µg/ml heparin (Sigma Aldrich, H4784-250MG) for 2 days. On day 7, the cells were washed with 1× Dulbecco's PBS (DPBS, Thermo Fisher Scientific,14190–250), then trypsinized using trypsin EDTA-0.05% (Thermo Fisher Scientific, 25300–062) at 37°C for 3 min. The cells were counted and divided to achieve 1×10⁶ cells per organoid and cultured into 3D organoid culture on 0.4-µm-pore polyester membrane of Corning 6-well Transwell cell culture plate (Corning-Sigma Aldrich, CLS3450-24EA). Four to five organoids were seeded on one membrane using a P100 wide-bore tip and cultured in APEL2 with 5 µM CHIR99021 at 37°C for 1 hr (CHIR99021 pulse). After the CHIR pulse, we changed the medium to APEL2 medium supplemented with 200 ng/ml FGF9 + 1 µg/ml heparin for 5 days with medium refreshing every 2 days. The organoids were then cultured only in APEL2 medium with 1 µg/ml heparin for additional 13 days. The total differentiation time is 25 days (7+18).

DNA isolation and PCR

DNA was isolated from cells using DNeasy Blood & Tissue Kits (Qiagen, 69504). CEP83 primers were designed using Primer3 webtool (*Supplementary file 1*). PCR was done using Phusion high-fidelity DNA polymerase (Biolabs, New England, M0530) according to the manufacturer's instructions. PCR results were visualized on 1.5% agarose gel using a BioDoc Analyze dark hood and software system (Biometra).

RNA isolation, RNA sequencing, and qPCR

Total RNA was isolated from the cells using RNAasy Mini Kit (QIAGEN, Hilden, Germany, 74104) following the manufacture's instructions. The concentration, quality, and integrity of the extracted RNA were evaluated using Nanodrop (Thermo Scientific, Waltham, MA; USA), an Agilent 2100 Bioanalyzer, and the Agilent RNA 6000 Nano kit (Agilent Technologies, 5067–1511). 0.4 µg total RNA was used to obtain a poly A–enriched RNA library by Novogene (Cambridge, United Kingdom). Library concentration was performed using a Qubit fluorometer (HS RNA assay kit, Agilent Technologies). Library size was measured by Agilent 2100 bioanalyzer. The libraries were then subjected to 150 bp paired-end next-generation sequencing (Illumina NovaSeq 6000 S4 flow cells). Mutation visualization was performed using the Integrative Genomic Viewer tool (*Robinson et al., 2011*). Read counts of the sequenced RNA were normalized to transcripts per million (TPM). The TPM values of the variables were used to plot heatmaps and for principle component analysis (PCA) based on Pearson correlation, using self-written scripts in R (R Development Core Team (2011)) (version 4.0.4).

RNA was reverse transcribed using the RevertAid First Strand cDNA Synthesis Kit (Thermo Scientific). qPCR was performed using the FastStart Universal SYBR Green Master (Rox) mix (Hoffmann-La Roche) according to the manufacturer's instructions. Glyceraldehyde-3-phosphate dehydrogenase (*GAPDH*) mRNA expression was calculated according to the ΔΔCt method. All primer pairs were designed using Primer3, purchased at BioTeZ (Berlin, Germany), and sequences are shown in *Supplementary file 1*.

Single-cell RNA sequencing (scRNA-seq)

Cells isolation and preparation

Differentiated cells at day 7 were washed twice with 1× DPBS, dissociated with Accumax solution, and resuspended in 1× DPBS. Then, cells were filtered, counted, and checked for viability.

Library preparation and single-cell sequencing

Single-cell 3′ RNA sequencing was performed using the 10× Genomics toolkit version v3.1 (*Alles et al., 2017*), according to the manufacturer's instructions aiming for 10,000 cells. Obtained libraries were sequenced on Illumina NextSeq 500 sequencers.

Single-cell sequencing data analysis and clustering

After sequencing and demultiplexing, fastq files were analyzed using Cellranger version 3.0.2. Gene expression matrices were then imported into R, and Seurat objects were created using the Seurat R package (version 4.0.5) (*Stuart et al., 2019*). The gene expression matrices were initially filtered by applying lower and upper cut-offs for the number of detected genes (500 and 6000, respectively). The filtered data were then log normalized and scaled according to the number of unique molecular

63

identifiers. The normalized and scaled data derived from the four samples were then merged into one Seurat object. Clustering was performed using the first 20 principal components. We used the Seurat FindAllMarkers function to extract marker gene lists that differentiate between clusters with log fold change threshold ± 0.25 using only positive markers expressed in a minimum of 25% of cells. PCA was done using the first 20 principle components in R using the following libraries factoextra, FactoMineR, and ggplot2.

Protein extraction and immunoblotting

Proteins were extracted from hiPSCs using radioimmunoprecipitation assay (RIPA) buffer (Sigma-Aldrich, R0278) as described in details in supplementary data. 30 µg protein in RIPA buffer were mixed with 1× reducing (10% b-mercaptoethanol) NuPAGE loading buffer (Life Technologies, Carlsbad, CA), loaded on a precast polyacrylamide NuPage 4–12% Bis-Tris protein gel (Invitrogen, Carlsbad, CA, USA) and blotted on 0.45 µm pore size Immobilon-P Polyvinylidene difluoride membrane (EMD Milli-pore, Billerica, MA; USA). The membrane was blocked in 5% bovine serum albumin for 1 hr at room temperature and incubated overnight at 4°C with primary antibodies: anti-CEP83 produced in rabbit (1:500, Sigma-Aldrich) and anti-α-Tubulin produced in mouse (1:500, Sigma-Aldrich, T9026). Then, the membrane was incubated for 1 hr at room temperature with horseradish peroxidase-conjugated secondary antibodies (1:2000, Sigma-Aldrich, Saint Louis, MO, USA). Chemiluminescent reagent (Super Signal–West Pico; Thermo Scientific, Waltham, MA; USA) was used to detect the proteins. The spectra Multicolor Broad Range Protein Ladder (Thermo Fisher Scientific, USA) was used to evaluate the molecular weight of corresponding protein bands.

Histology and immunofluorescence staining

Cells at different time points were checked regularly under a confocal microscope (Leica DMI 6000 CEL) for differentiation progress. Quantitative analysis of nephron-like structure formation within each organoid (D25) was done on tile scanning images of each organoid by estimating the percentage of the organoid area composed of nephron-like structures using 13 WT and 9 KO organoids. Organoids were fixed in BD Cytofix buffer (554655, BD Biosciences) for 1 hr on ice. Then organoids were grad-ually dehydrated in increasing ethanol concentrations, cleared in xylene, and embedded in paraffin. Organoids were cut into 3.5-µm thick sections. The sections were deparaffinized, dehydrated, and stained in hematoxylin (Sigma-Aldrich, Saint Louis, MO) for 3 min and in 1% eosin (Sigma-Aldrich) for 2 min. For immunostaining, cells (day 7) and organoids (day 25) were fixed with BD Cytofix, permea-bilized with BD Perm/Wash (554723, BD Biosciences), and blocked with blocking solution (1% BSA + 0.3% triton-X-100 in 1× DPBS) for 2 hr. Cells and organoids were incubated overnight at 4°C with primary antibodies (*Supplementary file 2*), then incubated with fluorescence-labeled secondary anti-bodies with 1:500 dilution including Cy3, Cy5, Alexa488, and Alexa647 (Jackson ImmunoResearch, Newmarket, UK) and Cy3 Streptavidin (Vector lab, Burlingame, USA) overnight at 4°C. DAPI was then used for nuclear staining (Cell signaling Technology, Danvers, MA, USA) with 1:300,000 dilution for 1 hr at RT. Finally, cells were mounted with Dako fluorescent mounting medium (Agilent Technolo-gies). Images were taken using a SP8 confocal microscope (Carl Zeiss GmbH, Oberkochen, Germany). Quantitative analyses of acquired images were performed using ImageJ software (1.48 v; National Institutes of Health, Bethesda, MD).

Comparison to zebrafish LPM

The upregulated genes in CEP83$^{-/-}$ cells on day 7 and day 25 were compared with the top 20 orthol-ogous genes identified in subclusters of zebrafish LPM identified by scRNA-seq, as deposited on ArrayExpress (E-MTAB-9727; *Prummel et al., 2022*).

Statistical analysis

scRNA-seq was done on two biological replicates representing two different clones of CEP83$^{-/-}$ and control cells, respectively. All other experiments were performed using three biological replicates representing three independent clones of *CEP83*$^{-/-}$ and control cells at different time points. A common excel sheet for the genes present in both bulk RNA and scRNA sequencing was generated in R. The sheet includes a total of 20,894 genes and represents the TPM values of both groups (*WT* and *KO*) on day 0, day 7, and day 25 of differentiation. The maximum TPM (TPMmax) and the minimum

64

TPM (TPMmin) were calculated for each gene across all samples. HVGs were calculated based on the ratio of TPMmax and TPMmin. For heatmaps and PCA analysis, the top 1000 HVGs were plotted with a selection of TPMmax >2 for each gene. Deregulated (upregulated and downregulated) genes between *WT* and *KO* groups were selected with expression criteria of TPM >2, fold change >1.5, and p-value calculated on log10 TPM <0.05. The unpaired two-tailed t-test was used to compare the two groups. All graphs were generated using GraphPad Prism 7.04 (GraphPad Software, San Diego, CA). Data are presented as mean ± SD.

Acknowledgements

Additional information

Author contributions

Fatma Mansour, Software, Formal analysis, Validation, Visualization, Methodology, Writing - original draft; Christian Hinze, Narasimha Swamy Telugu, Jelena Kresoja, Methodology; Iman B Shaheed, Writing – review and editing; Christian Mosimann, Methodology, Writing – review and editing; Sebastian Diecke, Supervision, Methodology; Kai M Schmidt-Ott, Conceptualization, Supervision, Writing – review and editing, Funding acquisition

Author ORCIDs

Fatma Mansour http://orcid.org/0000-0003-4808-3514
Christian Hinze http://orcid.org/0000-0003-2526-1621
Christian Mosimann http://orcid.org/0000-0002-0749-2576
Kai M Schmidt-Ott http://orcid.org/0000-0002-7700-7142

Decision letter and Author response

Decision letter https://doi.org/10.7554/eLife.80165.sa1
Author response https://doi.org/10.7554/eLife.80165.sa2

Additional files

Supplementary files

• MDAR checklist

65

- Supplementary file 1. The table shows the primers list used in the qPCR.
- Supplementary file 2. The table shows the list of primary antibodies used in IF staining.

Data availability

All data supporting the findings of this study are available within the article and its supplementary files. Source data files have been provided for Figures 1–6. Sequencing data have been deposited in GEO under accession code GSE205978.

The following dataset was generated:

Author(s)	Year	Dataset title	Dataset URL	Database and Identifier
Schmidt-Ott KM	2022	The centrosomal protein 83 (CEP83) regulates human pluripotent stem cell differentiation toward the kidney lineage	http://www.ncbi.nlm.nih.gov/geo/query/acc.cgi?acc=GSE205978	NCBI Gene Expression Omnibus, GSE205978

The following previously published dataset was used:

Author(s)	Year	Dataset title	Dataset URL	Database and Identifier
Hariharan K	2019	Parallel generation of easily selectable multiple nephronal cell types from human pluripotent stem cells	https://www.ncbi.nlm.nih.gov/geo/query/acc.cgi?acc=GSE75711	NCBI Gene Expression Omnibus, GSE75711

References

Alles J, Karaiskos N, Praktiknjo SD, Grosswendt S, Wahle P, Ruffault P-L, Ayoub S, Schreyer L, Boltengagen A, Birchmeier C, Zinzen R, Kocks C, Rajewsky N. 2017. Cell fixation and preservation for droplet-based single-cell transcriptomics. *BMC Biology* **15**:1–14. DOI: https://doi.org/10.1186/s12915-017-0383-5, PMID: 28526029

Anderson E, Peluso S, Lettice LA, Hill RE. 2012. Human limb abnormalities caused by disruption of Hedgehog signaling. *Trends in Genetics* **28**:364–373. DOI: https://doi.org/10.1016/j.tig.2012.03.012, PMID: 22534646

Angelo S, Lohr J, Lee KH, Ticho BS, Breitbart RE, Hill S, Yost HJ, Srivastava D. 2000. Conservation of sequence and expression of *Xenopus* and zebrafish dHAND during cardiac, branchial arch and lateral mesoderm development. *Mechanisms of Development* **95**:231–237. DOI: https://doi.org/10.1016/s0925-4773(00)00334-8, PMID: 10906469

Arsham MS, Barch MJ, Lawce HJ. 2017. The AGT Cytogenetics Laboratory Manual. Hoboken, NJ, USA: John Wiley & Sons. DOI: https://doi.org/10.1002/9781119061199

Baldini A. 2005. Dissecting contiguous gene defects: Tbx1. *Current Opinion in Genetics & Development* **15**:279–284. DOI: https://doi.org/10.1016/j.gde.2005.03.001, PMID: 15917203

Barasch J, Qiao J, McWilliams G, Chen D, Oliver JA, Herzlinger D. 1997. Ureteric bud cells secrete multiple factors, including bfgf, which rescue renal progenitors from apoptosis. *The American Journal of Physiology* **273**:F757–F767. DOI: https://doi.org/10.1152/ajprenal.1997.273.5.F757, PMID: 9374839

Barbosa AC, Funato N, Chapman S, McKee MD, Richardson JA, Olson EN, Yanagisawa H. 2007. Hand transcription factors cooperatively regulate development of the distal midline mesenchyme. *Developmental Biology* **310**:154–168. DOI: https://doi.org/10.1016/j.ydbio.2007.07.036, PMID: 17764670

Bilous RW, Murty G, Parkinson DB, Thakker RV, Coulthard MG, Burn J, Mathias D, Kendall-Taylor P. 1992. Brief report: autosomal dominant familial hypoparathyroidism, sensorineural deafness, and renal dysplasia. *The New England Journal of Medicine* **327**:1069–1074. DOI: https://doi.org/10.1056/NEJM199210083271506, PMID: 1522843

Bouchard M, Souabni A, Mandler M, Neubüser A, Busslinger M. 2002. Nephric lineage specification by Pax2 and Pax8. *Genes & Development* **16**:2958–2970. DOI: https://doi.org/10.1101/gad.240102, PMID: 12435636

Bowler M, Kong D, Sun S, Nanjundappa R, Evans L, Farmer V, Holland A, Mahjoub MR, Sui H, Loncarek J. 2019. High-Resolution characterization of centriole distal appendage morphology and dynamics by correlative storm and electron microscopy. *Nature Communications* **10**:993. DOI: https://doi.org/10.1038/s41467-018-08216-4, PMID: 30824690

Boyle S, Misfeldt A, Chandler KJ, Deal KK, Southard-Smith EM, Mortlock DP, Baldwin HS, de Caestecker M. 2008. Fate mapping using cited1-creert2 mice demonstrates that the cap mesenchyme contains self-renewing progenitor cells and gives rise exclusively to nephronic epithelia. *Developmental Biology* **313**:234–245. DOI: https://doi.org/10.1016/j.ydbio.2007.10.014, PMID: 18061157

66

Cai CL, Liang X, Shi Y, Chu PH, Pfaff SL, Chen J, Evans S. 2003. Isl1 identifies a cardiac progenitor population that proliferates prior to differentiation and contributes a majority of cells to the heart. *Developmental Cell* **5**:877–889. DOI: https://doi.org/10.1016/s1534-5807(03)00363-0, PMID: 14667410

Chen L, Fulcoli FG, Tang S, Baldini A. 2009. Tbx1 regulates proliferation and differentiation of multipotent heart progenitors. *Circulation Research* **105**:842–851. DOI: https://doi.org/10.1161/CIRCRESAHA.109.200295, PMID: 19745164

Chi L, Galtseva A, Chen L, Mo R, Hui CC, Rosenblum ND. 2013. Kif3A controls murine nephron number via Gli3 repressor, cell survival, and gene expression in a lineage-specific manner. *PLOS ONE* **8**:e65448. DOI: https://doi.org/10.1371/journal.pone.0065448, PMID: 23762375

Concordet JP, Haeussler M. 2018. CRISPOR: intuitive guide selection for CRISPR/Cas9 genome editing experiments and screens. *Nucleic Acids Research* **46**:W242–W245. DOI: https://doi.org/10.1093/nar/gky354, PMID: 29762716

Dammermann A, Merdes A. 2002. Assembly of centrosomal proteins and microtubule organization depends on PCM-1. *The Journal of Cell Biology* **159**:255–266. DOI: https://doi.org/10.1083/jcb.200204023, PMID: 12403812

Davidson AJ, Lewis P, Przepiorski A, Sander V. 2019. Turning mesoderm into kidney. *Seminars in Cell & Developmental Biology* **91**:86–93. DOI: https://doi.org/10.1016/j.semcdb.2018.08.016, PMID: 30172050

Desai PB, San Agustin JT, Stuck MW, Jonassen JA, Bates CM, Pazour GJ. 2018. Ift25 is not a cystic kidney disease gene but is required for early steps of kidney development. *Mechanisms of Development* **151**:10–17. DOI: https://doi.org/10.1016/j.mod.2018.04.001, PMID: 29626631

Dionne LK, Shim K, Hoshi M, Cheng T, Wang J, Marthiens V, Knoten A, Basto R, Jain S, Mahjoub MR. 2018. Centrosome amplification disrupts renal development and causes cystogenesis. *The Journal of Cell Biology* **217**:2485–2501. DOI: https://doi.org/10.1083/jcb.201710019, PMID: 29895697

Failler M, Gee HY, Krug P, Joo K, Halbritter J, Belkacem L, Filhol E, Porath JD, Braun DA, Schueler M, Frigo A, Alibeu O, Masson C, Brochard K, Hurault de Ligny B, Novo R, Pietrement C, Kayserili H, Salomon R, Gubler M-C, et al. 2014. Mutations of CEP83 cause infantile nephronophthisis and intellectual disability. *American Journal of Human Genetics* **94**:905–914. DOI: https://doi.org/10.1016/j.ajhg.2014.05.002, PMID: 24882706

Ferrante MI, Zullo A, Barra A, Bimonte S, Messaddeq N, Studer M, Dollé P, Franco B. 2006. Oral-Facial-Digital type I protein is required for primary cilia formation and left-right axis specification. *Nature Genetics* **38**:112–117. DOI: https://doi.org/10.1038/ng1684, PMID: 16311594

Filges I, Nosova E, Bruder E, Tercanli S, Townsend K, Gibson WT, Röthlisberger B, Heinimann K, Hall JG, Gregory-Evans CY, Wasserman WW, Miny P, Friedman JM. 2014. Exome sequencing identifies mutations in KIF14 as a novel cause of an autosomal recessive lethal fetal ciliopathy phenotype. *Clinical Genetics* **86**:220–228. DOI: https://doi.org/10.1111/cge.12301, PMID: 24128419

Firulli AB, McFadden DG, Lin Q, Srivastava D, Olson EN. 1998. Heart and extra-embryonic mesodermal defects in mouse embryos lacking the bHLH transcription factor HAND1. *Nature Genetics* **18**:266–270. DOI: https://doi.org/10.1038/ng0398-266, PMID: 9500550

Freedman BS, Brooks CR, Lam AQ, Fu H, Morizane R, Agrawal V, Saad AF, Li MK, Hughes MR, Werff RV, Peters DT, Lu J, Baccei A, Siedlecki AM, Valerius MT, Musunuru K, McNagny KM, Steinman TI, Zhou J, Lerou PH, et al. 2015. Modelling kidney disease with CRISPR-mutant kidney organoids derived from human pluripotent epiblast spheroids. *Nature Communications* **6**:8715. DOI: https://doi.org/10.1038/ncomms9715, PMID: 26493500

Gao R, Liang X, Cheedipudi S, Cordero J, Jiang X, Zhang Q, Caputo L, Günther S, Kuenne C, Ren Y, Bhattacharya S, Yuan X, Barreto G, Chen Y, Braun T, Evans SM, Sun Y, Dobreva G. 2019. Pioneering function of ISL1 in the epigenetic control of cardiomyocyte cell fate. *Cell Research* **29**:486–501. DOI: https://doi.org/10.1038/s41422-019-0168-1, PMID: 31024170

Gering M, Yamada Y, Rabbitts TH, Patient RK. 2003. Lmo2 and SCL/TAL1 convert non-axial mesoderm into haemangioblasts which differentiate into endothelial cells in the absence of GATA1. *Development* **130**:6187–6199. DOI: https://doi.org/10.1242/dev.00875, PMID: 14602685

Grote D, Souabni A, Busslinger M, Bouchard M. 2006. Pax 2/8-regulated GATA 3 expression is necessary for morphogenesis and guidance of the nephric duct in the developing kidney. *Development* **133**:53–61. DOI: https://doi.org/10.1242/dev.02184, PMID: 16319112

Grote P, Wittler L, Hendrix D, Koch F, Währisch S, Beisaw A, Macura K, Bläss G, Kellis M, Werber M, Herrmann BG. 2013. The tissue-specific lncRNA fendrr is an essential regulator of heart and body wall development in the mouse. *Developmental Cell* **24**:206–214. DOI: https://doi.org/10.1016/j.devcel.2012.12.012, PMID: 23369715

Guzzetta A, Koska M, Rowton M, Sullivan KR, Jacobs-Li J, Kweon J, Hidalgo H, Eckart H, Hoffmann AD, Back R, Lozano S, Moon AM, Basu A, Bressan M, Pott S, Moskowitz IP. 2020. Hedgehog-FGF signaling axis patterns anterior mesoderm during gastrulation. *PNAS* **117**:15712–15723. DOI: https://doi.org/10.1073/pnas.1914167117, PMID: 32561646

Haer-Wigman L, van Zelst-Stams WA, Pfundt R, van den Born LI, Klaver CC, Verheij JB, Hoyng CB, Breuning MH, Boon CJ, Kievit AJ, Verhoeven VJ, Pott JW, Sallevelt SC, van Hagen JM, Plomp AS, Kroes HY, Lelieveld SH, Hehir-Kwa JY, Castelein S, Nelen M, et al. 2017. Diagnostic exome sequencing in 266 Dutch patients with visual impairment. *European Journal of Human Genetics* **25**:591–599. DOI: https://doi.org/10.1038/ejhg.2017.9, PMID: 28224992

67

Han L, Xu J, Grigg E, Slack M, Chaturvedi P, Jiang R, Zorn AM. 2017. Osr1 functions downstream of hedgehog pathway to regulate foregut development. *Developmental Biology* **427**:72–83. DOI: https://doi.org/10.1016/j.ydbio.2017.05.005, PMID: 28501478

Haraksingh RR, Abyzov A, Urban AE. 2017. Comprehensive performance comparison of high-resolution array platforms for genome-wide copy number variation (CNV) analysis in humans. *BMC Genomics* **18**:1–14. DOI: https://doi.org/10.1186/s12864-017-3658-x, PMID: 28438122

Hariharan K, Stachelscheid H, Rossbach B, Oh SJ, Mah N, Schmidt-Ott K, Kurtz A, Reinke P. 2019. Parallel generation of easily selectable multiple nephronal cell types from human pluripotent stem cells. *Cellular and Molecular Life Sciences* **76**:179–192. DOI: https://doi.org/10.1007/s00018-018-2929-2, PMID: 30310934

Hildebrandt F. 2004. Pediatric Nephrology. Berlin, Heidelberg: Springer.

Ho EK, Stearns T. 2021. Hedgehog signaling and the primary cilium: implications for spatial and temporal constraints on signaling. *Development* **148**:dev195552. DOI: https://doi.org/10.1242/dev.195552, PMID: 33914866

Holtzinger A, Evans T. 2007. Gata5 and GATA6 are functionally redundant in zebrafish for specification of cardiomyocytes. *Developmental Biology* **312**:613–622. DOI: https://doi.org/10.1016/j.ydbio.2007.09.018, PMID: 17950269

Howden SE, Vanslambrouck JM, Wilson SB, Tan KS, Little MH. 2019. Reporter-based fate mapping in human kidney organoids confirms nephron lineage relationships and reveals synchronous nephron formation. *EMBO Reports* **20**:e47483. DOI: https://doi.org/10.15252/embr.201847483, PMID: 30858339

Joo K, Kim CG, Lee MS, Moon HY, Lee SH, Kim MJ, Kweon HS, Park WY, Kim CH, Gleeson JG, Kim J. 2013. CCDC41 is required for ciliary vesicle docking to the mother centriole. *PNAS* **110**:5987–5992. DOI: https://doi.org/10.1073/pnas.1220927110, PMID: 23530209

Kim D, Pertea G, Trapnell C, Pimentel H, Kelley R, Salzberg SL. 2013. TopHat2: accurate alignment of transcriptomes in the presence of insertions, deletions and gene fusions. *Genome Biology* **14**:R36. DOI: https://doi.org/10.1186/gb-2013-14-4-r36, PMID: 23618408

Knödler A, Feng S, Zhang J, Zhang X, Das A, Peränen J, Guo W. 2010. Coordination of rab8 and rab11 in primary ciliogenesis. *PNAS* **107**:6346–6351. DOI: https://doi.org/10.1073/pnas.1002401107, PMID: 20308558

Kobayashi A, Valerius MT, Mugford JW, Carroll TJ, Self M, Oliver G, McMahon AP. 2008. Six2 defines and regulates a multipotent self-renewing nephron progenitor population throughout mammalian kidney development. *Cell Stem Cell* **3**:169–181. DOI: https://doi.org/10.1016/j.stem.2008.05.020, PMID: 18682239

Koutsourakis M, Langeveld A, Patient R, Beddington R, Grosveld F. 1999. The transcription factor GATA6 is essential for early extraembryonic development. *Development* **126**:723–732. DOI: https://doi.org/10.1242/dev.126.4.723

Kress C, Vogels R, De Graaff W, Bonnerot C, Meijlink F, Nicolas JF, Deschamps J. 1990. Hox-2.3 upstream sequences mediate lacz expression in intermediate mesoderm derivatives of transgenic mice. *Development* **109**:775–786. DOI: https://doi.org/10.1242/dev.109.4.775, PMID: 1977573

Kugler MC, Joyner AL, Loomis CA, Munger JS. 2015. Sonic hedgehog signaling in the lung from development to disease. *American Journal of Respiratory Cell and Molecular Biology* **52**:1–13. DOI: https://doi.org/10.1165/rcmb.2014-0132TR, PMID: 25068457

Kumar S, Kimberling WJ, Weston MD, Schaefer BG, Berg MA, Marres HA, Cremers CW. 1998. Identification of three novel mutations in human EYA1 protein associated with branchio-oto-renal syndrome. *Human Mutation* **11**:443–449. DOI: https://doi.org/10.1002/(SICI)1098-1004(1998)11:6<443::AID-HUMU4>3.0.CO;2-S, PMID: 9603436

Kumar SV, Er PX, Lawlor KT, Motazedian A, Scurr M, Ghobrial I, Combes AN, Zappia L, Oshlack A, Stanley EG, Little MH. 2019. Kidney micro-organoids in suspension culture as a scalable source of human pluripotent stem cell-derived kidney cells. *Development* **146**:dev172361. DOI: https://doi.org/10.1242/dev.172361, PMID: 30846463

Kumar D, Rains A, Herranz-Pérez V, Lu Q, Shi X, Swaney DL, Stevenson E, Krogan NJ, Huang B, Westlake C, Garcia-Verdugo JM, Yoder BK, Reiter JF. 2021. A ciliopathy complex builds distal appendages to initiate ciliogenesis. *The Journal of Cell Biology* **220**:e202011133. DOI: https://doi.org/10.1083/jcb.202011133, PMID: 34241634

Kuraoka S, Tanigawa S, Taguchi A, Hotta A, Nakazato H, Osafune K, Kobayashi A, Nishinakamura R. 2020. PKD1-dependent renal cystogenesis in human induced pluripotent stem cell-derived ureteric bud/collecting duct organoids. *Journal of the American Society of Nephrology* **31**:2355–2371. DOI: https://doi.org/10.1681/ASN.2020030378, PMID: 32747355

Kurtulmus B, Yuan C, Schuy J, Neuner A, Hata S, Kalamakis G, Martin-Villalba A, Pereira G. 2018. LRRC45 contributes to early steps of axoneme extension. *Journal of Cell Science* **131**:jcs223594. DOI: https://doi.org/10.1242/jcs.223594, PMID: 30131441

Kwon C, Qian L, Cheng P, Nigam V, Arnold J, Srivastava D. 2009. A regulatory pathway involving notch1/beta-catenin/isl1 determines cardiac progenitor cell fate. *Nature Cell Biology* **11**:951–957. DOI: https://doi.org/10.1038/ncb1906, PMID: 19620969

LaFramboise T. 2009. Single nucleotide polymorphism arrays: a decade of biological, computational and technological advances. *Nucleic Acids Research* **37**:4181–4193. DOI: https://doi.org/10.1093/nar/gkp552, PMID: 19570852

Laugwitz K-L, Moretti A, Lam J, Gruber P, Chen Y, Woodard S, Lin L-Z, Cai C-L, Lu MM, Reth M, Platoshyn O, Yuan JX-J, Evans S, Chien KR. 2005. Postnatal isl1+ cardioblasts enter fully differentiated cardiomyocyte lineages. *Nature* **433**:647–653. DOI: https://doi.org/10.1038/nature03215, PMID: 15703750

Laverriere AC, MacNeill C, Mueller C, Poelmann RE, Burch JB, Evans T. 1994. Gata-4/5/6, a subfamily of three transcription factors transcribed in developing heart and gut. *The Journal of Biological Chemistry* **269**:23177–23184. DOI: https://doi.org/10.1016/S0021-9258(17)31636-8, PMID: 8083222

Lee J, Platt KA, Censullo P, Ruiz i Altaba A. 1997. Gli1 is a target of sonic hedgehog that induces ventral neural tube development. *Development* **124**:2537–2552. DOI: https://doi.org/10.1242/dev.124.13.2537

Liao Y, Smyth GK, Shi W. 2014. FeatureCounts: an efficient general purpose program for assigning sequence reads to genomic features. *Bioinformatics***30**:923–930. DOI: https://doi.org/10.1093/bioinformatics/btt656, PMID: 24227677

Liekens S, Schols D, Hatse S. 2010. CXCL12-CXCR4 axis in angiogenesis, metastasis and stem cell mobilization. *Current Pharmaceutical Design* **16**:3903–3920. DOI: https://doi.org/10.2174/138161210794455003, PMID: 21158728

Lo C-H, Lin I-H, Yang TT, Huang Y-C, Tanos BE, Chou P-C, Chang C-W, Tsay Y-G, Liao J-C, Wang W-J. 2019. Phosphorylation of CEP83 by TTBK2 is necessary for cilia initiation. *The Journal of Cell Biology* **218**:3489–3505. DOI: https://doi.org/10.1083/jcb.201811142, PMID: 31455668

Loh KM, Chen A, Koh PW, Deng TZ, Sinha R, Tsai JM, Barkal AA, Shen KY, Jain R, Morganti RM, Shyh-Chang N, Fernhoff NB, George BM, Wernig G, Salomon REA, Chen Z, Vogel H, Epstein JA, Kundaje A, Talbot WS, et al. 2016. Mapping the pairwise choices leading from pluripotency to human bone, heart, and other mesoderm cell types. *Cell* **166**:451–467. DOI: https://doi.org/10.1016/j.cell.2016.06.011, PMID: 27419872

Low JH, Li P, Chew EGY, Zhou B, Suzuki K, Zhang T, Lian MM, Liu M, Aizawa E, Rodriguez Esteban C, Yong KSM, Chen Q, Campistol JM, Fang M, Khor CC, Foo JN, Izpisua Belmonte JC, Xia Y. 2019. Generation of human PSC-derived kidney organoids with patterned nephron segments and a de novo vascular network. *Cell Stem Cell* **25**:373–387.. DOI: https://doi.org/10.1016/j.stem.2019.06.009, PMID: 31303547

Luo F, Tao YH. 2018. Nephronophthisis: a review of genotype-phenotype correlation. *Nephrology* **23**:904–911. DOI: https://doi.org/10.1111/nep.13393, PMID: 29717526

Mae SI, Shono A, Shiota F, Yasuno T, Kajiwara M, Gotoda-Nishimura N, Arai S, Sato-Otubo A, Toyoda T, Takahashi K, Nakayama N, Cowan CA, Aoi T, Ogawa S, McMahon AP, Yamanaka S, Osafune K. 2013. Monitoring and robust induction of nephrogenic intermediate mesoderm from human pluripotent stem cells. *Nature Communications* **4**:1367. DOI: https://doi.org/10.1038/ncomms2378, PMID: 23340407

Mahlapuu M, Ormestad M, Enerback S, Carlsson P. 2001. The forkhead transcription factor Foxf1 is required for differentiation of extra-embryonic and lateral plate mesoderm. *Development* **128**:155–166. DOI: https://doi.org/10.1242/dev.128.2.155

Mansour F, Boivin FJ, Shaheed IB, Schueler M, Schmidt-Ott KM. 2021. The role of centrosome distal appendage proteins (daps) in nephronophthisis and ciliogenesis. *International Journal of Molecular Sciences* **22**:12253. DOI: https://doi.org/10.3390/ijms222212253, PMID: 34830133

McFadden DG, Barbosa AC, Richardson JA, Schneider MD, Srivastava D, Olson EN. 2005. The HAND1 and HAND2 transcription factors regulate expansion of the embryonic cardiac ventricles in a gene dosage-dependent manner. *Development* **132**:189–201. DOI: https://doi.org/10.1242/dev.01562, PMID: 15576406

Moretti A, Caron L, Nakano A, Lam JT, Bernshausen A, Chen Y, Qyang Y, Bu L, Sasaki M, Martin-Puig S, Sun Y, Evans SM, Laugwitz K-L, Chien KR. 2006. Multipotent embryonic isl1+ progenitor cells lead to cardiac, smooth muscle, and endothelial cell diversification. *Cell* **127**:1151–1165. DOI: https://doi.org/10.1016/j.cell.2006.10.029, PMID: 17123592

Morikawa Y, Cserjesi P. 2004. Extra-embryonic vasculature development is regulated by the transcription factor HAND1. *Development* **131**:2195–2204. DOI: https://doi.org/10.1242/dev.01091, PMID: 15073150

Morizane R, Lam AQ, Freedman BS, Kishi S, Valerius MT, Bonventre JV. 2015. Nephron organoids derived from human pluripotent stem cells model kidney development and injury. *Nature Biotechnology* **33**:1193–1200. DOI: https://doi.org/10.1038/nbt.3392, PMID: 26458176

Mugford JW, Sipilä P, Kobayashi A, Behringer RR, McMahon AP. 2008a. Hoxd11 specifies a program of metanephric kidney development within the intermediate mesoderm of the mouse embryo. *Developmental Biology* **319**:396–405. DOI: https://doi.org/10.1016/j.ydbio.2008.03.044, PMID: 18485340

Mugford JW, Sipilä P, McMahon JA, McMahon AP. 2008b. Osr1 expression demarcates a multi-potent population of intermediate mesoderm that undergoes progressive restriction to an osr1-dependent nephron progenitor compartment within the mammalian kidney. *Developmental Biology* **324**:88–98. DOI: https://doi.org/10.1016/j.ydbio.2008.09.010, PMID: 18835385

Ormestad M, Astorga J, Carlsson P. 2004. Differences in the embryonic expression patterns of mouse Foxf1 and -2 match their distinct mutant phenotypes. *Developmental Dynamics* **229**:328–333. DOI: https://doi.org/10.1002/dvdy.10426, PMID: 14745957

Patterson LT, Potter SS. 2004. Atlas of Hox gene expression in the developing kidney. *Developmental Dynamics* **229**:771–779. DOI: https://doi.org/10.1002/dvdy.10474, PMID: 15042701

Pejskova P, Reilly ML, Bino L, Bernatik O, Dolanska L, Ganji RS, Zdrahal Z, Benmerah A, Cajanek L. 2020. Kif14 controls ciliogenesis via regulation of Aurora A and is important for hedgehog signaling. *The Journal of Cell Biology* **219**:e201904107. DOI: https://doi.org/10.1083/jcb.201904107, PMID: 32348467

Perens EA, Garavito-Aguilar ZV, Guio-Vega GP, Peña KT, Schindler YL, Yelon D. 2016. Hand2 Inhibits Kidney Specification While Promoting Vein Formation Within the Posterior Mesoderm. *bioRxiv*. DOI: https://doi.org/10.1101/075036

Pfeffer PL, Gerster T, Lun K, Brand M, Busslinger M. 1998. Characterization of three novel members of the zebrafish Pax2/5/8 family: dependency of Pax5 and Pax8 expression on the pax2.1 (Noi) function. *Development* **125**:3063–3074. DOI: https://doi.org/10.1242/dev.125.16.3063

69

Pikkarainen S, Tokola H, Kerkelä R, Ruskoaho H. 2004. Gata transcription factors in the developing and adult heart. *Cardiovascular Research* **63**:196–207. DOI: https://doi.org/10.1016/j.cardiores.2004.03.025, PMID: 15249177

Prummel KD, Nieuwenhuize S, Mosimann C. 2020. The lateral plate mesoderm. *Development* **147**:dev175059. DOI: https://doi.org/10.1242/dev.175059, PMID: 32561665

Prummel KD, Crowell HL, Nieuwenhuize S, Brombacher EC, Daetwyler S, Soneson C, Kresoja-Rakic J, Ronner M, Kocere A, Ernst A, Labbaf Z, Clouthier DE, Firulli AB, Sánchez-Iranzo H, Naganathan SR, O'Rourke R, Raz E, Mercader N, Burger A, Felley-Bosco E, et al. 2021. Hand2 Delineates Mesothelium Progenitors and Is Reactivated in Mesothelioma. *bioRxiv*. DOI: https://doi.org/10.1101/2020.11.11.355693

Prummel KD, Crowell HL, Nieuwenhuize S, Brombacher EC, Daetwyler S, Soneson C, Kresoja-Rakic J, Kocere A, Ronner M, Ernst A, Labbaf Z, Clouthier DE, Firulli AB, Sánchez-Iranzo H, Naganathan SR, O'Rourke R, Raz E, Mercader N, Burger A, Felley-Bosco E, et al. 2022. Hand2 delineates mesothelium progenitors and is reactivated in mesothelioma. *Nature Communications* **13**:1677. DOI: https://doi.org/10.1038/s41467-022-29311-7, PMID: 35354817

Quélin C, Loget P, Boutaud L, Elkhartoufi N, Milon J, Odent S, Fradin M, Demurger F, Pasquier L, Thomas S, Attié-Bitach T. 2018. Loss of function IFT27 variants associated with an unclassified lethal fetal ciliopathy with renal agenesis. *American Journal of Medical Genetics. Part A* **176**:1610–1613. DOI: https://doi.org/10.1002/ajmg.a.38685, PMID: 29704304

Reilly ML, Stokman MF, Magry V, Jeanpierre C, Alves M, Paydar M, Hellinga J, Delous M, Pouly D, Failler M, Martinovic J, Loeuillet L, Leroy B, Tantau J, Roume J, Gregory-Evans CY, Shan X, Filges I, Allingham JS, Kwok BH, et al. 2019. Loss-Of-Function mutations in KIF14 cause severe microcephaly and kidney development defects in humans and zebrafish. *Human Molecular Genetics* **28**:778–795. DOI: https://doi.org/10.1093/hmg/ddy381, PMID: 30388224

Reiter JF, Alexander J, Rodaway A, Yelon D, Patient R, Holder N, Stainier DY. 1999. Gata5 is required for the development of the heart and endoderm in zebrafish. *Genes & Development* **13**:2983–2995. DOI: https://doi.org/10.1101/gad.13.22.2983, PMID: 10580005

Risebro CA, Smart N, Dupays L, Breckenridge R, Mohun TJ, Riley PR. 2006. Hand1 regulates cardiomyocyte proliferation versus differentiation in the developing heart. *Development* **133**:4595–4606. DOI: https://doi.org/10.1242/dev.02625, PMID: 17050624

Robinson JT, Thorvaldsdóttir H, Winckler W, Guttman M, Lander ES, Getz G, Mesirov JP. 2011. Integrative genomics viewer. *Nature Biotechnology* **29**:24–26. DOI: https://doi.org/10.1038/nbt.1754, PMID: 21221095

Rojek A, Füchtbauer EM, Kwon TH, Frøkiaer J, Nielsen S. 2006. Severe urinary concentrating defect in renal collecting duct-selective AQP2 conditional-knockout mice. *PNAS* **103**:6037–6042. DOI: https://doi.org/10.1073/pnas.0511324103, PMID: 16581908

Ruf RG, Xu PX, Silvius D, Otto EA, Beekmann F, Muerb UT, Kumar S, Neuhaus TJ, Kemper MJ, Raymond RM, Brophy PD, Berkman J, Gattas M, Hyland V, Ruf EM, Schwartz C, Chang EH, Smith RJH, Stratakis CA, Weil D, et al. 2004. SIX1 mutations cause branchio-oto-renal syndrome by disruption of EYA1-SIX1-DNA complexes. *PNAS* **101**:8090–8095. DOI: https://doi.org/10.1073/pnas.0308475101, PMID: 15141091

Sajithlal G, Zou D, Silvius D, Xu PX. 2005. Eya 1 acts as a critical regulator for specifying the metanephric mesenchyme. *Developmental Biology* **284**:323–336. DOI: https://doi.org/10.1016/j.ydbio.2005.05.029, PMID: 16018995

Salcedo R, Oppenheim JJ. 2003. Role of chemokines in angiogenesis: CXCL12/SDF-1 and CXCR4 interaction, a key regulator of endothelial cell responses. *Microcirculation* **10**:359–370. DOI: https://doi.org/10.1038/sj.mn.7800200, PMID: 12851652

Schindler YL, Garske KM, Wang J, Firulli BA, Firulli AB, Poss KD, Yelon D. 2014. Hand2 elevates cardiomyocyte production during zebrafish heart development and regeneration. *Development* **141**:3112–3122. DOI: https://doi.org/10.1242/dev.106336, PMID: 25038045

Shao W, Yang J, He M, Yu X-Y, Lee CH, Yang Z, Joyner AL, Anderson KV, Zhang J, Tsou M-FB, Shi H, Shi S-H. 2020. Centrosome anchoring regulates progenitor properties and cortical formation. *Nature* **580**:106–112. DOI: https://doi.org/10.1038/s41586-020-2139-6, PMID: 32238932

Srinivas S, Wu Z, Chen CM, D'Agati V, Costantini F. 1999. Dominant effects of RET receptor misexpression and ligand-independent RET signaling on ureteric bud development. *Development* **126**:1375–1386. DOI: https://doi.org/10.1242/dev.126.7.1375, PMID: 10068631

Stennard FA, Harvey RP. 2005. T-box transcription factors and their roles in regulatory hierarchies in the developing heart. *Development* **132**:4897–4910. DOI: https://doi.org/10.1242/dev.02099, PMID: 16258075

Stinchcombe JC, Randzavola LO, Angus KL, Mantell JM, Verkade P, Griffiths GM. 2015. Mother centriole distal appendages mediate centrosome docking at the immunological synapse and reveal mechanistic parallels with ciliogenesis. *Current Biology* **25**:3239–3244. DOI: https://doi.org/10.1016/j.cub.2015.10.028, PMID: 26670998

Stuart T, Butler A, Hoffman P, Hafemeister C, Papalexi E, Mauck WM III, Hao Y, Stoeckius M, Smibert P, Satija R. 2019. Comprehensive integration of single-cell data. *Cell* **177**:1888–1902.. DOI: https://doi.org/10.1016/j.cell.2019.05.031

Subramanian A, Sidhom EH, Emani M, Vernon K, Sahakian N, Zhou Y, Kost-Alimova M, Slyper M, Waldman J, Dionne D, Nguyen LT, Weins A, Marshall JL, Rosenblatt-Rosen O, Regev A, Greka A. 2019. Single cell census of human kidney organoids shows reproducibility and diminished off-target cells after transplantation. *Nature Communications* **10**:5462. DOI: https://doi.org/10.1038/s41467-019-13382-0, PMID: 31784515

70

Taguchi A, Kaku Y, Ohmori T, Sharmin S, Ogawa M, Sasaki H, Nishinakamura R. 2014. Redefining the in vivo origin of metanephric nephron progenitors enables generation of complex kidney structures from pluripotent stem cells. *Cell Stem Cell* **14**:53–67. DOI: https://doi.org/10.1016/j.stem.2013.11.010, PMID: 24332837

Takahashi K, Tanabe K, Ohnuki M, Narita M, Ichisaka T, Tomoda K, Yamanaka S. 2007. Induction of pluripotent stem cells from adult human fibroblasts by defined factors. *Cell* **131**:861–872. DOI: https://doi.org/10.1016/j.cell.2007.11.019, PMID: 18035408

Takasato M, Er PX, Chiu HS, Maier B, Baillie GJ, Ferguson C, Parton RG, Wolvetang EJ, Roost MS, Chuva de Sousa Lopes SM, Little MH. 2015. Kidney organoids from human iPS cells contain multiple lineages and model human nephrogenesis. *Nature* **526**:564–568. DOI: https://doi.org/10.1038/nature15695, PMID: 26444236

Takeda S, Yonekawa Y, Tanaka Y, Okada Y, Nonaka S, Hirokawa N. 1999. Left-Right asymmetry and kinesin superfamily protein KIF3A: new insights in determination of laterality and mesoderm induction by KIF3A-/- mice analysis. *The Journal of Cell Biology* **145**:825–836. DOI: https://doi.org/10.1083/jcb.145.4.825, PMID: 10330409

Tan Z, Shan J, Rak-Raszewska A, Vainio SJ. 2018. Embryonic stem cells derived kidney organoids as faithful models to target programmed nephrogenesis. *Scientific Reports* **8**:1–10. DOI: https://doi.org/10.1038/s41598-018-34995-3, PMID: 30413738

Tanos BE, Yang HJ, Soni R, Wang WJ, Macaluso FP, Asara JM, Tsou MFB. 2013. Centriole distal appendages promote membrane docking, leading to cilia initiation. *Genes & Development* **27**:163–168. DOI: https://doi.org/10.1101/gad.207043.112, PMID: 23348840

Tsuchihashi T, Maeda J, Shin CH, Ivey KN, Black BL, Olson EN, Yamagishi H, Srivastava D. 2011. Hand2 function in second heart field progenitors is essential for cardiogenesis. *Developmental Biology* **351**:62–69. DOI: https://doi.org/10.1016/j.ydbio.2010.12.023, PMID: 21185281

Veldman BCF, Kuper WFE, Lilien M, Schuurs-Hoeijmakers JHM, Marcelis C, Phan M, Hettinga Y, Talsma HE, van Hasselt PM, Haijes HA. 2021. Beyond nephronophthisis: retinal dystrophy in the absence of kidney dysfunction in childhood expands the clinical spectrum of CEP83 deficiency. *American Journal of Medical Genetics. Part A* **185**:2204–2210. DOI: https://doi.org/10.1002/ajmg.a.62225, PMID: 33938610

Villavicencio EH, Walterhouse DO, Iannaccone PM. 2000. The sonic hedgehog-patched-gli pathway in human development and disease. *American Journal of Human Genetics* **67**:1047–1054. DOI: https://doi.org/10.1016/S0002-9297(07)62934-6, PMID: 11001584

Vincent C, Kalatzis V, Abdelhak S, Chaib H, Compain S, Helias J, Vaneecloo FM, Petit C. 1997. Bor and bo syndromes are allelic defects of EYA1. *European Journal of Human Genetics* **5**:242–246 PMID: 9359046.

Wagner GP, Kin K, Lynch VJ. 2012. Measurement of mRNA abundance using RNA-Seq data: RPKM measure is inconsistent among samples. *Theory in Biosciences = Theorie in Den Biowissenschaften* **131**:281–285. DOI: https://doi.org/10.1007/s12064-012-0162-3, PMID: 22872506

Wellik DM, Hawkes PJ, Capecchi MR. 2002. Hox11 paralogous genes are essential for metanephric kidney induction. *Genes & Development* **16**:1423–1432. DOI: https://doi.org/10.1101/gad.993302, PMID: 12050119

Wheway G, Schmidts M, Mans DA, Szymanska K, Nguyen T-MT, Racher H, Phelps IG, Toedt G, Kennedy J, Wunderlich KA, Sorusch N, Abdelhamed ZA, Natarajan S, Herridge W, van Reeuwijk J, Horn N, Boldt K, Parry DA, Letteboer SJF, Roosing S, et al. 2015. An siRNA-based functional genomics screen for the identification of regulators of ciliogenesis and ciliopathy genes. *Nature Cell Biology* **17**:1074–1087. DOI: https://doi.org/10.1038/ncb3201, PMID: 26167768

Wilm B, James RG, Schultheiss TM, Hogan BLM. 2004. The forkhead genes, FOXC1 and FOXC2, regulate paraxial versus intermediate mesoderm cell fate. *Developmental Biology* **271**:176–189. DOI: https://doi.org/10.1016/j.ydbio.2004.03.034, PMID: 15196959

Wotton KR, Mazet F, Shimeld SM. 2008. Expression of foxc, foxf, FoxL1, and Foxq1 genes in the dogfish Scyliorhinus canicula defines ancient and derived roles for Fox genes in vertebrate development. *Developmental Dynamics* **237**:1590–1603. DOI: https://doi.org/10.1002/dvdy.21553, PMID: 18498098

Xu PX, Adams J, Peters H, Brown MC, Heaney S, Maas R. 1999. Eya1-deficient mice lack ears and kidneys and show abnormal apoptosis of organ primordia. *Nature Genetics* **23**:113–117. DOI: https://doi.org/10.1038/12722, PMID: 10471511

Yang TT, Chong WM, Wang W-J, Mazo G, Tanos B, Chen Z, Tran TMN, Chen Y-D, Weng RR, Huang C-E, Jane W-N, Tsou M-FB, Liao J-C. 2018. Super-Resolution architecture of mammalian centriole distal appendages reveals distinct blade and matrix functional components. *Nature Communications* **9**:1–11. DOI: https://doi.org/10.1038/s41467-018-04469-1, PMID: 29789620

Yumlu S, Stumm J, Bashir S, Dreyer AK, Lisowski P, Danner E, Kühn R. 2017. Gene editing and clonal isolation of human induced pluripotent stem cells using CRISPR/cas9. *Methods* **121–122**:29–44. DOI: https://doi.org/10.1016/j.ymeth.2017.05.009, PMID: 28522326

Zhao R, Watt AJ, Battle MA, Li J, Bondow BJ, Duncan SA. 2008. Loss of both GATA4 and GATA6 blocks cardiac myocyte differentiation and results in acardia in mice. *Developmental Biology* **317**:614–619. DOI: https://doi.org/10.1016/j.ydbio.2008.03.013, PMID: 18400219

71

Appendix 1

Supplemental methods

hiPSCs culture

We used the human iPSC cell line BIHi005-A, which was generated from a healthy donor by the Berlin Institute of Health (BIH) and supplied by the stem cell core facility at Max Delbrück Center for Molecular Medicine (Berlin). The hiPSCs were maintained in six-well plates (Corning, 353046), coated with Matrigel (Corning, 354277), and cultured in Essential 8 medium (E8, Gibco-Thermo Fisher Scientific, A1517001) supplemented with 10 µM Y-27632 (Rocki, Wako, 253–00513). The cells were split twice per week using EDTA/PBS or Accumax (Stem cell technology, 07921).

CRISPR CAS9 technology to generate CEP83$^{-/-}$ hiPSCs clones

Clustered regularly interspaced short palindromic repeats (CRISPR)-Cas9 technology was used to generate CEP83$^{-/-}$ hiPSCs clones. Two 20 bp-long CRISPR RNAs (crRNAs) were designed using CRISPOR software (*Concordet and Haeussler, 2018*) to selectively target exon7: (5'- GGCTGAAG TAGCGGAATTAA-AGG-3'); (5'-AAGAATACAGGTGCGGCAGT-TGG-3'). The crRNAs were ordered from Integrated DNA Technologies (IDT). The crRNAs (IDT) were annealed in equimolar concentrations with trans-activating CRISPR RNA (tracrRNA) to form two guide RNAs (gRNA1 and gRNA2), which were then conjugated separately with Alt-R S.p. Cas9 Nuclease V3 (1 µM concentration, IDT, 1081058) at room temperature for 1 hr to form ribonucleoprotein (RNP) complexes (RNP1 and RNP2).

One day prior to transfection, hiPSCs were split using Accumax solution and cultured in an equal proportion of E8 medium and StemFlex medium (Thermo Fisher Scientific, A3349401). The hiPSCs were transfected using a Neon transfection system (Thermo Fisher Scientific, MPK5000). Immediately before the transfection, the cells were dissociated, collected, and resuspended in Resuspension Buffer (Buffer R) that included in Neon transfection 100 µl kit (Thermo Fisher Scientific, MPK10025; *Yumlu et al., 2017*). Cells were transfected in 3 ml Electrolytic buffer (Buffer E) that included in the neon transfection kit and by using the Neon transfection system 10 µl tip. The used Neon Transfection parameters were voltage (1200 V), width (30 ms), and pulse (1). The transfected cells were cultured in StemFlex Medium with Rocki for 48 hr.

Then, quick DNA extraction and PCR were then done to test transfection efficiency according to the manufacturer's instructions using Phire Tissue Direct PCR Master Mix (Thermo Scientific, F170S). The size of the PCR products was visualized on 1.5% agarose gel. After confirming the transfection's success in the knockout cells, as shown in *Figure 1B*, the cells were dissociated and seeded at low densities for 24 hr. Then, 24 single cells were picked under a picking hood S1 (stem cell core facility-MDC, Buch) and cultured in StemFlex medium for 2 weeks. The clones were then tested for CEP83 mutation on the DNA level by PCR using Phire Tissue Direct PCR Master Mix. Finally, the selected clones were expanded and frozen in the Bambanker medium (Nippon Genetics, BB01) for further characterization. The selected clones were characterized for the mutation induction on the DNA, protein, and RNA level.

Differentiation protocol

We used the protocol of *Takasato* to differentiate the hiPSCs into nephron organoids (*Takasato et al., 2015*), the experiment was performed using three replicates per each group wildtype hiPSCs (*WT1*, *WT2*, and *WT3*) and CEP83$^{-/-}$ hiPSCs (*KO1*, *KO2*, and *KO3*). Two days prior to the differentiation, cultured hiPSCs on matrigel with 70–80% density were prepared for the differentiation. The cells were washed twice with 1× Dulbecco's PBS (Thermo Fisher Scientific,14190–250), then cells were trypsinized using 1× Trypl E Select (Thermo Fisher Scientific, 12563011). Cells were incubated at 37°C for 3 min. Then, DMEM/F-12 medium (Thermo Fisher Scientific, 11320–033) was added to the cells to neutralize Trypl E. The cell suspension was mixed by pipetting (pipetting is maximum twice), then centrifuged at 300 g for 5 min. The cell pellet was washed and resuspended in 1 ml of E8 medium. Then the cells were counted using Countess chamber slide and Countess II Automated Cell Counter (Thermo Fisher Scientific). Then cells were centrifuged and resuspended in E8 media supplemented with 10 µM Rocki. Last, cells were cultured on a prepared coated matrigel six-well culture plates to obtain a density of 15×10^3 cells per cm^2 and incubated overnight at 37°C CO$_2$ incubator for 48 hr with daily medium change.

Immediately before the differentiation, the cells were checked under the microscope. Cells with 40–50% confluency were used for the differentiation. The E8 medium was changed into APEL2

medium (Stem Cell Technologies, 05270) with 5% Protein Free Hybridoma Medium II (PFHMII, GIBCO, 12040077) and 8 µM CHIR99021 (2 ml medium per a well of 6- well plate). Cells were incubated in a 37°C CO_2 incubator for 5 days, with medium refreshing every 2 dys. Following the CHIR99021 phase, the medium was changed into a double volume of APEL2 medium (4 ml medium per a well of six-well plate) supplemented with 200 ng/ml FGF9 (R&D, 273-F9-025) and 1 µg/ml heparin (Sigma Aldrich, H4784-250MG) and were incubated in a 37°C CO_2 incubator.

On day 7 of differentiation, the cells were washed, trypsinized with trypsin EDTA (0.05%), and incubated at 37°C for 3 min. Then, the cell suspension was transferred to a 50 ml tube containing 9 ml of MEF conditioned medium (R&D, AR005) to neutralize the trypsin. The cells were centrifuged and resuspended in APEL2 medium. Using a hemocytometer, the cells were counted, and the cell suspension was divided to achieve 1×10^6 cells (organoid) per 1.5 ml tube. All the tubes were centrifuged at 400× g for 3 min at RT. During centrifugation, six-well transwell cell culture plates (Corning-Sigma Aldrich, CLS3450-24EA) were prepared by adding 1.2 ml of APEL2 supplemented with 5 µM CHIR99021 to each well. Cell pellets were picked up by using a P1000 or P200 wide-bore tip. Pellets were carefully seeded onto the six-well transwell membrane with minimal APEL2 medium carryover and incubated at 37°C for 1 hr. Then the medium was changed into APEL2 medium supplemented with 200 ng/ml FGF9 plus 1 µg/ml heparin for further 5 days, with medium refreshing every 2 days. Finally, the medium to APEL2 medium with only heparin for further 13 days, with medium refreshing every 2 days.

DNA isolation and PCR

Cultured *WT* and *CEP83*$^{-/-}$ hiPSCs were washed, scrapped gently using a cell scraper (VWR, part of Avantor, 734–2602), and collected with a maximum 5×10^6 cell/ml for proper DNA extraction. The DNA was extracted using DNeasy Blood & Tissue Kits (Qiagen, 69504) following the manufacturer's instructions. The concentrations and quality of the DNA were evaluated using Nanodrop (Thermo Scientific, Waltham, MA; USA). To detect CEP83 expression, 200 µg DNA was amplified by a standard PCR using Phusion high-fidelity DNA polymerase (Biolabs, New England, M0530). The master mix was calculated according to the manufacturer's instructions. Primers are designed using Primer3 webtool, *Supplementary file 2*. PCR was carried out in a thermocycler as follow: initial denaturation at 98°C for 30 s, 35–40 cycles of 30 s at 98°C, 30 s at 63.5°C, and 30 s at 72°C; final elongation step at 72°C for 10 min. The PCR results were checked on 1.5% agarose gel and analyzed using a BioDoc Analyze dark hood and software system (Biometra).

RNA isolation, RNA sequencing, and qPCR

Total RNA was isolated from the cells at three time points: day 0 (hiPSCs), day 7 (IM), and day 25 (organoids) with a maximum of 1×10^7 cells using RNAasy Mini Kit (QIAGEN, Hilden, Germany, 74104,) following the manufacture instructions. The RNA was treated with RNase-free DNase I (QIAGEN, 79254) for 15 min at room temperature during the extraction. The concentration, quality, and integrity of the extracted RNA were evaluated using Nanodrop (Thermo Scientific, Waltham, MA; USA), an Agilent 2100 Bioanalyzer, and the Agilent RNA 6000 Nano kit (5067–1511, Agilent Technologies). More than 0.4 µg total RNA with high integrity (more than 6.8) and high purity (OD260/280=1.8–2.2 and OD260/230≥1.8) were collected and sent to Illumina NovaSeq 6000RNA sequencing by Novogene. RNA-Seq library preparation and next-generation sequencing: cDNA libraries with paired-end 150 bp enriched were prepared by Novogene. First, the mRNA was randomly fragmented and supplemented with oligo (dT) beads. Then cDNA synthesis was done using the random hexamers and reverse transcriptase. Second, second-strand synthesis was done using: a custom second-strand synthesis buffer from Illumina, deoxyribose nucleoside triphosphates (dNTPs), RNase H, and *Escherichia coli* polymerase I. The final obtained cDNA library was purified, terminally repaired, A-tailed ligated to sequencing adapters, size-selected, and PCR-enriched. Quantification of library concentration was performed using a Qubit 2.0 fluorometer. Library size was measured by Agilent 2100 bioanalyzer and was quantified by qPCR (library activity >2 nM). Libraries were sequenced on Illumina NovaSeq 6000 S4 flow cells (paired end, 150 bp).

Raw data were transformed into sequenced reads and recorded in a FASTQ file. FASTQ files were aligned to build 19 of the human genome provided by the Genome Reference Consortium (GRCh19), performed by Christian Hinze using TOPHAT2 aligner tool (*Kim et al., 2013*). Up to four mismatches with the reference genome were accepted. Raw counts were obtained using featureCounts (*Liao et al., 2014*). Mutation visualization in the knockout samples was performed using the Integrative

73

Genomic Viewer tool (*Robinson et al., 2011*). For gene expression analysis reads were normalized to the sequence length and transcripts per million (TPM) values were calculated (*Wagner et al., 2012*). TPM values of the samples were used to plot heatmaps and for PCA analysis based on Pearson correlation, using R (R Development Core Team, 4.0.4)

500 ng of RNA was reverse transcribed using the RevertAid First Strand cDNA synthesis kit (Thermo Scientific, K1622) according to the manufacturer's instructions. The qPCR was carried out using the Fast Universal SYBR Green Master Mix (ROX, Roche Diagnostics, 04 913 850 001,) according to the manufacturer's instructions. For expression analysis, relative mRNA expression levels were normalized for GAPDH mRNA expression and calculated according to the ΔΔCt method. All primer pairs were designed using the free-online primer design tool Primer3, purchased at BioTeZ (Berlin, Germany), and sequences are shown in (*Supplementary file 1*). The statistical significance of differences between two groups (WT and KO) was analyzed using a two-sided Student's t-test.

Single-cell RNA (scRNA) experiment

Cells isolation and preparation

The differentiated hiPSCs to intermediate mesodermal cells were collected at day 7 of the differentiation from two different experiments. The cells of the first experiment were derived from *WT1* and *KO1* differentiated hiPSCs, while the second experiment comprises the differentiated cells of *WT2* and *KO2* cells. The cells were washed twice with 1× DPBS and dissociated with Accumax for 7 min at 37°C. Cells were centrifuged at 350× g for 5 min and resuspended in 1× DPBS. Then, cells were filtered with a 40 μm filter (Corning, 352340), counted (10,000 cells per sample), and checked for viability using Trypan blue staining.

Protein extraction and Immunoblotting

Protein extraction

Up to 1×10⁶ hiPSCs per sample (*WT1, WT2, WT3, KO1, KO2*, and *KO3*) were washed with cold 1× PBS, then centrifuged at 3500 g for 5 min. Next, the cell pellet was resuspended in pre-ice cold 100 μl of radioimmunoprecipitation assay (RIPA) buffer (Sigma-Aldrich, R0278) supplemented with protease inhibitor (Roche, 11697498001) and maintained with constant agitation for 30 min at 4°C. Then the suspension was centrifuged at 4°C for 20 min at 12,000 rpm. The supernatant was collected as protein extract and quantified using BCA Protein Assay (Thermo Scientific, 23228).

Immunoblotting

30 μg of the extracted protein in RIPA buffer were mixed with 1RIPA reducing (10% b-mercaptoethanol) NuPAGE loading buffer (Life Technologies, Carlsbad, CA). After denaturation at 70°C for 10 min. The protein was loaded on a precast polyacrylamide NuPage 4–12% Bis-Tris protein gel (Invitrogen, Carlsbad, CA, USA) and 1× MOPS (1 M MOPS, 1 M TrisBase, 69.3 mM SDS, 20.5 mM EDTA) to be separated according to the length using SDS -PAGE (100 V, 200mA, 2 hr). Proteins were blotted on 0.45 μm pore size Immobilon-P polyvinylidene difluoride membrane (EMD Millipore, Billerica, MA; USA). The membrane was pre-activated for 20 s in methanol and equilibrated in 1× NuPage Transfer buffer (1.25 mM bicine, 1.25 mM BisTris, 0.05 mM EDTA, and 10% ethanol) for 30 min at RT. The membrane was blocked in 5% bovine serum albumin for 1 hr at RT and incubated overnight at 4°C with primary antibodies: Anti-CEP83 produced in rabbit (1:500, Sigma-Aldrich) and Anti-α-Tubulin produced in mouse (1:500, T9026, Sigma-Aldrich). The membrane was incubated for 1 hr at RT with horseradish peroxidase-conjugated secondary antibodies (Sigma-Aldrich, Saint Louis, MO, USA) with 1:2000 dilution. Chemiluminescent reagent (Super Signal–West Pico; Thermo Scientific, Waltham, MA; USA) was used to detect the proteins. The spectra Multicolor Broad Range Protein Ladder (Thermo Fisher Scientific, USA) was used to evaluate the molecular weight of corresponding protein bands.

Histology and immunofluorescence staining

After organoid fixation in BD Cytofix buffer (554655, BD Biosciences) for 1 hr on ice, the organoids were gradually dehydrated in increasing ethanol concentrations for 15 min each. Then organoids were cleared in xylene for three times 20 min each. After infiltration with melted paraffin at 65°C

74

three times for 30 min each, the organoids were embedded in paraffin and processed in 3.5-μm thick sections using a HM 355 S microtome. The sections were deparaffinized, dehydrated, and stained with hematoxylin (Sigma-Aldrich, Saint Louis, MO) for 3 min and in 1% eosin (Sigma-Aldrich) for 2 min. The sections were mounted using Kaiser's glycerol gelatin-based mounting medium. Images were captured with a Leica CTR 6000 microscope (Leica Biosystems, Wetzlar, Germany).

For immunostaining, cultured cells (D7) and organoids (D25) were fixed with BD Cytofix for 10 min on ice. Then cells were permeabilized with BD Perm/Wash (554723, BD Biosciences), twice, 15 min per each. Cells were blocked with a blocking solution (1% BSA + 0.3% triton-X-100 in 1× DPBS) for 2 hr at RT or overnight at 4°C. Cells were incubated overnight at 4°C with primary antibodies (*Supplementary file 2*). Cells were then washed twice (10 min each) and incubated with fluorescence-labeled secondary antibodies with 1:500 dilution including Cy3, Cy5, Alexa488, and Alexa647 (Jackson ImmunoResearch, Newmarket, UK) and Cy3 Streptavidin (Vector lab, Burlingame, USA) overnight at 4°C. DAPI was then used for nuclear staining (Cell signaling Technology, Danvers, MA, USA) with 1:300,000 dilution for 1 hour at RT. Finally, cells were mounted with Dako fluorescent mounting medium (Agilent Technologies). The images were taken using a SP8 confocal microscope (Carl Zeiss GmbH, Oberkochen, Germany). All the quantitative analyses of the taken images were performed using ImageJ (1.48 v; National Institutes of Health, Bethesda, MD) software.

75

(My curriculum vitae does not appear in the electronic version of my paper for reasons of data protection) .

(My curriculum vitae does not appear in the electronic version of my paper for reasons of data protection).

Publication list

1. **<u>Fatma Mansour</u>**; Christian Hinze; Narasimha Swamy Telugu; Jelena Kresoja; Iman B. Shaheed; Christian Mosimann; Sebastian Diecke; Kai M. Schmidt-Ott. The centrosomal protein 83 (CEP83) regulates human pluripotent stem cell differentiation towards the kidney lineage. **eLife** 11:e80165. https://doi.org/10.7554/eLife.80165 (**IF: 8.71).**

2. **<u>Fatma Mansour</u>**, Felix J. Boivin, Iman B. Shaheed, Markus Schueler, and Kai M. Schmidt-Ott (2021). The Role of Centrosome Distal Appendage Proteins (DAPs) in Nephronophthisis and Ciliogenesis. **International Journal of Molecular Sciences,** 22: 12253. https://doi.org/10.3390/ijms222212253 (**IF: 5.54)**.

3. **<u>Mansour, F.A.A</u>**., Shaheed, I., Hassan, N.R.A. (2015). Use of Bone Marrow-Derived Mesenchymal Stem Cells in Improving Thioacetamide Induced Liver Fibrosis in Rats. In: Polychroniadis, E., Oral, A., Ozer, M. (eds) 2nd International Multidisciplinary Microscopy and Microanalysis Congress. Springer Proceedings in Physics, vol 164. Springer, Cham. https://doi.org/10.1007/978-3-319-16919-4_29.

Acknowledgments

Fatma Mansour